

# **TRANSITION METAL-CATALYZED NON-DIRECTED C–H FUNCTIONALIZATION OF ARENES AND ALKANES**

by

Amanda Karena Cook-Sneathen

A dissertation submitted in partial fulfillment  
of the requirements for the degree of  
Doctor of Philosophy  
(Chemistry)  
in the University of Michigan  
2015

Doctoral Committee:

Professor Melanie S. Sanford, Chair  
Professor John Montgomery  
Professor Johannes Schwank  
Assistant Professor Nathaniel Szymczak

© Amanda K. Cook-Sneathen  
2015

**To Mom**

## ACKNOWLEDGEMENTS

Everything I have accomplished during my five years working on this thesis would not have been possible without an army of support. Melanie, you have been a better mentor and role model than I ever could have hoped for. Your knowledge, creativity, and ambition both amazed and intimidated me when I was a rotator in the lab, and still do so today. I admire your willingness to diversify and how you encourage your students to do the same. The focus of the group has expanded so much since I first joined, and I have learned so much because of it. You have encouraged and pushed me out of my comfort zone (Methane as a substrate? Really?), and I have become a better and more confident chemist because of it. The ways in which you have influenced me are innumerable, and I cannot thank you enough.

To my committee members, Professors Montgomery, Szymczak, and Schwank, I thank you for your support and guidance over my time here. Prof. Montgomery, thank you for asking me the difficult questions about chemistry and not being too harsh if I didn't know the answers. Also, the exchange program with ICIQ was one of the best experiences of my life and I thank you for organizing and initiating it. Prof. Szymczak, my first semester here I spend working in your lab. Thinking about chemistry from an inorganic chemist's viewpoint has greatly influenced the direction of my graduate work and will continue to do so. Prof. Schwank, I am very grateful for the perspective that you have brought to my projects, especially in regards to the focus of our work on methane functionalization.

Over my five years here at Michigan, I have been extremely lucky to have such great mentors and peers to look up to. Marion, you took me under your wing, taught me how to take over your project, and held me to your standards. You have shaped my expectations of what a good chemists should be, and I hope one day to live up to them. Brannon, you were my first bay-mate and although I teased you a lot, I really looked up

to you. I wouldn't have made it through my candidacy exam without you. To Anna, Chelsea, Sharon, and Kara, you guys are everything I wanted to be when I first joined the group and I thank you for being great examples for me to follow. Ansis, thank you for asking me difficult questions at every group meeting and especially in your help preparing my ORP.

My bay-mates have been constant supports in everything from broken vials to presentation preparation. Kate, you have been such a great friend and lab-mate during my time here. I love how we could talk about anything and how you remind me that chemistry shouldn't be my entire life. Signe, although your time here was short, your smile and relaxed attitude was a beacon in the midst of graduate school stress. I'll always remember our trip through Canada, the Ferris wheel, and the never-ending search for wifi. Christo, I don't think I've ever gotten along with someone as quickly as I have with you. You're one of the smartest and most focused people I've ever met. I have thoroughly enjoyed talking about chemistry with you, and even though my last year here has been stressful (I swear I'm not always a ball of anxiety), you have definitely made it easier and actually enjoyable. So, thank you for that, for your Nespresso machine, and for Stuff you Missed in History Class.

To Doug and Monica, you guys have helped me through my toughest times during grad school. Doug, a big regret I have is that I only really got to know you in the months before you left. I reached out to you because I greatly admire your ability to handle tough situations, and your perspective and support through a situation that both blindsided and devastated me was incredibly invaluable. You helped me regain a confidence in myself that I thought was stolen from me. You're the example of what a post-doc should be, and I hope I can be like you. Monica, on days when I don't want to talk to anyone, you are the one person I can go to who can make everything better. I'm so grateful to you for simply being there when I need someone to talk to. I thoroughly enjoyed teaching with you last semester, and your bravery in coming to a foreign country, learning the language, and flourishing as you do is awe inspiring. I can't wait to visit you in Tarragona and watch you excel in your new career by the sea.

As my time at Michigan has gone on, incredible younger scientists have joined the lab. Naoko, I wish you could see how great I think you are. You're hard working, smart,

and fearless. I love joking around with you, teaching you bad words, and talking about chemistry with you. I hope you find the balance you're searching for. Nomaan, I see a bit of myself in you. You have a fire and ambition that I recognize, and I hope that you can learn to use that to challenge yourself and find your motivation from within. Sydonie, you've done amazing things in your work so far, and your initiative to change projects is admirable. I'm so lucky to be leaving my project in your hands. To Melissa, I'm so impressed with the progress you've made on your project and I can't wait to see where your research takes you. To Nicole, Ian, James, BJ, Danielle, Devin, and Katarina, I am impressed with your guys' enthusiasm to talk about chemistry and with how hard you work; I encourage all of you to step outside of your comfort zones and challenge yourself.

The true foundation of who I am as a scientist was laid by my family. Mom, you sacrificed so much for your kids, and everything I do, I do to make you proud. Thank you for never just telling me the answer to my questions, but for making me actually look it up. I've learned to be independent and to have the confidence to pursue my goals because of you. To Mimi, thank you for being the most forgiving person I know and the best sister I could ask for. To Tar, I try every day to be as happy and carefree as you. You are the best brother anyone could hope for. To Uncle Mikey and JoJo, thank you for helping me start in college- without your help and encouragement I would have never even stepped foot in a college classroom.

Stefan, the nine months that you were here were the best of my life. You have taught me so much, from how to count in Schwiizerdütsch, to why my shoulder hurts, to how to setup a Soxhlet extraction. You know me better than I know myself, and words cannot express how much I have grown because of you. I'm so proud of you for risking everything to find a lab and a project that you are passionate about, and it is amazing seeing that fire in you again. As I close this chapter of my life, I'm so grateful for the time I've spent with you, listening to The Xx, drinking beer, and watching Netflix. We've gone through so much together, and I can't wait to see what's next for us.

# TABLE OF CONTENTS

Dedication .....	ii
Acknowledgements .....	iii
List of Schemes.....	viii
List of Figures.....	ix
List of Tables.....	xii
Abstract.....	xiv
CHAPTER 1. Introduction .....	1
1.1 Functional Group Interconversion and C–H Activation.....	1
1.2 Mechanisms of C–H Activation .....	2
1.3 Development of Catalytic Ligand Directed C–H Functionalization .....	4
1.4 Catalytic Arene C–H Functionalization .....	5
1.5 Catalytic Alkane C–H Functionalization .....	8
1.6 References.....	11
CHAPTER 2. Pyridine and its Derivatives as Ligands for Palladium: Remarkably High Reactivity in the Non-Directed C–H Acetoxylation of Arenes.....	13
2.1 Introduction .....	13
2.2 Results and Discussion.....	15
2.3 Conclusions.....	29
2.4 Perspective and Outlook .....	29
2.5 Experimental .....	30
2.6 Characterization.....	32
2.7 References.....	33
CHAPTER 3. On the Mechanism of the Palladium-Catalyzed Arene C–H Acetoxylation: A Comparison of Catalysts and Ligand Effects .....	35

3.1	Introduction .....	35
3.2	Results and Discussion .....	37
3.3	Conclusions.....	64
3.4	Perspective and Outlook .....	64
3.5	Experimental .....	65
3.6	Characterization .....	70
3.7	References.....	71
CHAPTER 4. Steric Control of Site Selectivity in the Pd-Catalyzed C–H Acetoxylation of Simple Arenes.....		74
4.1	Introduction .....	74
4.2	Results and Discussion .....	75
4.3	Conclusions.....	81
4.4	Perspective and Outlook .....	82
4.5	Experimental .....	83
4.6	Characterization .....	84
4.7	References.....	92
CHAPTER 5. The Development of Catalytic Methane C–H Borylation and a comparison of Rh and Ir catalysts .....		94
5.1	Introduction .....	94
5.2	Results and Discussion .....	97
5.3	Conclusion .....	107
5.4	Perspective and Outlook .....	108
5.5	Experimental .....	108
5.6	Characterization .....	114
5.7	References.....	116



## LIST OF SCHEMES

<b>Scheme 1.1.</b> Functional group interconversion.....	1
<b>Scheme 2.1.</b> Balanced equations of the acetoxylation of benzene.....	14
<b>Scheme 2.2.</b> Low catalyst loading showing the robustness of the Pd(OAc) <sub>2</sub> /pyr catalyst system.....	18
<b>Scheme 2.3.</b> Testing the viability of peracetic acid as the oxidant.....	28
<b>Scheme 3.1.</b> Comparison of directed and non-directed C–H functionalization.....	35
<b>Scheme 3.2.</b> Pyridine ligand effects in the Pd-catalyzed C–H acetoxylation of benzene .....	36
<b>Scheme 3.3.</b> Proposed mechanism of the Pd(OAc) <sub>2</sub> -catalyzed C–H acetoxylation of benzene .....	41
<b>Scheme 3.4.</b> Proposed mechanism for the (pyr) <sub>2</sub> Pd(OAc) <sub>2</sub> -catalyzed C–H acetoxylation of benzene .....	47
<b>Scheme 3.5.</b> Proposed mechanism with Pd(OAc) <sub>2</sub> /pyr (1:1) as catalyst .....	62
<b>Scheme 3.6.</b> Explanation for lack of pyridine electronic effect with catalyst <b>8b</b> .....	63
<b>Scheme 5.1.</b> Methods of methane functionalization known in the literature .....	95
<b>Scheme 5.2.</b> (a) Stoichiometric borylation of <i>n</i> -pentane using [W]–B(OR) <sub>2</sub> complex. (b) Borylation of 1° or 2° alkanes using a Rh or Ir catalyst and B <sub>2</sub> pin <sub>2</sub> .....	96
<b>Scheme 5.3.</b> The borylation of methane and potential by-products.....	97

## LIST OF FIGURES

<b>Figure 1.1.</b> Bond dissociation energies and $pK_a$ values of common C–H bonds <sup>3</sup> .....	2
<b>Figure 1.2.</b> (a) Mechanism of oxidative addition. (b) Representative example of stoichiometric C–H activation via oxidative addition. ....	3
<b>Figure 1.3.</b> (a) General mechanism of C–H activation via $\sigma$ -bond metathesis. (b) General mechanism of C–H activation via 1,2-addition. ....	4
<b>Figure 1.4.</b> (a) General mechanism of C–H activation via CMD. (b) Representative example of CMD transition state. ....	4
<b>Figure 1.5.</b> Concept of how directing groups facilitate C–H activation and some examples of substrates .....	5
<b>Figure 1.6.</b> Early work on the acetoxylation of benzene by Ebersson and Crabtree .....	6
<b>Figure 1.7.</b> Catalyst development for the acetoxylation of benzene (Chapter 2) .....	7
<b>Figure 1.8.</b> Comparison of catalysts and the mechanism of benzene acetoxylation (Chapter 3) .....	7
<b>Figure 1.9.</b> Representative example of the catalyst controlled site-selective C–H acetoxylation of simple arenes (Chapter 4) .....	8
<b>Figure 1.10.</b> (a) Shilov’s methane oxidation to methanol and/or methyl chloride using Pt(II) catalyst and Pt(IV) oxidant. (b) Periana’s methane oxidation to methyl bisulfate using (bpm)PtCl <sub>2</sub> catalyst and SO <sub>3</sub> oxidant. (c) Alkane carbonylation. (d) Alkane dehydrogenation using a hydrogen acceptor. (e) Alkane borylation using B <sub>2</sub> Pin <sub>2</sub> . ....	9
<b>Figure 1.11.</b> Comparison of catalysts and substrates for the borylation of alkanes (Chapter 5) .....	10
<b>Figure 2.1.</b> Activity of Pd(OAc) <sub>2</sub> /pyr (1:X) catalyst systems .....	16
<b>Figure 2.2.</b> Varying the equivalents of pyridine: 2 hour reaction time .....	17
<b>Figure 2.3.</b> Varying the equivalents of pyridine: 1 hour reaction time, 1-2.6 mol % pyr	18

<b>Figure 2.4.</b> Cationic pyridine derivatives.....	21
<b>Figure 2.5.</b> Time study comparing catalyst systems using $K_2S_2O_8$ .....	23
<b>Figure 2.6.</b> Time study comparing electronics of pyridine derivatives in the acetoxylation of benzene using $K_2S_2O_8$ .....	25
<b>Figure 2.7.</b> Time study comparing <b>L2</b> and pyridine as ligands using $PhI(OAc)_2$ .....	26
<b>Figure 2.8.</b> Time study demonstrating the initial rate enhancement of $NEt_4BF_4$ as a PTC .....	28
<b>Figure 3.1.</b> Order in $Pd(OAc)_2$ .....	38
<b>Figure 3.2.</b> Order in $Pd(OTFA)_2$ .....	38
<b>Figure 3.3.</b> Order in benzene using $Pd(OAc)_2$ as the catalyst .....	39
<b>Figure 3.4.</b> Order in $PhI(OAc)_2$ using $Pd(OAc)_2$ as the catalyst.....	40
<b>Figure 3.5.</b> H/D kinetic isotope effect for benzene using $Pd(OAc)_2$ as the catalyst.....	40
<b>Figure 3.6.</b> C–H acetoxylation of benzene monitored by $^1H$ NMR spectroscopy (aromatic region shown) using $Pd(OAc)_2$ /pyr (1:2) as catalyst.....	42
<b>Figure 3.7.</b> $^1H$ - $^1H$ ROESY NMR experiment showing exchange between free (8.48 ppm) and bound (8.59 ppm) pyridine. Spectrum acquired in $C_6D_6/CD_3CO_2D$ (1:1) at 80 °C .....	43
<b>Figure 3.8.</b> Order in $[Pd]$ with the $(pyr)_2Pd(OAc)_2$ catalyst in <i>Regime 1</i> .....	44
<b>Figure 3.9.</b> Order in benzene with $(pyr)_2Pd(OAc)_2$ catalyst in <i>Regime 1</i> .....	44
<b>Figure 3.10.</b> Order in $PhI(OAc)_2$ with $(pyr)_2Pd(OAc)_2$ as catalyst in <i>Regime 1</i> .....	45
<b>Figure 3.11.</b> H/D kinetic isotope effect for benzene using $(pyr)_2Pd(OAc)_2$ as catalyst in <i>Regime 1</i> .....	46
<b>Figure 3.12.</b> Hammett plot showing the effect of pyridine electronics for $(pyr)_2Pd(OAc)_2$ catalyst in <i>Regime 1</i> .....	47
<b>Figure 3.13.</b> C–H acetoxylation of benzene monitored by $^1H$ NMR spectroscopy (aromatic region shown) using <b>4-NO<sub>2</sub></b> as the catalyst.....	49
<b>Figure 3.14.</b> Order in $[Pd]$ for the <b>4-NO<sub>2</sub></b> catalyst in <i>Regime 1</i> .....	50
<b>Figure 3.15.</b> Order in benzene for the <b>4-NO<sub>2</sub></b> catalyst in <i>Regime 1</i> .....	50
<b>Figure 3.16.</b> Order in $PhI(OAc)_2$ for the <b>4-NO<sub>2</sub></b> catalyst in <i>Regime 1</i> .....	51
<b>Figure 3.17.</b> Order in $[Pd]$ for the <b>4-NO<sub>2</sub></b> catalyst in <i>Regime 2</i> .....	52
<b>Figure 3.18.</b> Order in (excess) 3-NO <sub>2</sub> Pyr for the <b>4-NO<sub>2</sub></b> catalyst in <i>Regime 2</i> .....	52

<b>Figure 3.19.</b> Order in benzene for the <b>4-NO<sub>2</sub></b> catalyst in <i>Regime 2</i> .....	53
<b>Figure 3.20.</b> Order in PhI(OAc) <sub>2</sub> for the <b>4-NO<sub>2</sub></b> catalyst in <i>Regime 2</i> .....	53
<b>Figure 3.21.</b> New species ( <b>8</b> ) observed by <sup>1</sup> H NMR spectroscopy along with <b>4</b> when combining a 1:1 ratio of Pd(OAc) <sub>2</sub> :pyr .....	54
<b>Figure 3.22.</b> C–H acetoxylation of benzene monitored by <sup>1</sup> H NMR spectroscopy (aromatic region shown) using a Pd(OAc) <sub>2</sub> :pyr ratio of 1:1 .....	55
<b>Figure 3.23.</b> DOSY data used to approximate the molecular weight of <b>8</b> (blue data point) in solution .....	56
<b>Figure 3.24.</b> Mixed pyridines experiment. (a) <sup>1</sup> H NMR spectrum when Pd(OAc) <sub>2</sub> and OMe-pyr (1:1) are mixed. (b) <sup>1</sup> H NMR spectrum when Pd(OAc) <sub>2</sub> and <i>t</i> -Bu-pyr (1:1) are mixed. (c) <sup>1</sup> H NMR spectrum when Pd(OAc) <sub>2</sub> , <i>t</i> -Bu-pyr, and OMe-pyr (1:0.5:0.5) are mixed. Two new peaks are observed. (Spectra shown are the region corresponding to the signals of the 2-position of the mono-pyridine complexes.).....	59
<b>Figure 3.25.</b> Order in [Pd] with Pd(OAc) <sub>2</sub> /pyr (1:1) as catalyst .....	60
<b>Figure 3.26.</b> Order in benzene with Pd(OAc) <sub>2</sub> /pyr (1:1) as catalyst .....	60
<b>Figure 3.27.</b> Order in PhI(OAc) <sub>2</sub> with Pd(OAc) <sub>2</sub> /pyr (1:1) as catalyst.....	61
<b>Figure 3.28.</b> H/D kinetic isotope effect for benzene using Pd(OAc) <sub>2</sub> /pyr (1:1) as catalyst .....	61
<b>Figure 3.29.</b> Hammett plot showing the effect of pyridine electronics with Pd(OAc) <sub>2</sub> /pyr (1:1) as catalyst.....	63
<b>Figure 5.1.</b> Challenges associated with methane C–H functionalization .....	94
<b>Figure 5.2.</b> Reactor setup for in situ liquid sampling.....	103
<b>Figure 5.3.</b> Time studies for methane and ethane borylation.....	104
<b>Figure 5.4.</b> CH <sub>4</sub> and MeBpin competition for the (a) Rh and (b) Ir catalysts .....	106

## LIST OF TABLES

<b>Table 2.1.</b> Substrate scope .....	19
<b>Table 2.2.</b> Yield of C–H acetoxylation of benzene as a function of pyridine structure...	20
<b>Table 2.3.</b> Initial evaluation of Pd catalyst activity for benzene C–H acetoxylation as a function of pyridine ligand using $K_2S_2O_8$ as the oxidant .....	21
<b>Table 2.4.</b> Effect of temperature on initial (t = 2 h) and final (t = 18 h) yield .....	24
<b>Table 2.5.</b> PTCs tested in the acetoxylation of benzene using $K_2S_2O_8$ .....	27
<b>Table 3.1.</b> Results from DOSY experiment and internal standards used .....	57
<b>Table 3.2.</b> Amounts of pyridine derivatives for the mixed pyridines experiment.....	70
<b>Table 4.1.</b> Effect of pyridine ligands on site selectivity and yield for the C–H acetoxylation of 1,2-dichlorobenzene .....	76
<b>Table 4.2.</b> Optimization of $Pd(OAc)_2$ /acridine-catalyzed C–H acetoxylation of 1,2-dichlorobenzene .....	77
<b>Table 4.3.</b> Effect of the oxidant on site selectivity for the C–H acetoxylation of 1,2-dichlorobenzene .....	78
<b>Table 4.4.</b> Optimization of catalyst loading .....	79
<b>Table 4.5.</b> $Pd(OAc)_2$ /acridine-catalyzed C–H acetoxylation of tri- and di-substituted arenes .....	80
<b>Table 4.6.</b> $Pd(OAc)_2$ /acridine-catalyzed C–H acetoxylation of mono-substituted arenes .....	82
<b>Table 5.1.</b> Evaluating Rh and Ir complexes as catalysts for methane borylation .....	98
<b>Table 5.2.</b> Optimization of reaction parameters .....	100
<b>Table 5.3.</b> Testing various solvents for methane borylation .....	101
<b>Table 5.4.</b> Comparison of Rh and Ir catalysts for $CH_4$ vs. CyH borylation .....	102
<b>Table 5.5.</b> Rates of reaction for methane, ethane, hexane, and cyclohexane using both the Rh and Ir catalysts.....	105

**Table 5.6.** Independent rates for methane and MeBpin ..... 107

## ABSTRACT

The development of novel methods to convert chemical feedstocks is highly desirable, as it holds the potential for significant valorization. Today, the chemicals readily available for functionalization are converted to more useful products using functional group interconversion. However, these processes are costly in terms of waste and effort. To improve upon these processes, using functional groups readily available in the feedstock is desirable. One of the most abundant functional groups is the C–H bond, but despite this availability, there are challenges associated with C–H functionalization. The challenges are primarily associated with inertness; the bond dissociation energy is high, the acidity is low, and the kinetic barriers for C–H bond breakage are prohibitive. Using homogeneous transition metal complexes to facilitate C–H bond activation and functionalization is a promising method for C–H functionalization. This thesis describes the development of methods and mechanistic analysis of C–H functionalization of alkanes and arenes, both of which are the primary components of chemical feedstocks.

Chapter 1 describes in detail the challenges in C–H activation and functionalization, as well as the relevant history and precedent for the work detailed herein.

Chapter 2 begins with our initial development of a palladium/pyridine-based catalyst that is highly active for the C–H oxygenation of benzene and other simple arenes using a powerful iodine(III) oxidant. This novel catalyst system proves to show increased reaction rates when compared to previously developed catalysts for this transformation. This chapter also addresses a major challenge of C–H oxidation chemistry: typically expensive and wasteful oxidants are required. Using a cationic ligand for the palladium catalyst, the iodine(III) oxidant was successfully replaced with potassium persulfate, a highly economical oxidant. The cationic ligand proved essential for high activity with this oxidant, and the origins of this effect are explored and detailed.

Chapter 3 further investigates the mechanism of the palladium/pyridine catalyzed conversion of benzene to phenyl acetate using the iodine(III) oxidant. Detailed mechanistic and kinetic analyses were used to determine that the active catalyst in solution is a dimer with one pyridine ligated per palladium. The mechanism by which this precatalyst enters into the catalytic cycle and functionalized benzene was elucidated using kinetic analysis. Additionally, these studies were performed for the previously developed catalysts, and the three catalyst systems and their mechanisms are compared.

In Chapter 4, a catalyst system was developed for the site selective C–H oxygenation of simple arenes. Site-selectivity is a major challenge of C–H functionalization reactions, as C–H bonds are ubiquitous in organic molecules. Using an acridine/palladium catalyst with a sterically bulky iodine(III) ligand, high site selectivities are obtained, favoring functionalization at the least sterically hindered C–H bond.

Chapters 2-4 detail the accomplishments regarding arene C–H functionalization. However, alkanes are another abundant feedstock available and their functionalization has proved more challenging than arene functionalization. In this context, one of the most challenging substrates is methane, whose availability is increasing. In Chapter 5, the borylation of methane using Ir and Rh catalysts is explored. Methane is converted to a methyl boronic ester using a diboron reagent, and the activities and selectivities of the Rh and the Ir catalysts are compared

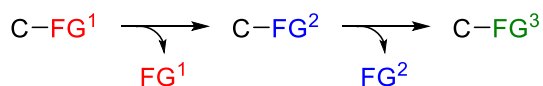


# CHAPTER 1. INTRODUCTION

## 1.1 FUNCTIONAL GROUP INTERCONVERSION AND C–H ACTIVATION

The paradigm of synthesis, whether it be of small molecules or large natural products, is that one functional group must be converted into another. The fields of organic and inorganic chemistry revolve around this school of thought. However, functional group interconversion sequences have inherent flaws including the generation of significant waste, as the starting material must lose one functional group in place of another (Scheme 1.1). Additionally, much effort is invested in the starting material's design, installation, protection, etc. To avoid this waste of materials and effort, using a functional group readily available in our chemical feedstocks is a desirable solution. One functional group that is ubiquitous is the C–H bond. Because functional groups are handles for reactivity, the C–H bond is rarely thought of as such (although that has been changing over the past two decades), and has even been labelled as the “un-functional group” because of its inherent stability.<sup>1</sup>

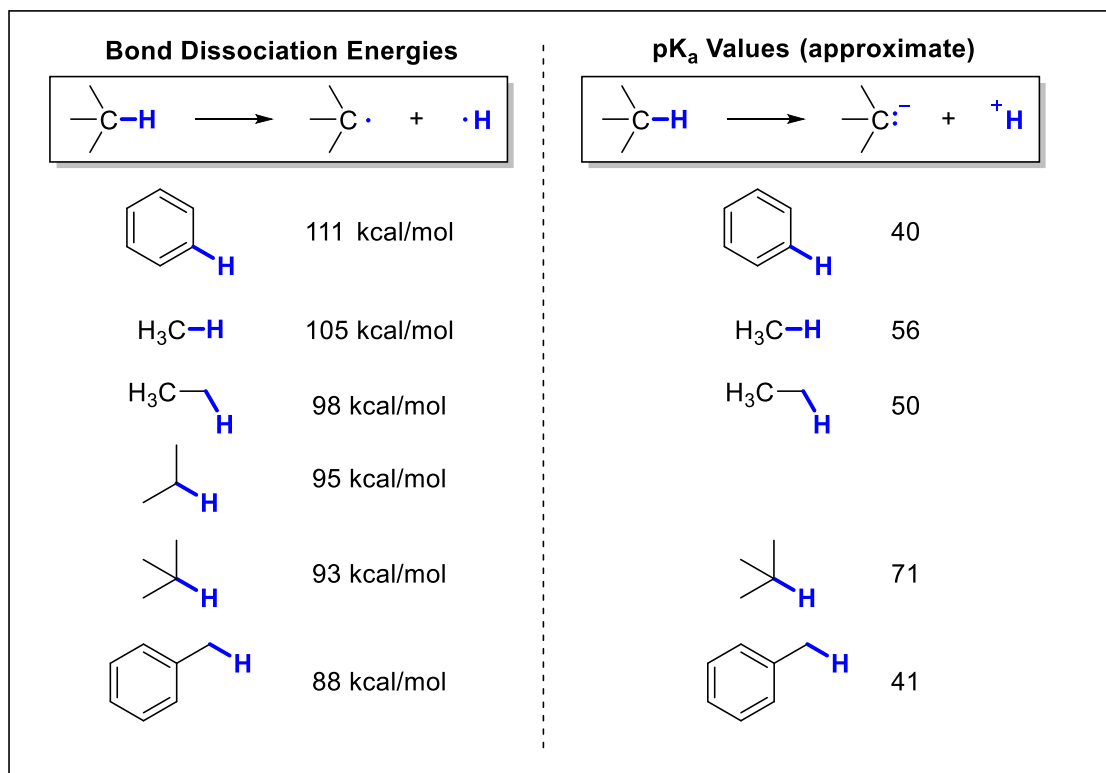
**Scheme 1.1.** Functional group interconversion



Bonds are broken and formed according to their reactivity, which is often quantified as bond dissociation energies (BDEs) or, in the special case of bonds to hydrogen, as acidity. The C–H bond is so unreactive because of its high pK<sub>a</sub> and high BDE.<sup>2</sup> The BDEs and acidities of various types of C–H bonds are compared in Figure 1.1 below.<sup>3</sup> Despite the strength of C–H bonds, there have been numerous examples of their cleavage in the literature, primarily with the aid of transition metals.<sup>1,2,4</sup> In the early years of homogeneous C–H activation, transition metals such as palladium, iridium, and rhodium were shown to

react with the C–H bonds of alkanes and arenes stoichiometrically, forming [M]–C bonds.<sup>2,4a,4e</sup> These pioneering examples opened the door for catalytic C–H functionalization, which has started to become synthetically useful in recent years.<sup>5</sup>

**Figure 1.1.** Bond dissociation energies and pK<sub>a</sub> values of common C–H bonds<sup>3</sup>



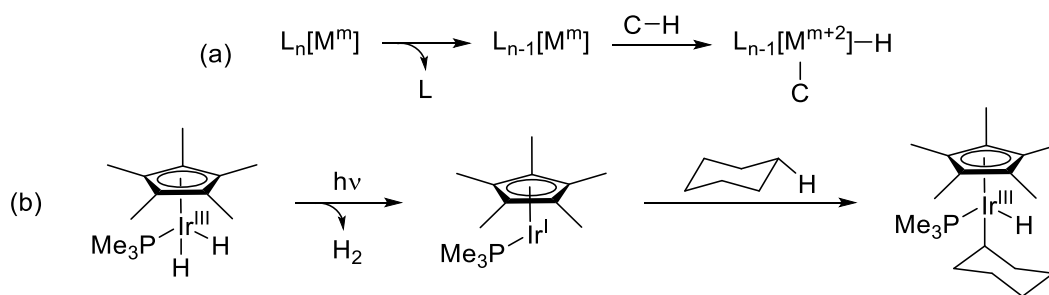
Challenges in the field of C–H activation are abundant. The main attraction of using C–H bonds as the reactive group in starting materials (i.e., that it is highly abundant) is also one of the primary setbacks. The key challenge that must be addressed is how does one functionalize *this* C–H bond, and not *that* one? This challenge includes proper catalyst choice and development, as the catalyst can exert control over both selectivity and activity. Detailed below is the relevant history and advances in C–H bond activation, followed by the challenges addressed in this dissertation.

## 1.2 MECHANISMS OF C–H ACTIVATION

Exploration of C–H activation by homogeneous transition metal complexes began with stoichiometric studies.<sup>2,4a,4b,4d</sup> Classical examples involve ligand dissociation from an ML<sub>n</sub> complex, forming ML<sub>n-1</sub>, which has an open coordination site (Figure 1.2a). It is

through this open coordination site that the C–H bond can interact with the metal. After the C–H bond coordinates to the metal, it undergoes oxidative addition, forming a metal hydride and a metal–C bond. This type of C–H activation has been seen in many forms, and the low valent intermediate  $[(L_{n-1})M]$  has been accessed a variety of ways. Work by the Bergman,<sup>6</sup> Jones,<sup>7</sup> and Graham<sup>8</sup> groups showed that low valent  $(Cp^*)(L)Ir$  species, which contain an open coordination site, can be generated from either the dihydride via photo-induced reductive elimination of  $H_2$  (Figure 1.2b) or from the carbonyl complex via photo-induced dissociation of CO. These fleeting intermediates can then react with substrates such as cyclohexane to form  $(Cp^*)(L)Ir(Cy)(H)$ . Work in this area has built upon this foundation and has expanded to other metals and supporting ligands.

**Figure 1.2.** (a) Mechanism of oxidative addition. (b) Representative example of stoichiometric C–H activation via oxidative addition.



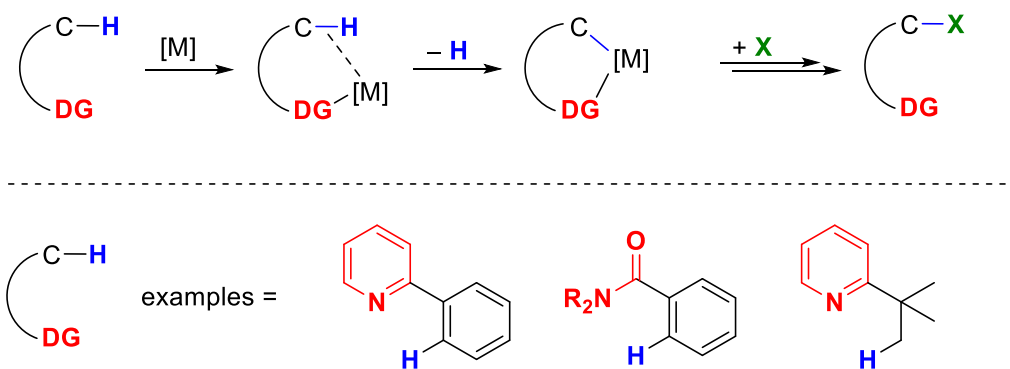
In addition to oxidative addition, other methods<sup>9</sup> for C–H bond activation have been explored stoichiometrically, including sigma-bond metathesis<sup>10</sup> and 1,2-addition across  $M=X$  double bonds. The sigma-bond metathesis pathway (Figure 1.3a) most often occurs using early transition metals with a  $d^0$  electron count, but examples do exist for late transition metals and these will be discussed in more detail in Chapter 5. The 1,2-addition across  $M=X$  double bonds (Figure 1.3b) has mechanistic similarities with both the oxidative addition and sigma-bond metathesis pathways.<sup>2,9</sup> The reactive  $M=Y$  species is formed after elimination of  $XH$ . This highly reactive intermediate then reacts with the C–H bond of interest. The C–H bond adds across the  $M=Y$  double bond, forming a M–C bond, via a 4-membered transition state. This type of transition state, along with the tendency of early metals to perform this mechanism, is similar to that of sigma-bond metathesis.



directing groups, C–H bonds can be transformed into a wide variety of C–X bonds, where X = B, C, N, O, halide, etc.<sup>4c</sup> Despite these advantages, there are significant drawbacks to the use of DGs. The DG and the C–H bond to be functionalized are fixed in their orientation, and this relationship, which is dictated by the metallacycle formed, is not always desirable. For example, in the C–H acetoxylation of 2-phenylpyridine, the pyridyl directing group and the acetoxy group are *ortho* to each other and this relationship is dictated by the 5-membered palladacyclic intermediate that forms upon C–H activation. Additionally, the installation and removal of DGs can be costly, both in terms of time, synthetic effort, and waste.

Because of these disadvantages, significant effort has been invested in developing catalysts that will functionalize C–H bonds of substrates lacking directing groups. Catalyst development is the key to enabling selective, non-directed C–H functionalization, as it has the potential to increase and control the rate, site selectivity, and chemoselectivity of these transformations.<sup>14</sup>

**Figure 1.5.** Concept of how directing groups facilitate C–H activation and some examples of substrates

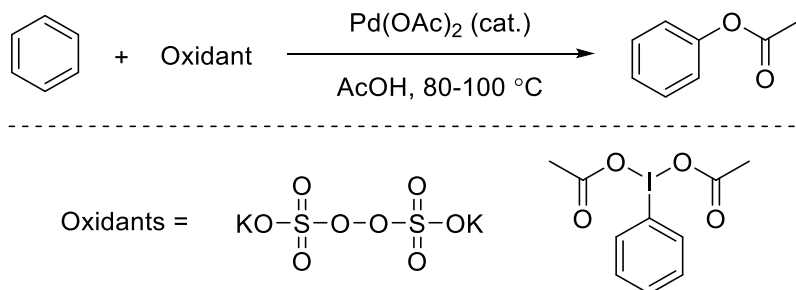


## 1.4 CATALYTIC ARENE C–H FUNCTIONALIZATION

Arenes are a class of abundant feedstocks whose functionalization would add significant value. There is a wealth of literature for arene functionalization via C–H activation, including C–O, C–N, C–C, C–B, and C–Si bond formation.<sup>14a</sup> For arene C–H oxygenation, amination, arylation, and olefination (C–O, C–N, and C–C bond formation),

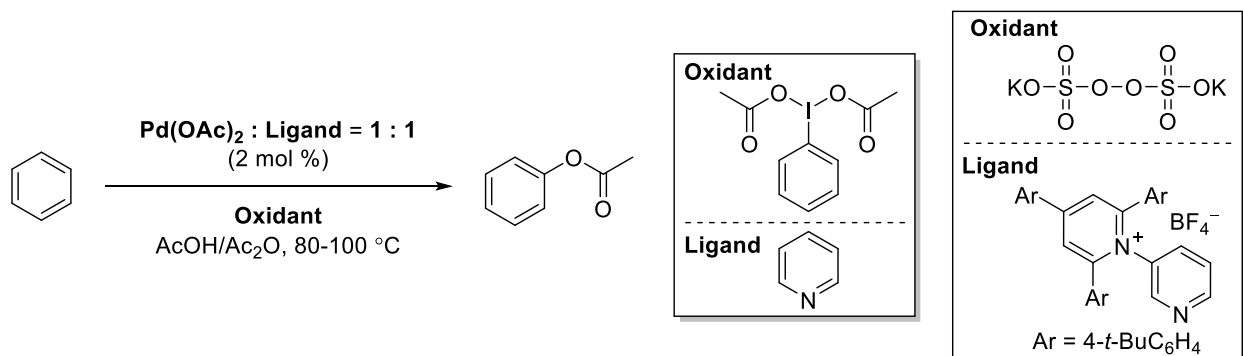
the catalysts found to be optimal were often simple palladium salts, such as Pd(OAc)<sub>2</sub>. For borylation and silylation, success has been met with iridium and rhodium catalysts.<sup>26</sup> Much effort was invested in the C–H hydroxylation and carbonylation of benzene and other simple arenes in the 1970s and 1980s, but the yields of these reactions remained low.<sup>15</sup> Until recently, these reactions remained underdeveloped.

**Figure 1.6.** Early work on the acetoxylation of benzene by Ebersson and Crabtree



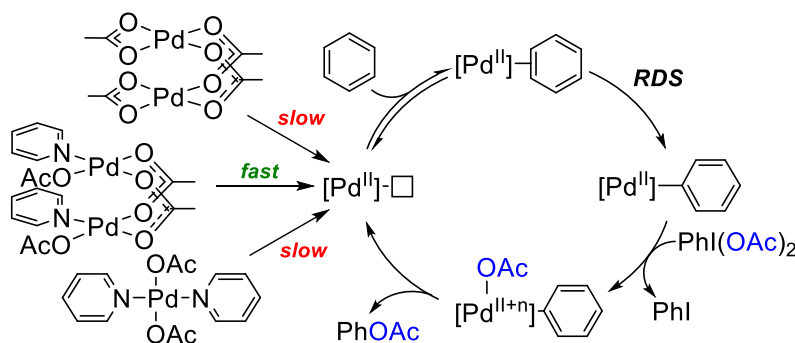
Of special importance to this dissertation is the C–H acetoxylation of simple arenes, such as benzene. Prior to our work in the field (described in Chapters 2-4), the yields and turnover numbers remained low (Figure 1.6).<sup>15b-e, 16</sup> Previous efforts in catalyst development met with little success, and for >30 years, Pd(OAc)<sub>2</sub> remained the best catalyst. One of the first oxidants used for the acetoxylation of arenes was potassium persulfate.<sup>15b-e</sup> While there are many advantages to this oxidant, such as low cost and easily removable by-products, the kinetics of the reaction remained slow due to low solubility. In the 1990s, the I(III) oxidant PhI(OAc)<sub>2</sub> was shown to provide much higher activity, giving 70 turnovers of PhOAc.<sup>16</sup> Despite this advancement, yields with electron poor arenes remained low. In Chapter 2, the development of ligated palladium complexes for improved reactivity for both the PhI(OAc)<sub>2</sub> and K<sub>2</sub>S<sub>2</sub>O<sub>8</sub> oxidants is discussed (Figure 1.7).<sup>17</sup>

**Figure 1.7.** Catalyst development for the acetoxylation of benzene (Chapter 2)



For many of these C–H functionalization reactions, the mechanism of the reaction, including details about the nature of the active catalyst, is unknown or under-explored. Through detailed mechanistic studies, we compared several catalyst systems for the C–H acetoxylation of benzene (Figure 1.8). We found that our highly active catalyst is dimeric in structure and can readily dissociate to enter the catalytic cycle. The less active catalysts,  $[\text{Pd}(\text{OAc})_2]_2$  and  $(\text{pyr})_2\text{Pd}(\text{OAc})_2$  exhibit lower activity because they are slower to enter into the catalytic cycle.<sup>18</sup>

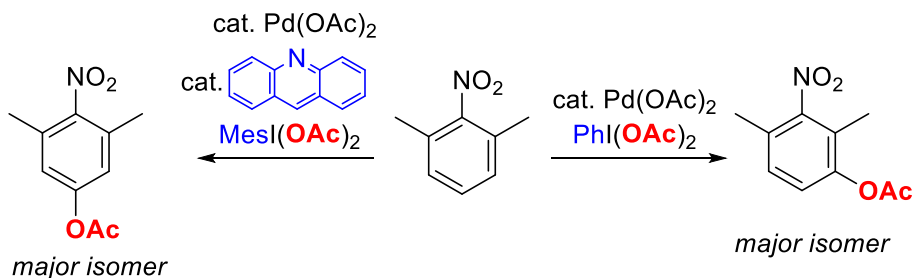
**Figure 1.8.** Comparison of catalysts and the mechanism of benzene acetoxylation (Chapter 3)



One of the main challenges in arene functionalization is site selectivity.<sup>14</sup> While catalytic systems for the sterically controlled C–H amination,<sup>19</sup> borylation,<sup>27</sup> and silylation<sup>20</sup> have been reported, a void in the literature remained for the site selective C–H oxygenation of arenes. Our work discussed in Chapter 4 shows the development of a catalyst system for the site selective C–H acetoxylation of simple arenes (Figure 1.9). Here, the use of a sterically bulky ligand (acridine) and oxidant ( $\text{MesI}(\text{OAc})_2$ ) increased

the site selectivity for a wide range of substrates, favoring C–H functionalization at the least sterically hindered position.<sup>21</sup>

**Figure 1.9.** Representative example of the catalyst controlled site-selective C–H acetoxylation of simple arenes (Chapter 4)



## 1.5 CATALYTIC ALKANE C–H FUNCTIONALIZATION

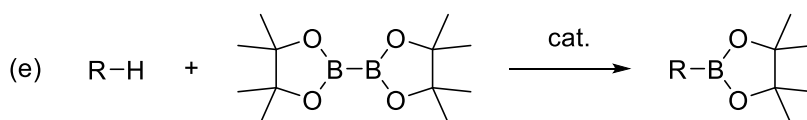
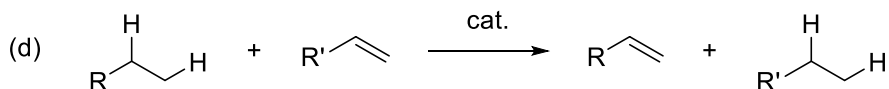
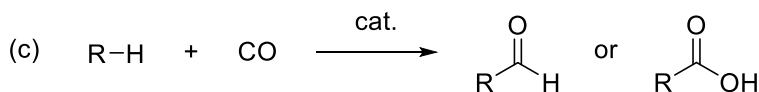
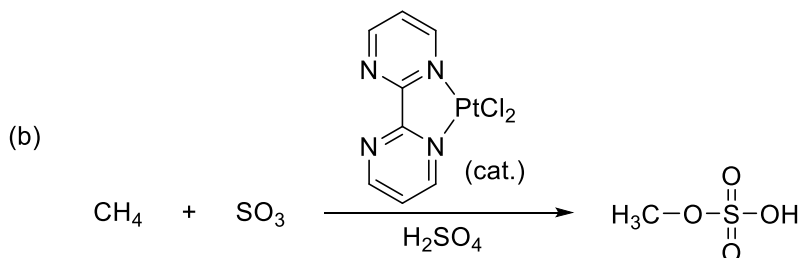
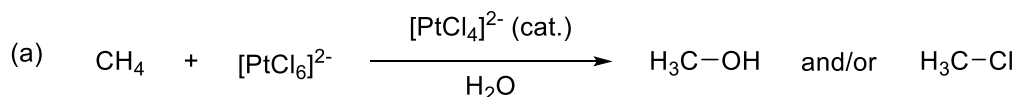
The catalytic functionalization of alkanes is a highly sought after goal of homogeneous catalysis. The primary motivation for alkane functionalization is the potential to turn cheap and abundant feedstock chemicals into value-increased commodity chemicals. Of particular importance is the functionalization of methane, which is the primary component of natural gas.<sup>22</sup> With the world's capture of natural gas ever increasing, the price drops concurrently, and storing and transporting such a volatile gas is problematic.<sup>22a</sup> However, there are relatively few reports of methane functionalization, despite its desirability.<sup>22</sup> Developed in the 1960s by Shilov, the Pt(II)-catalyzed oxidation of alkanes, including methane, to alcohols or alkyl chlorides has become the gold standard for alkane oxidation (Figure 1.10a).<sup>4e</sup> However, the use of Pt(IV) as the stoichiometric oxidant and requirement of high temperatures and acidic conditions has limited its usefulness. Improvements on the Shilov system have been sought after, especially in the context of methane functionalization, and progress has been made. One notable example is the Periana system, which uses SO<sub>3</sub> as the oxidant and (bpm)PtCl<sub>2</sub> as the catalyst to convert methane to methylbisulfate (Figure 1.10b).<sup>23</sup> The downside of this reaction is the use of high temperatures (200 °C) and an extremely acidic solvent (fuming sulfuric acid, which is also the source of the SO<sub>3</sub> oxidant).

Further significant advancements in alkane functionalization include carbonylation (Figure 1.10c), dehydrogenation (Figure 1.10d), and borylation (Figure 1.10e), which is



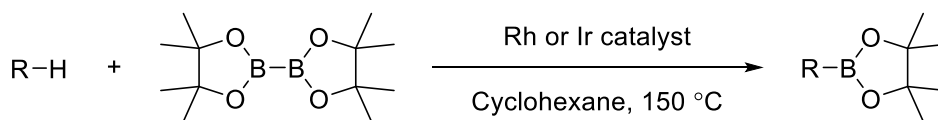
the subject of Chapter 5 of this dissertation. Carbonylation of alkanes to make valuable aldehydes and carboxylic acids requires the use of strongly acidic solvents, such as hydrochloric acid, or irradiation.<sup>24</sup> Alkane dehydrogenation to form an alkene and H<sub>2</sub> is thermodynamically uphill, and therefore requires the use of a hydrogen acceptor.<sup>25</sup> Catalytic alkane borylation was developed much later than the other types of alkane functionalization, and it uses bis(pinacolato)diboron (B<sub>2</sub>pin<sub>2</sub>) as the coupling partner to form alkyl boronic esters.<sup>26</sup> Rhodium and iridium catalysts have been developed and optimized for this process. The products are synthetically useful intermediates, as the C–B bond formed can be transformed into a wide variety of other functional groups.<sup>27</sup> In Chapter 5, this chemistry is applied to methane, and a systematic comparison of the Rh and Ir catalysts highlights their ability to borylate different types of C–H bonds.

**Figure 1.10.** (a) Shilov’s methane oxidation to methanol and/or methyl chloride using Pt(II) catalyst and Pt(IV) oxidant. (b) Periana’s methane oxidation to methyl bisulfate using (bpm)PtCl<sub>2</sub> catalyst and SO<sub>3</sub> oxidant. (c) Alkane carbonylation. (d) Alkane dehydrogenation using a hydrogen acceptor. (e) Alkane borylation using B<sub>2</sub>Pin<sub>2</sub>.

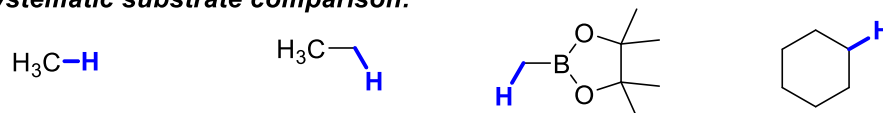


Late transition metal-catalyzed alkane functionalizations have all shown varying degrees of preference for the primary (terminal) C(sp<sup>3</sup>)-H sites in a substrate. Primary C(sp<sup>3</sup>)-H bonds have higher bond dissociation energies than secondary and tertiary C(sp<sup>3</sup>)-H bonds. However, with many catalysts, C-H functionalization occurs selectively at terminal sites because they are the least sterically hindered. It is also important to mention carbenoid,<sup>28</sup> nitrenoid,<sup>29</sup> and O-atom<sup>4b,30</sup> insertions into C-H bonds. The use of these methods, while beyond the scope and direct relevance of this dissertation, have seen fruitful advancements over the past years and have helped advance the field of C-H activation into the realm of utility. The selectivity of these transformations is complementary. Carbenoid, nitrenoid, and O-atom insertion pathways generally selectively target the C(sp<sup>3</sup>)-H bond with low BDE. As such, they are generally selective for 3° and/or 2° C-H sites and are unreactive with 1° C-H bonds.

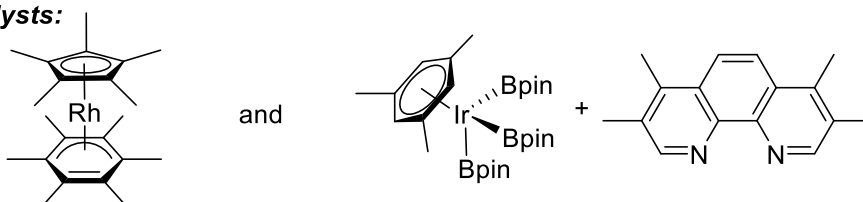
**Figure 1.11.** Comparison of catalysts and substrates for the borylation of alkanes (Chapter 5)



**Systematic substrate comparison:**



**Catalysts:**



In summary, this dissertation contains our work in the development of highly active catalysts (Chapter 2), mechanism elucidation (Chapter 3), and site selective catalysts (Chapter 4) for the C-H acetoxylation of arenes. These chapters are followed by the development of the borylation of light alkanes like methane (Figure 1.11; Chapter 5), which concludes the work detailed herein.

## 1.6 REFERENCES

- (1) Alan, S. G.; Karen, I. G. In *Activation and Functionalization of C–H Bonds*; American Chemical Society: 2004; Vol. 885, p 1.
- (2) Arndtsen, B. A.; Bergman, R. G.; Mobley, T. A.; Peterson, T. H. *Acc. Chem. Res.* **1995**, *28*, 154.
- (3) Anslyn, E. V.; Dougherty, D. A. *Modern Physical Organic Chemistry*, © 2006, University Science Books
- (4) (a) Crabtree, R. H. *Chem. Rev.* **1985**, *85*, 245. (b) Crabtree, R. H. *J. Chem. Soc., Dalton Trans.* **2001**, 2437. (c) Dick, A. R.; Sanford, M. S. *Tetrahedron* **2006**, *62*, 2439. (d) Labinger, J. A.; Bercaw, J. E. *Nature* **2002**, *417*, 507. (e) Shilov, A. E.; Shul'pin, G. B. *Chem. Rev.* **1997**, *97*, 2879.
- (5) (a) Kakiuchi, F.; Chatani, N. *Adv. Synth. Catal.* **2003**, *345*, 1077. (b) McMurray, L.; O'Hara, F.; Gaunt, M. J. *Chem. Soc. Rev.* **2011**, *40*, 1885. (c) Newhouse, T.; Baran, P. S. *Angew. Chem., Int. Ed.* **2011**, *50*, 3362.
- (6) (a) Janowicz, A. H.; Bergman, R. G. *J. Am. Chem. Soc.* **1982**, *104*, 352. (b) Janowicz, A. H.; Bergman, R. G. *J. Am. Chem. Soc.* **1983**, *105*, 3929.
- (7) Jones, W. D.; Feher, F. J. *J. Am. Chem. Soc.* **1984**, *106*, 1650.
- (8) Hoyano, J. K.; McMaster, A. D.; Graham, W. A. G. *J. Am. Chem. Soc.* **1983**, *105*, 7190.
- (9) Balcells, D.; Clot, E.; Eisenstein, O. *Chem. Rev.* **2010**, *110*, 749.
- (10) (a) Lin, Z. *Coord. Chem. Rev.* **2007**, *251*, 2280. (b) Perutz, R. N.; Sabo-Etienne, S. *Angew. Chem., Int. Ed.* **2007**, *46*, 2578.
- (11) Winstein, S.; Traylor, T. G. *J. Am. Chem. Soc.* **1955**, *77*, 3747.
- (12) (a) Boutadla, Y.; Davies, D. L.; Macgregor, S. A.; Poblador-Bahamonde, A. I. *Dalton Trans.* **2009**, 5820. (b) Lapointe, D.; Fagnou, K. *Chem. Lett.* **2010**, *39*, 1118.
- (13) Lyons, T. W.; Sanford, M. S. *Chem. Rev.* **2010**, *110*, 1147.
- (14) (a) Kuhl, N.; Hopkinson, M. N.; Wencel-Delord, J.; Glorius, F. *Angew. Chem., Int. Ed.* **2012**, *51*, 10236. (b) Neufeldt, S. R.; Sanford, M. S. *Acc. Chem. Res.* **2012**, *45*, 936.
- (15) (a) Davidson, J. M.; Triggs, C. *Chemistry & Industry* **1966**, 457. (b) Ebersson, L.; Jonsson, E. *Acta Chem. Scand. B* **1974**, *28*, 771. (c) Ebersson, L.; Jonsson, L. *J. Chem. Soc., Chem. Comm.* **1974**, 885. (d) Ebersson, L.; Jonsson, L. *Acta Chem. Scand. B* **1976**, *30*, 361. (e) Ebersson, L.; Jonsson, L. *Justus Liebigs Ann. Chem.* **1977**, 233. (f) Henry, P. M. *J. Org. Chem.* **1971**, *36*, 1886. (g) Jintoku, T.; Takaki, K.; Fujiwara, Y.; Fuchita, Y.; Hiraki, K. *B. Chem. Soc. Jpn.* **1990**, *63*, 438. (h) Jintoku, T.; Taniguchi, H.; Fujiwara, Y. *Chem. Lett.* **1987**, 1865. (i) Stock, L. M.; Tse, K.; Vorvick, L. J.; Walstrum, S. A. *J. Org. Chem.* **1981**, *46*, 1757.
- (16) Yoneyama, T.; Crabtree, R. H. *J. Mol. Catal. A-Chem.* **1996**, *108*, 35.
- (17) (a) Emmert, M. H.; Cook, A. K.; Xie, Y. J.; Sanford, M. *Angew. Chem., Int. Ed.* **2011**, *50*, 9409. (b) Gary, J. B.; Cook, A. K.; Sanford, M. S. *ACS Catalysis* **2013**, *3*, 700.
- (18) Cook, A. K.; Sanford, M. S. *J. Am. Chem. Soc.* **2015**, *137*, 3109.
- (19) Shrestha, R.; Mukherjee, P.; Tan, Y.; Litman, Z. C.; Hartwig, J. F. *J. Am. Chem. Soc.* **2013**, *135*, 8480.
- (20) (a) Cheng, C.; Hartwig, J. F. *J. Am. Chem. Soc.* **2014**, *136*, 12064. (b) Cheng, C.; Hartwig, J. F. *Science* **2014**, *343*, 853.
- (21) Cook, A. K.; Emmert, M. H.; Sanford, M. S. *Org. Lett.* **2013**, *15*, 5428.
- (22) (a) Crabtree, R. H. *Chem. Rev.* **1995**, *95*, 987. (b) Caballero, A.; Perez, P. J. *Chem. Soc. Rev.* **2013**, *42*, 8809.
- (23) Periana, R. A.; Taube, D. J.; Gamble, S.; Taube, H.; Satoh, T.; Fujii, H. *Science* **1998**, *280*, 560.
- (24) (a) Sakakura, T.; Tanaka, M. *J. Chem. Soc., Chem. Commun.* **1987**, 758. (b) Sakakura, T.; Sodeyama, T.; Sasaki, K.; Wada, K.; Tanaka, M. *J. Am. Chem. Soc.* **1990**, *112*, 7221. (c) Nakata, K.; Miyata, T.; Jintoku, T.; Kitani, A.; Taniguchi, Y.; Takaki, K.; Fujiwara, Y. *B. Chem. Soc. Jpn.* **1993**, *66*, 3755.
- (25) (a) Choi, J.; MacArthur, A. H. R.; Brookhart, M.; Goldman, A. S. *Chem. Rev.* **2011**, *111*, 1761. (b) Dobereiner, G. E.; Crabtree, R. H. *Chem. Rev.* **2010**, *110*, 681.
- (26) (a) Hartwig, J. F. *Chem. Soc. Rev.* **2011**, *40*, 1992. (b) Mkhaliid, I. A. I.; Barnard, J. H.; Marder, T. B.; Murphy, J. M.; Hartwig, J. F. *Chem. Rev.* **2010**, *110*, 890.
- (27) Hartwig, J. F. *Acc. Chem. Res.* **2012**, *45*, 864.

- 
- (28) (a) Davies, H. M. L.; Beckwith, R. E. J. *Chem. Rev.* **2003**, *103*, 2861. (b) Davies, H. M. L.; Manning, J. R. *Nature* **2008**, *451*, 417. (c) Doyle, M. P.; Duffy, R.; Ratnikov, M.; Zhou, L. *Chem. Rev.* **2010**, *110*, 704.
- (29) Davies, H. M. L.; Long, M. S. *Angew. Chem., Int. Ed.* **2005**, *44*, 3518.
- (30) (a) Mansuy, D. *Coord. Chem. Rev.* **1993**, *125*, 129. (b) Meunier, B. *Chem. Rev.* **1992**, *92*, 1411.

# CHAPTER 2. PYRIDINE AND ITS DERIVATIVES AS LIGANDS FOR PALLADIUM: REMARKABLY HIGH REACTIVITY IN THE NON-DIRECTED C–H ACETOXYLATION OF ARENES<sup>1,\*</sup>

## 2.1 INTRODUCTION

Over the past fifteen years there has been tremendous progress in the development of Pd<sup>II/IV</sup>-catalyzed, ligand-directed C–H oxidation reactions to form C–O, C–N, C–S, C–halogen, and C–C bonds.<sup>2</sup> In marked contrast, analogous C–H oxidation reactions of substrates that do not contain directing groups remain challenging.<sup>3</sup> The lack of a directing group typically renders C–H oxidation reactions (as exemplified by C–H oxygenation) kinetically slow (generally <2 turnovers h<sup>-1</sup>), particularly with electron-deficient arene substrates.<sup>3g,3q-x</sup> The palladium-catalyzed C–H oxygenation of simple arenes is also plagued by low turnover numbers (often <10)<sup>3d-t</sup> and competing biaryl formation, which often leads to catalyst decomposition through precipitation of heterogeneous palladium.<sup>3h-j,3n-p,3s,4</sup> Furthermore, with substituted aromatic substrates, the site selectivity is typically low and difficult to control. Our group has sought to identify supporting ligands that would address these limitations and promote the Pd<sup>II/IV</sup>-catalyzed C–H acetoxylation of arenes.<sup>3u-x</sup>

The vast majority of known palladium-catalyzed arene C–H oxygenation reactions utilize simple palladium salts as catalysts (e.g., Pd(OAc)<sub>2</sub> or PdCl<sub>2</sub>).<sup>3d-p</sup> Literature studies have provided conflicting data about the influence of added ligands on these reactions. Several reports have shown that most common ligands (e.g., 2,2'-bipyridine, 1,10-phenanthroline, pyridine, triphenylphosphine oxide, etc.) inhibit the palladium-catalyzed

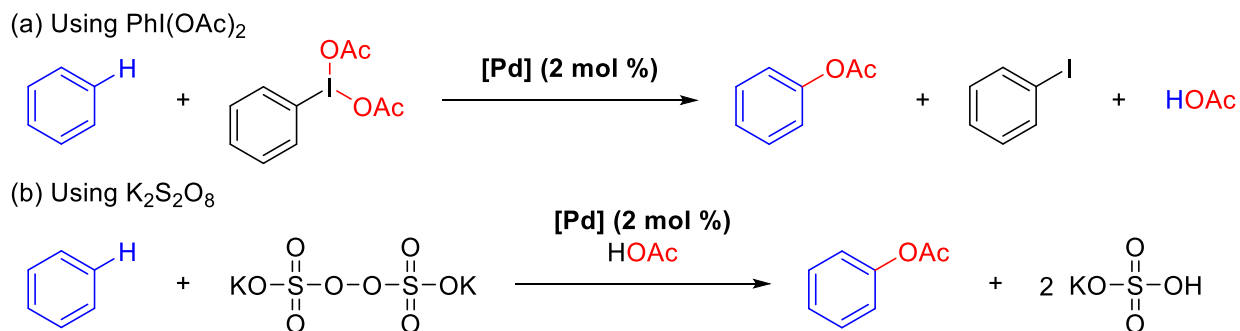
---

\* Work in this chapter was collaborative with Marion H. Emmert (Pd/pyr catalyst system development with PhI(OAc)<sub>2</sub>) and J. Brannon Gary (Cationic ligands and K<sub>2</sub>S<sub>2</sub>O<sub>8</sub>). My contribution to the Pd/pyr catalyst system focused on the data using Pd/pyr (1 : 2) as the catalyst system. My contribution to the cationic ligands and K<sub>2</sub>S<sub>2</sub>O<sub>8</sub> portion of this chapter include time study data for all ligands and all oxidants and evaluating all phase-transfer catalysts and their comparison to **L2**.

C–H acetoxylation of arenes.<sup>3a,3b,3e,3g-j,3n,3s,4</sup> In contrast, related systems with bidentate N(sp<sup>2</sup>)-donor ligands (e.g., 2,2'-bipyridine and/or 1,10-phenanthroline) were shown to provide modest enhancement of catalytic activity.<sup>3j,3k,3q-t</sup> However, these latter reactions exhibited low turnover numbers (typically <10); furthermore, the origin of the increased turnovers was not explored in detail.

In addition to improvements in the catalyst, the choice of oxidant is vital to the development of more practical arene C–H oxygenation reactions. The state of the art, prior to our work, utilized PhI(OAc)<sub>2</sub> as the terminal oxidant.<sup>3g</sup> This reagent is expensive (approximately \$450/mol) when considering the value of the products.<sup>5</sup> Furthermore, it produces iodobenzene and AcOH as stoichiometric by-products (Scheme 2.1a). In addition, PhI(OAc)<sub>2</sub> and PhI both contain aromatic C–H bonds that can undergo competing C–H oxygenation under the reaction conditions. This side reaction significantly reduces the yield of phenyl acetate.

**Scheme 2.1.** Balanced equations of the acetoxylation of benzene



Persulfate-based oxidants are attractive alternatives for these transformations. K<sub>2</sub>S<sub>2</sub>O<sub>8</sub> is more than an order of magnitude less expensive than PhI(OAc)<sub>2</sub>.<sup>6</sup> Furthermore, the by-products of this oxidant are easily separable, water-soluble salts (Scheme 2.1b). Our group has previously shown that K<sub>2</sub>S<sub>2</sub>O<sub>8</sub> serves as an effective oxidant for Pd(OAc)<sub>2</sub>-catalyzed, ligand-directed C–H oxidation reactions of pyridine and oxime ether derivatives.<sup>7</sup> This precedent confirms that K<sub>2</sub>S<sub>2</sub>O<sub>8</sub> is sufficiently reactive to promote C–O bond formation at Pd. However, despite this promising example, the use of K<sub>2</sub>S<sub>2</sub>O<sub>8</sub> in non-directed arene oxidations catalyzed by Pd has historically proven challenging. The most successful example was reported more than 30 years ago and involved the

Pd(OAc)<sub>2</sub>-catalyzed conversion of benzene to phenyl acetate with K<sub>2</sub>S<sub>2</sub>O<sub>8</sub> with extremely low turnover numbers (<10) and reaction yields (<30%).<sup>3s</sup>

This chapter describes our development of Pd-pyridine complexes as catalysts for the oxidation of benzene with PhI(OAc)<sub>2</sub> and K<sub>2</sub>S<sub>2</sub>O<sub>8</sub>. First, we describe the use of careful mechanistic analysis to identify new, active, and general palladium catalysts for the C–H acetoxylation of benzene derivatives using PhI(OAc)<sub>2</sub>. These catalysts can be formed in situ from Pd(OAc)<sub>2</sub> and the simple ligand pyridine (pyr). Furthermore, their catalytic activities can be modulated through variation of the palladium/pyridine ratio. Second, we demonstrate that the combination of Pd(OAc)<sub>2</sub> and a monodentate, pyridinium-substituted pyridine ligand provides a particularly active catalyst for the C–H acetoxylation of benzene using K<sub>2</sub>S<sub>2</sub>O<sub>8</sub> as the oxidant. The mechanistic origins of this high activity are discussed.

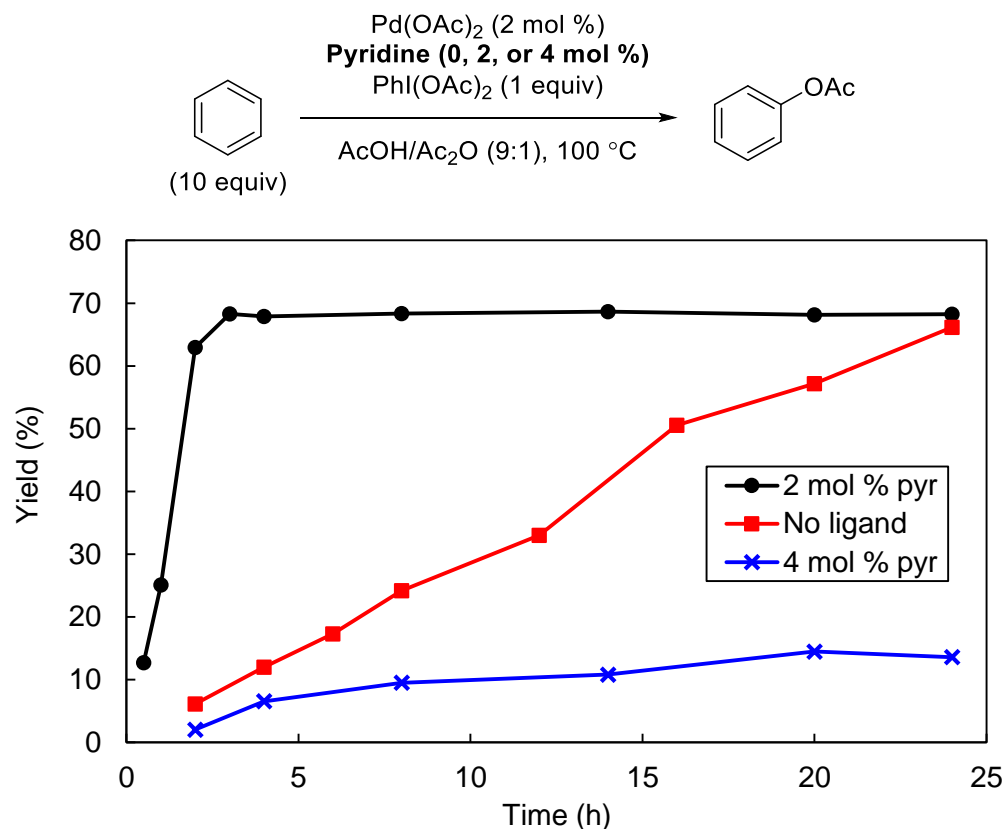
## 2.2 RESULTS AND DISCUSSION

**Development of Pd(OAc)<sub>2</sub>/pyr (1:1) catalyst systems using PhI(OAc)<sub>2</sub>.** Inspired by recent reports of Pd<sup>0/II</sup>-catalyzed C–H functionalizations,<sup>8,9</sup> our initial explorations focused on pyridine as a ligand for the Pd<sup>II/IV</sup>-catalyzed C–H acetoxylation of benzene with PhI(OAc)<sub>2</sub>. At 2 mol % Pd(OAc)<sub>2</sub> (catalyst loading relative to the oxidant), the transformation was complete after 24 hours at 100 °C (Figure 2.1, red squares). In marked contrast, [(pyr)<sub>2</sub>Pd(OAc)<sub>2</sub>] (generated in situ from 2 mol % of Pd(OAc)<sub>2</sub> and 4 mol % of pyr) performed very poorly, providing less than 20% yield under the same reaction conditions (Figure 2.1, blue Xs).

We hypothesized that the low reactivity of [(pyr)<sub>2</sub>Pd(OAc)<sub>2</sub>] might be due to the lack of open coordination sites at the palladium center. Therefore, we next explored the use of a palladium/pyridine ratio of 1:1 (by adding 2 mol % pyr) to more easily access a coordinatively unsaturated, mono-pyridine-ligated palladium species in situ. Importantly, several literature reports have implicated monopyridine Pd<sup>II</sup> complexes as reactive intermediates in Pd<sup>II/0</sup>-catalyzed oxidation reactions.<sup>9,10</sup> The combination of 2 mol % of Pd(OAc)<sub>2</sub> and 2 mol % of pyridine (1:1 ratio of [Pd] to [pyr]) provided a dramatic rate enhancement, with the reaction proceeding to completion in less than 3 hours (Figure 2.1, black circles). Yields are based on the oxidant PhI(OAc)<sub>2</sub>, which has been shown to decompose upon heating through metal-catalyzed<sup>11</sup> and uncatalyzed<sup>12</sup> pathways. By-

products detected include  $(\text{OAc})\text{C}_6\text{H}_4\text{I}$  and  $\text{C}_6\text{H}_4(\text{OAc})_2$ . Both pathways presumably contribute to the moderate yields of acetoxyated products (ca. 70%) upon complete conversion of the oxidant.

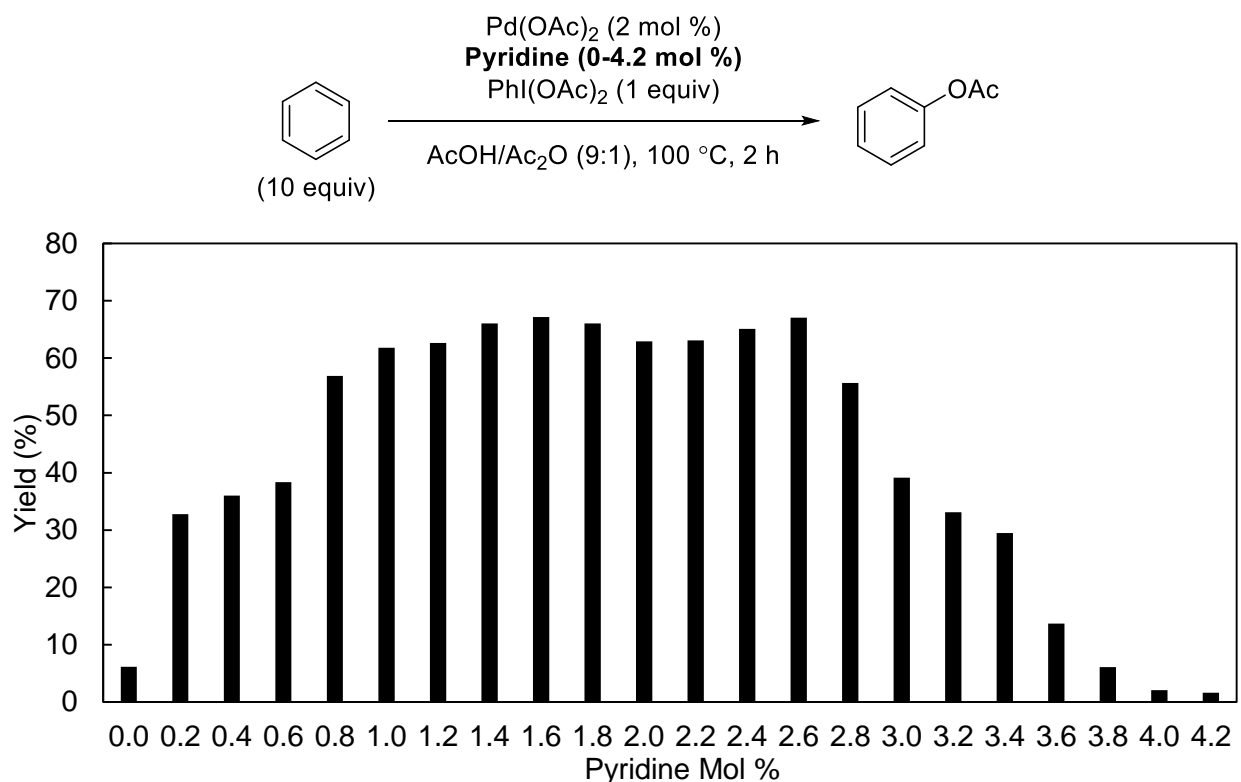
**Figure 2.1.** Activity of  $\text{Pd}(\text{OAc})_2/\text{pyr}$  (1:X) catalyst systems



To test whether the observed yield is due to decomposition of the oxidant or the catalyst, a second equivalent of oxidant was added after 3 h reaction time (when the yield stops increasing). This “second run” afforded an additional 54% yield of  $\text{PhOAc}$ , indicating that the catalyst is still active at 3 h and that the first batch of oxidant had been consumed. A systematic study of the initial reaction rate (approximated by the yield of  $\text{PhOAc}$  after 2 h) as a function of the palladium/pyridine ratio is shown in Figure 2.2. A large dependence was observed, with the highest initial yields at palladium/pyridine ratios between 1:0.5 and 1:1.3. Further experimentation revealed that a palladium/pyridine ratio of 1:0.9 is optimal. The observed sensitivity of the catalyst activity to the ligand-to-metal ratio is likely the reason that ancillary ligands were previously reported to inhibit C–H acetoxylation.<sup>3e,3g</sup>



**Figure 2.2.** Varying the equivalents of pyridine: 2 hour reaction time

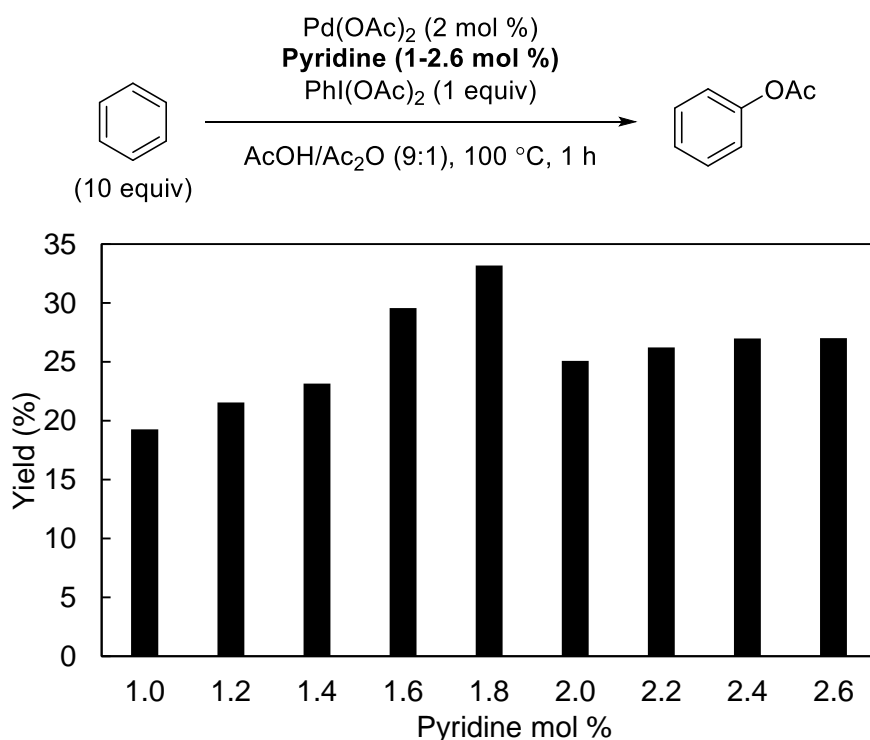


We next sought to probe the longevity of the palladium/pyridine catalysts. Importantly, literature reports suggest that monopyridine/palladium catalysts are short-lived in Pd<sup>II/0</sup>-catalyzed reactions because of fast aggregation of palladium black from coordinatively-unsaturated Pd<sup>0</sup> intermediates.<sup>10</sup> We anticipated that such catalyst decomposition pathways should not be accessible in the current transformation because of the Pd<sup>II/IV</sup> catalytic cycle. Indeed, we found that the palladium/pyridine (1:0.9) catalyst system maintained high activity for C–H acetoxylation over days at 100 °C. For example, under our optimal conditions, the catalyst loading could be lowered to 0.01 mol % Pd(OAc)<sub>2</sub>/0.009 mol % pyridine, which provided a 48% yield of PhOAc (TON of 4756) after 306 hours at 100 °C (Scheme 2.2). To our knowledge, this is the highest reported TON for a homogeneous palladium-catalyzed arene C–H oxygenation reaction.

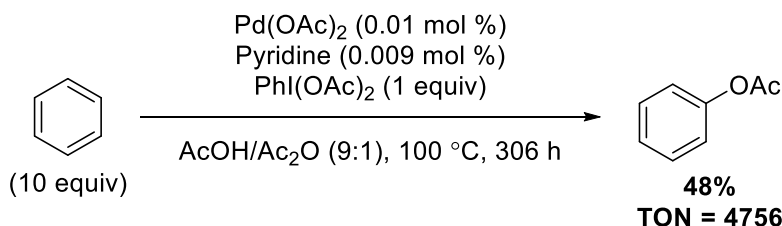
As summarized in Table 2.1, the increased reactivity of the Pd(OAc)<sub>2</sub>/pyridine system is general across a wide scope of arene substrates. Our studies particularly focused on electron-deficient arenes such as bromobenzene, chlorobenzene, ethylbenzoate, α,α,α-trifluorotoluene, and 1,3-bis(trifluoromethyl)benzene, since these

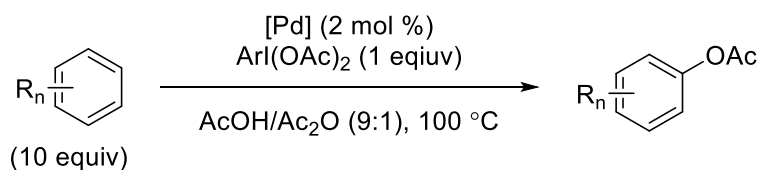
are typically challenging substrates for palladium-catalyzed C–H functionalization.<sup>3g,3q-t,3v</sup> In all cases, the yield of monoacetylated product under our optimal reaction conditions [Pd(OAc)<sub>2</sub>/pyr 1:0.9] was compared to that obtained with Pd(OAc)<sub>2</sub> and with [(pyr)<sub>2</sub>Pd(OAc)<sub>2</sub>] (generated in situ from a 1:2.1 ratio of Pd(OAc)<sub>2</sub> to pyr). A Pd(OAc)<sub>2</sub>/pyr ratio of 1:0.9 provided significantly enhanced yields in all cases. With many substrates, the yield could be further improved by substituting PhI(OAc)<sub>2</sub> with iodomesitylene diacetate (MesI(OAc)<sub>2</sub>; Table 2.1, entries 4, 6, 8, 10, and 12). This may be due to greater stability of MesI(OAc)<sub>2</sub> under the reaction conditions and/or to diminished formation of the by-product (OAc)ArI, which is formed by C(sp<sup>2</sup>)-acetoxylation of the oxidant-derived ArI.

**Figure 2.3.** Varying the equivalents of pyridine: 1 hour reaction time, 1-2.6 mol % pyr



**Scheme 2.2.** Low catalyst loading showing the robustness of the Pd(OAc)<sub>2</sub>/pyr catalyst system



**Table 2.1.** Substrate scope

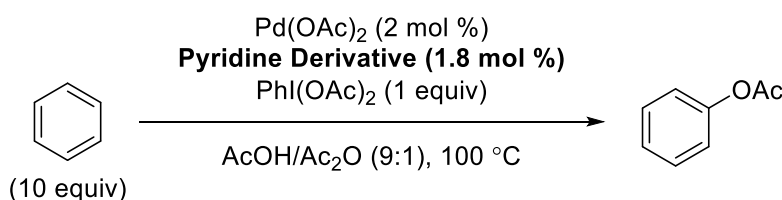
Entry	Oxidant	Product	Yield (%) <sup>a</sup>		
			Pd(OAc) <sub>2</sub>	Pd(OAc) <sub>2</sub> /pyr (1:0.9)	Pd(OAc) <sub>2</sub> /pyr (1:2.1)
1 <sup>b</sup>	PhI(OAc) <sub>2</sub>		8	70	5
2 <sup>c</sup>	MesI(OAc) <sub>2</sub>		n.d.	70	n.d.
3 <sup>b</sup>	PhI(OAc) <sub>2</sub>		7	62	3
4 <sup>d</sup>	MesI(OAc) <sub>2</sub>		n.d.	68	n.d.
5 <sup>e</sup>	PhI(OAc) <sub>2</sub>		8	68	4
6 <sup>f</sup>	MesI(OAc) <sub>2</sub>		n.d.	62	n.d.
7 <sup>e</sup>	PhI(OAc) <sub>2</sub>		5	68	3
8 <sup>g</sup>	MesI(OAc) <sub>2</sub>		n.d.	70	n.d.
9 <sup>h</sup>	PhI(OAc) <sub>2</sub>		5	47	3
10 <sup>i</sup>	MesI(OAc) <sub>2</sub>		n.d.	61	n.d.
11 <sup>j</sup>	PhI(OAc) <sub>2</sub>		1	24	3
12 <sup>k</sup>	MesI(OAc) <sub>2</sub>		n.d.	56	n.d.

<sup>a</sup>Yields are averages of at least 2 runs and were determined by calibrated GC using PhCl or PhCH<sub>2</sub>C(CH<sub>3</sub>)<sub>3</sub> as a standard. Reaction endpoints for the most active catalyst system (Pd(OAc)<sub>2</sub>/pyr 1:0.9) are determined by observation of palladium black formation which indicates complete conversion of the oxidant. The less reactive catalysts are compared at the same reaction times. <sup>b</sup>5 h. <sup>c</sup>9 h. <sup>d</sup>10 h. <sup>e</sup>8 h. <sup>f</sup>12 h. <sup>g</sup>21 h. <sup>h</sup>18 h. <sup>i</sup>17 h. <sup>j</sup>22 h. <sup>k</sup>10 mol % [Pd], 50 h. n.d.=not determined.

We next initiated studies to gain more detailed insights into the role of pyridine in the catalytic cycle. As discussed above, we originally hypothesized that pyridine was acting as a ligand for the active palladium catalyst; however, this additive could also serve as an external base to accelerate C–H activation. To preliminarily distinguish these roles,

we examined the effect of a series of 2- and 2,6-substituted pyridine derivatives on this transformation. As shown in Table 2.2, the initial rate (as approximated by the yield after 1 and 2 hours) tracked extremely well with the steric environment around the pyridine nitrogen atom. For example, moving from unsubstituted pyridine to 2-picoline to 2,6-lutidine significantly slowed the reaction (Table 2.2, entries 1–3, respectively). Furthermore, highly sterically hindered 2,6-di-*tert*-butylpyridine afforded a similar initial rate to that with Pd(OAc)<sub>2</sub> alone. These results implicate a primary role for pyridine as a ligand that binds to the palladium center during one or more key steps of the catalytic cycle.

**Table 2.2.** Yield of C–H acetoxylation of benzene as a function of pyridine structure



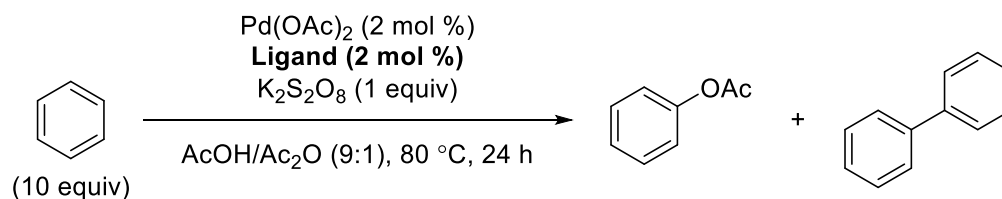
Entry	Additive	Yield (%) after 1h <sup>a</sup>	Yield (%) after 2h <sup>a</sup>
1		33	66
2		13	26
3		6	14
4		3	8
5	None	2	6

<sup>a</sup>Yields were determined by calibrated GC using PhCl as a standard.

**Development of cationic ligands for Pd to enable the use of K<sub>2</sub>S<sub>2</sub>O<sub>8</sub> as the oxidant.** Having developed this highly active Pd(OAc)<sub>2</sub>/pyr catalyst system using PhI(OAc)<sub>2</sub>, we next sought to expand this system to the more economical oxidant, K<sub>2</sub>S<sub>2</sub>O<sub>8</sub>. The C–H oxygenation of benzene (10 equiv) with K<sub>2</sub>S<sub>2</sub>O<sub>8</sub> (1 equiv) as the terminal oxidant and limiting reagent was evaluated at 80 °C in AcOH/Ac<sub>2</sub>O (9:1). As shown in Table 2.3,

entry 1, Pd(OAc)<sub>2</sub> is a poor catalyst for this reaction; the use of 2 mol % of Pd(OAc)<sub>2</sub> resulted in only 0.8% yield of phenyl acetate (approximately 0.5 turnovers) after 24 h.

**Table 2.3.** Initial evaluation of Pd catalyst activity for benzene C–H acetoxylation as a function of pyridine ligand using K<sub>2</sub>S<sub>2</sub>O<sub>8</sub> as the oxidant

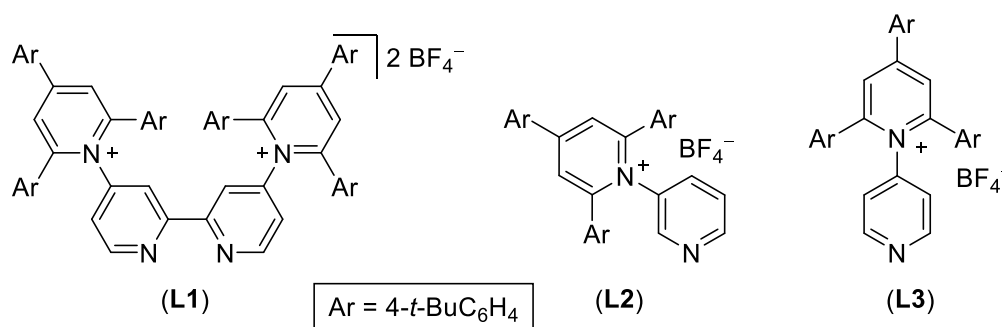


Entry	Ligand	Yield PhOAc (%) <sup>a</sup>	Yield PhPh (%) <sup>a</sup>
1	None	0.8	0.6
2	Pyridine	37	2.0
3	<b>L2</b>	71	1.9
4	<b>L3</b>	65	1.1

<sup>a</sup>Yields were determined by calibrated GC using PhCl as a standard.

Pyridine-ligated catalysts were next examined for this transformation. Similar to the effects seen with PhI(OAc)<sub>2</sub> as the oxidant, the addition of 2 mol % of pyridine to the K<sub>2</sub>S<sub>2</sub>O<sub>8</sub> reaction led to an enhancement in both yield and catalyst turnovers (Table 2.3, entry 2). However, the rate of this reaction remained slow and only 37% yield of phenyl acetate was obtained after 24 hours. Furthermore, a significant quantity of biphenyl (2% yield, PhOAc:PhPh ratio – 14:1) was formed in this transformation.

**Figure 2.4.** Cationic pyridine derivatives



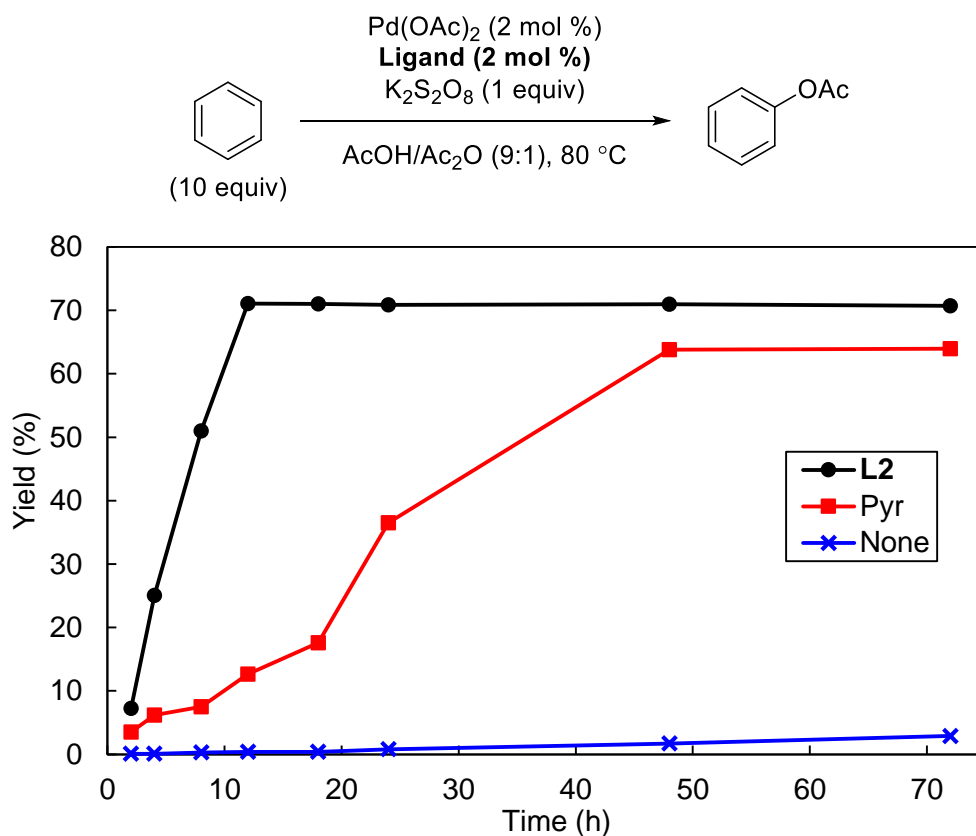
In an effort to identify more reactive catalysts, we next examined cationic pyridinium-substituted pyridine ligands **L2** and **L3** (Figure 2.4). We hypothesized that these ligands might enhance catalyst reactivity based on our prior studies of the bidentate

analogue **L1**.<sup>3v</sup> Our previous work showed that Pd and Pt complexes of **L1** catalyze benzene C–H activation (as measured by H/D exchange) with 10-100-fold faster rates than those containing neutral bipyridine derivatives.<sup>3v</sup> By analogy, we anticipated that monodentate **L2** and **L3** might outperform pyridine as ligands in Pd-catalyzed benzene C–H activation/acetoxylation.

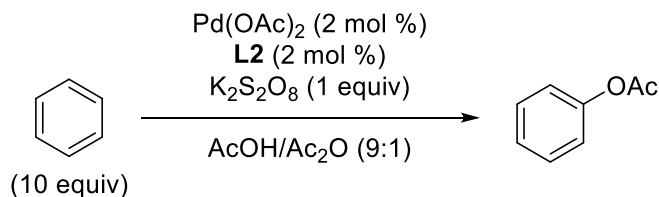
As predicted, ligands **L2** and **L3** provided significant improvements in the rate and chemoselectivity of Pd-catalyzed benzene acetoxylation with  $K_2S_2O_8$ . The use of **L2** or **L3** (2 mol %) in conjunction with  $Pd(OAc)_2$  (2 mol %) afforded PhOAc in 71% and 65% yield, respectively, after 24 hours (Table 2.3, entries 3 and 4). Additionally, the selectivity for PhOAc versus PhPh was high in both cases (approximately 36:1 for **L2** and 65:1 for **L3**).

A more detailed comparison of the reactivity of  $Pd(OAc)_2$  (blue Xs),  $Pd(OAc)_2$ /pyridine (red squares), and  $Pd(OAc)_2$ /**L2** (black circles) is shown in Figure 2.5. The initial rate with  $Pd(OAc)_2$ /**L2** is approximately 5 times faster than that with  $Pd(OAc)_2$ /pyridine and at least two orders of magnitude faster than that with  $Pd(OAc)_2$  alone. Furthermore, the  $Pd(OAc)_2$ /**L2**-catalyzed reaction proceeds to higher overall yield at completion than the analogous  $Pd(OAc)_2$ /pyridine system (71% versus 64%, respectively).

**Figure 2.5.** Time study comparing catalyst systems using  $K_2S_2O_8$

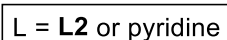
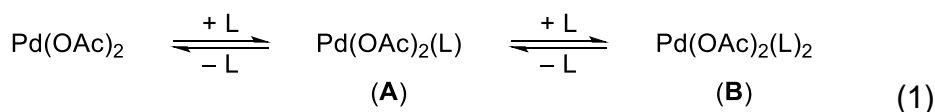


As noted in Figure 2.5, this C–H acetoxylation reaction proceeded to less than 75% yield in all cases (the yields are based on  $K_2S_2O_8$  as the limiting reagent). This is not due to over-oxidation of the benzene substrate. Under the standard conditions, <4% yield of diacetoxybenzene was observed. Instead, the observed yields are believed to be due to competing thermal decomposition of  $K_2S_2O_8$  in acetic acid: a well preceded process.<sup>13</sup> Increasing the reaction temperature to  $120\text{ }^\circ C$  appears to accelerate competing oxidant decomposition (Table 2.4). While the initial rate of C–H acetoxylation is significantly faster at  $120\text{ }^\circ C$  than at  $80\text{ }^\circ C$  (yield after 2 h was 24% versus 7%; Table 2.4, entries 3 and 1, respectively), the reaction proceeds to a maximum of only 44% yield at  $120\text{ }^\circ C$  (Table 2.4, entry 4). We attribute this to increased background decomposition of  $K_2S_2O_8$ .

**Table 2.4.** Effect of temperature on initial (t = 2 h) and final (t = 18 h) yield

Entry	Temperature (° C)	Time (h)	Yield PhOAc (%)
1	80	2	7
2	80	18	71
3	120	2	24
4	120	18	44

We next sought to obtain evidence on the origin of the improved catalytic activity. The combination of 1 equiv of pyridine or **L2** with 1 equiv of  $\text{Pd(OAc)}_2$  is expected to generate a number of equilibrating species in solution, including mono-pyridine complex **A** and bis-pyridine adduct **B** (eq. 1). We and others<sup>8c</sup> hypothesize that **A**, or a related acetate bridged dimer, is the primary active catalyst generated under these conditions.

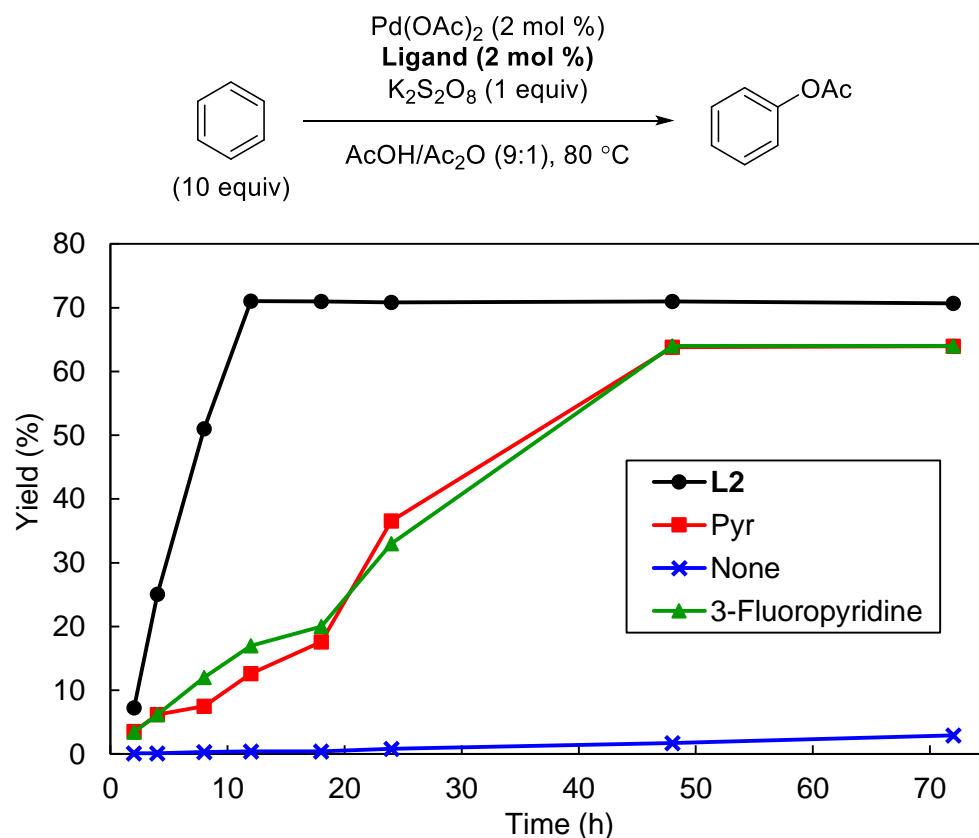


On the basis of this mechanistic framework, there are several possible factors that could contribute to the observed rate enhancement with cationic ligand **L2**. These include: (1) electronic effects (i.e., the electron withdrawing pyridinium substituent leads to a more electrophilic Pd catalyst **A** that is more reactive towards benzene C–H activation); (2) equilibrium effects (i.e., the large size and cationic charge of ligand **L2** result in an increased equilibrium population of the active mono-pyridine catalyst **A**); or (3) phase transfer effects (i.e., the cationic pyridine ligand serves as a phase transfer catalyst to bring poorly soluble  $[\text{S}_2\text{O}_8]^{2-}$  into solution and into contact with the Pd catalyst). Experiments designed to preliminarily test each of these possibilities are described in detail below.



*Electronic effects.* To test the role of electronic effects, we compared catalyst activity in the presence of **L2** to that with 3-fluoropyridine. The Hammett value for a *meta*-fluoro group is the same as that for a *meta*-pyridinium substituent ( $\rho = 0.34$  in both cases),<sup>14</sup> indicating that these ligands should have comparable electronic properties. As shown in Figure 2.6, the Pd(OAc)<sub>2</sub>/3-fluoropyridine catalyst system (green triangles) showed essentially identical reactivity to Pd(OAc)<sub>2</sub>/pyridine (red squares). In addition, the chemoselectivity with pyr and 3-fluoropyridine were both lower than with **L2** (PhOAc:PhPh ratio = 14:1, 20:1, and 36:1 respectively). These data suggest against a purely electronic effect.

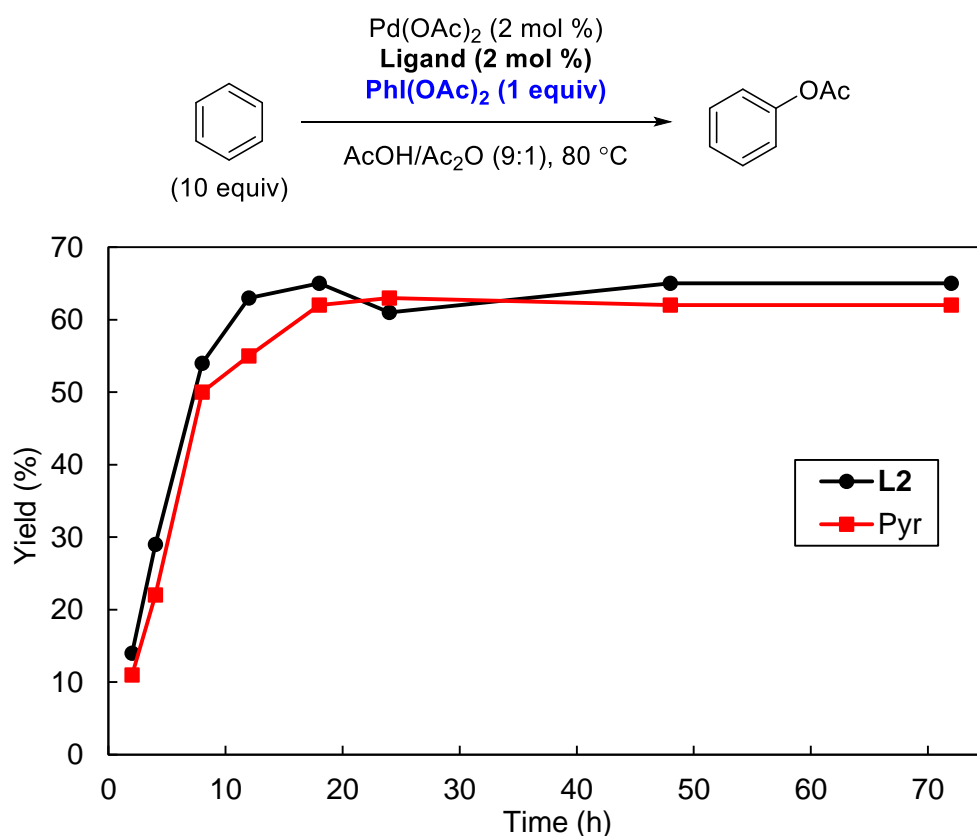
**Figure 2.6.** Time study comparing electronics of pyridine derivatives in the acetoxylation of benzene using K<sub>2</sub>S<sub>2</sub>O<sub>8</sub>



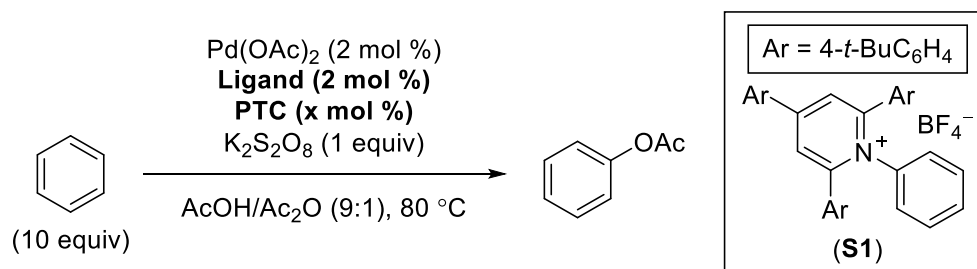
*Equilibrium effects.* If equilibrium effects were the main factor responsible for the enhanced reactivity of Pd(OAc)<sub>2</sub>/**L2**, this catalyst would be expected to outperform Pd(OAc)<sub>2</sub>/pyridine in other C–H oxidation reactions as well. To test this possibility, we compared the two catalysts using PhI(OAc)<sub>2</sub> as the oxidant under otherwise identical

conditions. As shown in Figure 2.7, with  $\text{PhI}(\text{OAc})_2$ , the pyridine (red squares) and pyridinium-derived (black circles) catalysts afforded nearly identical reaction rates. This suggests that the favorable effect of ligand **L2** does not transfer to other C–H oxidation reactions.

**Figure 2.7.** Time study comparing **L2** and pyridine as ligands using  $\text{PhI}(\text{OAc})_2$



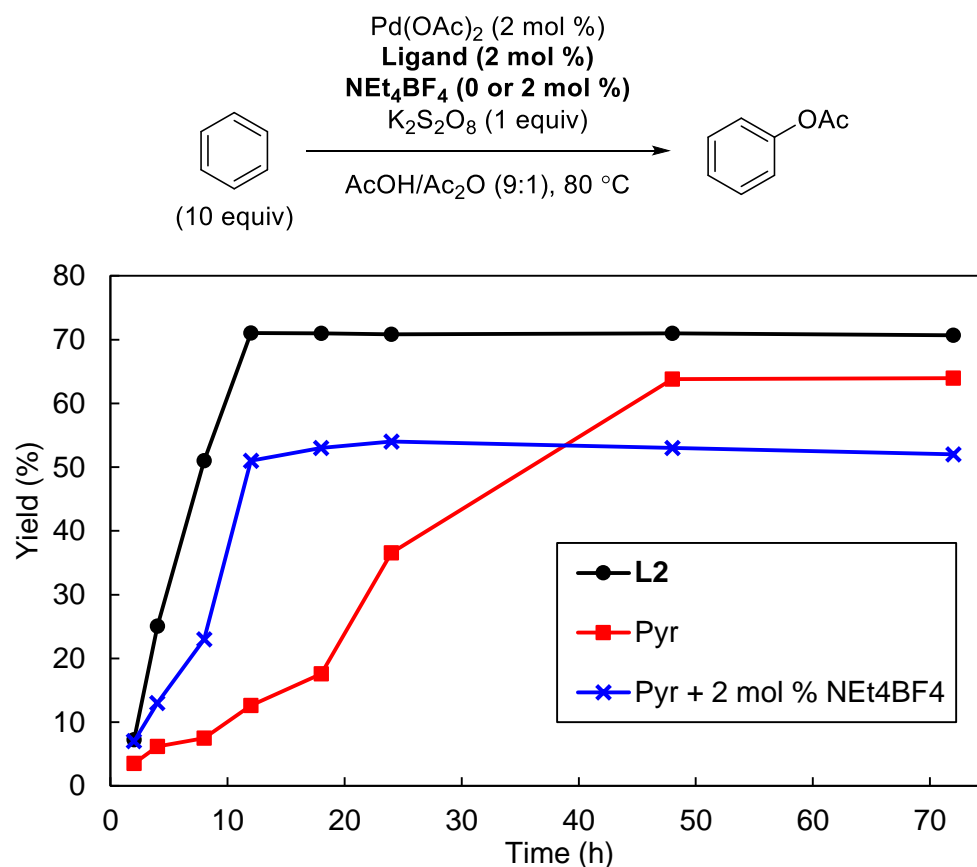
*Phase transfer effects.* To test the effect of phase transfer catalysts on this system, we examined a variety of phase transfer catalysts (PTCs) in conjunction with pyridine as the ligand using  $\text{K}_2\text{S}_2\text{O}_8$  as the oxidant (Table 2.5). We chose to record yields after 2 h to approximate the influence on the initial rate of the reaction in addition to the yield upon completion of the reaction for the highly active systems. As seen in entry 5 of Table 2.5,  $\text{NEt}_4\text{BF}_4$  at 15 mol % gave a good initial yield of 8.5% when used as a PTC in conjunction with pyridine as the ligand for Pd. An important control is shown in entry 3 in which the PTC **S1** has the same general structure of **L2** except it lacks the ability to act as a ligand; **S1** does indeed act as a PTC, giving an improved yield of 4.7% compared to the conditions lacking a PTC (3.5%, entry 2).

**Table 2.5.** PTCs tested in the acetoxylation of benzene using  $K_2S_2O_8$ 

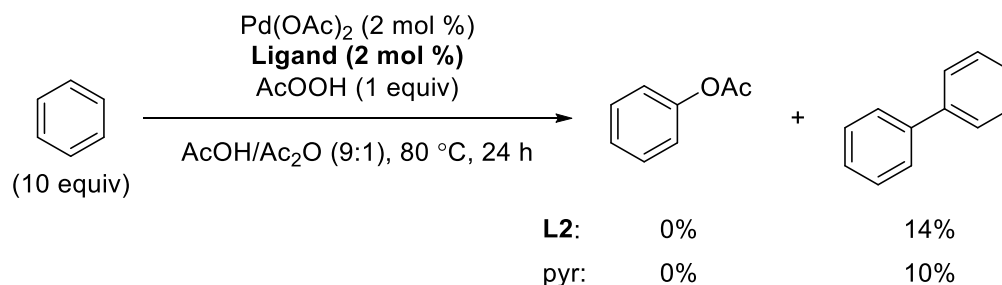
Entry	Ligand	PTC	Mol % PTC	Yield (%) 2 h	Yield (%) Reaction completion
1	<b>L2</b>	None	---	7.3	71 (12 h)
2	Pyr	None	---	3.5	64 (48 h)
3	Pyr	<b>S1</b>	2	4.7	60 (58 h)
4	Pyr	$NEt_4BF_4$	2	7.0	52 (12 h)
5	Pyr	$NEt_4BF_4$	15	8.5	42 (12 h)
6	Pyr	$NBu_4BF_4$	2	2.4	---
7	Pyr	$LiBF_4$	2	7.0	---
8	Pyr	$NH_4BF_4$	2	2.8	---
9	Pyr	$NBu_4PF_6$	2	3.8	---
10	Pyr	$NBu_4SO_3CF_3$	2	3.6	---
11	Pyr	18-crown-6	2	3.3	---

A more detailed study was undertaken by adding 2 mol % of  $NEt_4BF_4$  (a known phase transfer catalyst) to the  $Pd(OAc)_2$ /pyridine-catalyzed reaction. As shown in Figure 2.8, the  $NEt_4BF_4$  led to a significant acceleration of the initial reaction rate, very similar to that observed with **L2**. However, the overall yield was lower with  $Pd(OAc)_2$ /pyridine/ $NEt_4BF_4$  versus  $Pd(OAc)_2$ /**L2** (52% versus 71%). The lower overall yields observed in the presence of tetraalkylammonium salts are likely due to their well-precedented ability to catalyze the conversion of  $K_2S_2O_8$  to peracetic acid in  $AcOH$ .<sup>13b</sup> Importantly, peracetic acid is not a viable oxidant for the C–H acetoxylation transformation (Scheme 2.3), as no  $PhOAc$  was observed after 24 h using either **L2** or pyridine as the ligand; however, after 24 h, 14% and 10% yield of  $PhPh$  were obtained using **L2** and pyridine, respectively.

**Figure 2.8.** Time study demonstrating the initial rate enhancement of  $\text{NEt}_4\text{BF}_4$  as a PTC



**Scheme 2.3.** Testing the viability of peracetic acid as the oxidant



Overall, these results lead us to conclude that phase transfer catalysis is a key factor in the enhanced reaction rate with ligand **L2**. The differences in yield observed between **L2** and more conventional phase transfer catalysts like  $\text{NEt}_4\text{BF}_4$  may be due to differences in the rate of undesired  $\text{K}_2\text{S}_2\text{O}_8$  to  $\text{AcOOH}$  conversion between these systems. Notably, Neumann has proposed similar accelerative effects of interactions between cationic ligands and anionic oxidants in Pd/polyoxometallate-catalyzed Wacker oxidation reactions<sup>15</sup> and in Pt/polyoxometalate-catalyzed  $\text{CH}_4$  oxidation.<sup>16</sup>

## 2.3 CONCLUSIONS

In conclusion, this chapter describes two catalytic systems based on  $[\text{Pd}(\text{OAc})_2]$  and pyridine derivatives that show the highest reactivity reported to date for the acetoxylation of unactivated aromatic C–H bonds. In the  $\text{PhI}(\text{OAc})_2$  system, the ratio of palladium/pyridine proved critical and the use of ca. 1 equivalent of pyridine per palladium center led to dramatic enhancements in reactivity. These studies highlight the importance of exploring the ligand to metal ratio, along with the structure of spectator ligands, during the optimization of reaction conditions for catalytic C–H functionalization.

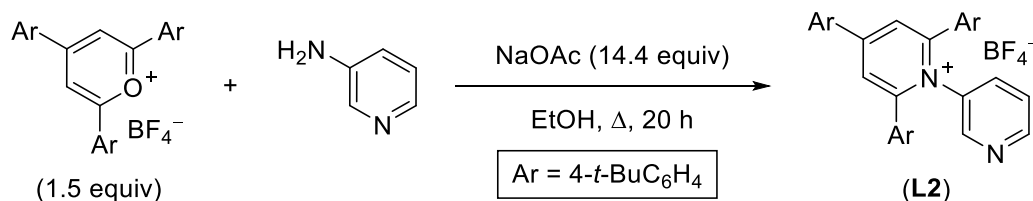
Additionally, this chapter describes the development of Pd catalysts containing pyridinium-substituted pyridine ligands for the C–H oxygenation of benzene with the economical oxidant potassium persulfate. These new catalyst systems provide significantly improved activity compared to  $\text{Pd}(\text{OAc})_2$  and the  $\text{Pd}(\text{OAc})_2/\text{pyridine}$  system in this transformation. Furthermore, the reaction proceeds with high selectivity for phenyl acetate over biphenyl. Preliminary mechanistic investigations suggest that a key role for the cationic ligand is to serve as a phase transfer catalyst to bring poorly soluble  $[\text{S}_2\text{O}_8]^{2-}$  into solution and into contact with the Pd catalyst. This represents one of an expanding number of examples suggesting that ionic association between ligands and oxidants can serve as a valuable design principle in oxidation catalysis.

## 2.4 PERSPECTIVE AND OUTLOOK

While the catalyst systems developed in this chapter for the acetoxylation of simple arenes using  $\text{PhI}(\text{OAc})_2$  and  $\text{K}_2\text{S}_2\text{O}_8$  mark a significant advancement in the area of C–H activation, there remain directions for improvement. The first is the limited overall yield of the acetoxyated products, which are maximized at about 75-80%. Developing milder conditions and catalysts that operate at lower temperatures will likely be the most fruitful in this regard, as oxidant decomposition is the yield-limiting factor. The second is the use of an acidic solvent, acetic acid. Moving towards polar aprotic solvents and solvent mixtures would be an appropriate direction to pursue.

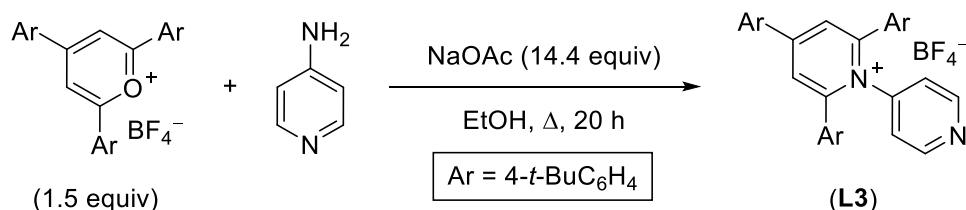
## 2.5 EXPERIMENTAL

### Synthesis of L2



2,4,6-Tri-(4-*t*-butylphenyl)pyrylium tetrafluoroborate (4.50 g, 7.97 mmol, 1.50 equiv), 3-aminopyridine (0.50 g, 5.3 mmol, 1.0 equiv), and sodium acetate (6.27 g, 76.4 mmol, 14.4 equiv) were combined in a 500 mL round bottomed flask. Absolute ethanol (200 mL) was added, and the reaction was heated at reflux under nitrogen for 20 h. The reaction was allowed to cool to room temperature, the volatiles were removed by rotary evaporation, and the residue was suspended in water (200 mL). The suspension was filtered and the resulting solids were washed with water (3 x 20 mL). The solid was dissolved in methylene chloride and dried over MgSO<sub>4</sub> and then concentrated under vacuum. The resulting residue was triturated with Et<sub>2</sub>O, resulting in a white solid that was collected by vacuum filtration. The product was obtained as a white solid (2.96 g, 87% yield).

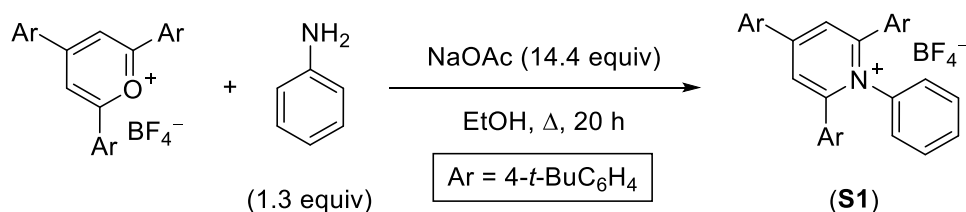
### Synthesis of L3



2,4,6-Tri-(4-*t*-butylphenyl)pyrylium tetrafluoroborate (9.00 g, 15.9 mmol, 1.50 equiv), 4-aminopyridine (1.00 g, 10.6 mmol, 1.00 equiv), and sodium acetate (12.6 g, 153 mmol, 14.4 equiv) were combined in a 1 L round bottomed flask. Absolute ethanol (400 mL) was added, and the reaction was heated at reflux under nitrogen for 20 h. The reaction was allowed to cool to room temperature, the volatiles were removed by rotary evaporation, and the residue was suspended in water (200 mL). The suspension was filtered and the resulting solids were washed with water (3 x 20 mL). The solids were dissolved in methylene chloride, and this solution was dried over MgSO<sub>4</sub> and then

concentrated under vacuum. The resulting residue was triturated with Et<sub>2</sub>O, resulting in a white solid that was collected by vacuum filtration. The product was obtained as a white solid (5.63 g, 83% yield).

### Synthesis of S1



2,4,6-Tri-(4-*t*-butylphenyl)pyrylium tetrafluoroborate (2.31 g, 4.09 mmol, 1.00 equiv), aniline (0.50 g, 5.37 mmol, 1.31 equiv), and sodium acetate (4.84 g, 59.0 mmol, 14.4 equiv) were combined in a 500 mL round bottomed flask. Absolute ethanol (200 mL) was added, and the reaction was heated at reflux under nitrogen for 20 h. The reaction was allowed to cool to room temperature, the volatiles were removed by rotary evaporation, and the residue was suspended in water (200 mL). The suspension was filtered and the resulting solids were washed with water (3 x 20 mL). The solids were then dissolved in methylene chloride and this solution was dried over MgSO<sub>4</sub> and then concentrated under vacuum. The resulting residue was triturated with Et<sub>2</sub>O, resulting in a white solid that was collected by vacuum filtration. The product was obtained as a white solid (0.640 g, 24% yield).

### General Procedure for the Acetoxylation of Arenes using no ligand or solid ligands (L2 or L3)

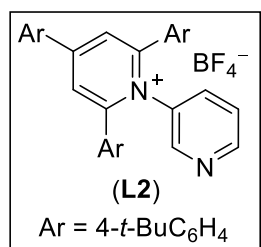
Solids were weighed into a 1-dram scintillation vial equipped with a stirbar, followed by addition of the liquid reagents. The vial was then sealed and allowed to heat to 100 °C or 80 °C using a preheated hotplate. At the end of the reaction, the vial was allowed to cool to room temperature and a known amount of phenyl chloride or neopentylbenzene (measured by difference using a gas-tight Hamilton syringe) was added as an internal standard for quantitative GC analysis. The mixture was diluted with EtOAc (2 mL) and filtered through a plug of celite. The filtrate was extracted with a saturated, aqueous solution of K<sub>2</sub>CO<sub>3</sub> (9 M in deionized H<sub>2</sub>O) to quench and separate the acid. The organic layer was carefully separated and diluted with additional EtOAc to a total volume of 20

mL. The resulting solution was analyzed by GC. Yields are reported as an average of at least two runs.

### General Procedure for the Acetoxylation of Arenes using liquid ligands (pyridine, 3-fluoropyridine, 2-picoline, 2,6-lutidine, 2,6-di-*tert*-butylpyridine)

Solids were weighed into a 1-dram scintillation vial equipped with a stirbar. The pyridine derivative was added as a stock solution in AcOH, followed by addition of the remaining liquid reagents. The vial was then sealed and heated to 100 °C or 80 °C using a preheated hotplate. At the end of the reaction, the vial was cooled to room temperature and a known amount of phenyl chloride or neopentylbenzene (measured by difference using a gas-tight Hamilton syringe) was added as an internal standard for quantitative GC analysis. The mixture was diluted with EtOAc (2 mL) and filtered through a plug of celite. The filtrate was extracted with a saturated, aqueous solution of K<sub>2</sub>CO<sub>3</sub> (9 M in deionized H<sub>2</sub>O) to quench and separate the acid. The organic layer was carefully separated and diluted with additional EtOAc to a total volume of 20 mL. The resulting solution was analyzed by GC. Yields are reported as an average of at least two runs.

## 2.6 CHARACTERIZATION



<sup>1</sup>H NMR (CDCl<sub>3</sub>, 500.099 MHz): 8.35 (dd, J = 4.8 Hz, J = 2.1 Hz, 1H), 8.24 (d, J = 2.1 Hz, 1H), 8.08 (s, 2H), 8.02 (m, 1H), 7.81 (d, J = 8.4 Hz, 2H), 7.55 (d, J = 8.4 Hz, 2H), 7.28-7.34 (multiple peaks, 8H), 7.13 (dd, J = 8.0 Hz, J = 4.8 Hz, 1H), 1.35 (s, 9H), 1.22 (s, 18H).

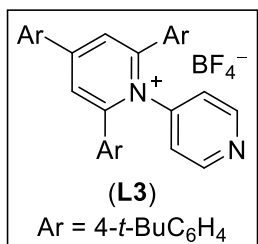
<sup>13</sup>C NMR (CDCl<sub>3</sub>, 125.762 MHz): 157.5, 156.8, 156.3, 153.8, 150.2, 147.8, 137.2, 136.6, 131.4, 129.7, 129.5, 128.2, 126.7, 125.6, 125.5, 123.7, 35.0, 34.8, 31.0, 31.0.

<sup>19</sup>F NMR (CDCl<sub>3</sub>, 470.520 MHz): -150.3 (<sup>10</sup>B), -150.4 (<sup>11</sup>B).

HRMS electrospray (m/z): [M-BF<sub>4</sub>]<sup>+</sup> calcd for [C<sub>40</sub>H<sub>45</sub>N<sub>2</sub>]<sup>+</sup> 553.3577; found 553.3574.

Anal. calcd for C<sub>40</sub>H<sub>45</sub>N<sub>2</sub>BF<sub>4</sub>: C, 75.00; H, 7.08; N, 4.37. Found: C, 74.45; H, 7.09; N, 4.38.





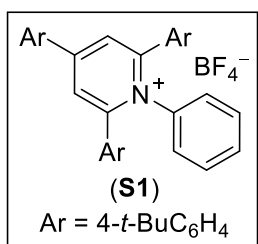
<sup>1</sup>H NMR (CD<sub>3</sub>CN, 500.099 MHz): 8.39 (d, J = 5.8 Hz, 2H), 8.35 (s, 2H), 8.06 (d, J = 8.5 Hz, 2H), 7.69 (d, J = 8.5 Hz, 2H), 7.40 (d, J = 8.3 Hz, 4H), 7.31 (d, J = 8.3 Hz, 4H), 7.23 (d, J = 5.8 Hz, 2H), 1.38 (s, 9H), 1.25 (s, 18H).

<sup>13</sup>C NMR (CDCl<sub>3</sub>, 125.762 MHz): 157.6, 156.2, 156.0, 154.0, 150.7, 146.5, 131.5, 129.6, 129.5, 128.2, 126.7, 125.7, 125.5, 123.4, 35.1, 34.8, 31.1, 31.0.

<sup>19</sup>F NMR (CD<sub>3</sub>CN, 470.520 MHz): -150.3 (<sup>10</sup>B), -150.4 (<sup>11</sup>B).

HRMS electrospray (m/z): [M-BF<sub>4</sub>]<sup>+</sup> calcd for [C<sub>40</sub>H<sub>45</sub>N<sub>2</sub>]<sup>+</sup> 553.3577; found 553.3581.

Anal. calcd for C<sub>40</sub>H<sub>45</sub>N<sub>2</sub>BF<sub>4</sub>: C, 75.00; H, 7.08; N, 4.37. Found: C, 74.55; H, 7.16; N, 4.37.



<sup>1</sup>H NMR (CD<sub>3</sub>CN, 500.099 MHz): 8.31 (s, 2H), 8.05 (d, J = 8.4 Hz, 2H), 7.68 (d, J = 8.4 Hz, 2H), 7.36 (d, J = 8.3 Hz, 4H), 7.27 (d, J = 8.3 Hz, 4H), 7.21 (multiple peaks, 3H), 7.17 (m, 2H), 1.37 (s, 9H), 1.23 (s, 18H).

<sup>13</sup>C NMR (CD<sub>3</sub>CN, 125.762 MHz): 157.6, 157.5, 157.0, 154.5, 140.0, 131.7, 131.2, 130.7, 130.4, 129.6, 129.4, 129.3, 127.7, 126.2, 126.1, 35.7, 35.3, 31.1 (this resonance comprises 2 signals).

<sup>19</sup>F NMR (CD<sub>3</sub>CN, 470.520 MHz): -151.8 (<sup>10</sup>B), -151.9 (<sup>11</sup>B).

HRMS electrospray (m/z): [M-BF<sub>4</sub>]<sup>+</sup> calcd. for [C<sub>41</sub>H<sub>46</sub>N]<sup>+</sup> 552.3626; found 552.3636.

## 2.7 REFERENCES

- (1) Adapted with permission from (a) Emmert, M. H.; Cook, A. K.; Xie, Y. J.; Sanford, M. *Angew. Chem., Int. Ed.* **2011**, *50*, 9409. © 2011 WILEY-VCH Verlag GmbH & Co. KGaA, Weinheim. (b) Gary, J. B.; Cook, A. K.; Sanford, M. S. *ACS Catalysis* **2013**, *3*, 700. © American Chemical Society.
- (2) (a) Lyons, T. W.; Sanford, M. S. *Chem. Rev.* **2010**, *110*, 1147. (b) Muniz, K. *Angew. Chem., Int. Ed.* **2009**, *48*, 9412. (c) Sehnal, P.; Taylor, R. J. K.; Fairlamb, I. J. S. *Chem. Rev.* **2010**, *110*, 824.
- (3) (a) Alonso, D. A.; Najera, C.; Pastor, I. M.; Yus, M. *Chem. Eur. J.* **2010**, *16*, 5274. (b) Tsuji, J. *Synthesis* **1990**, 739. (c) Kuhl, N.; Hopkinson, M. N.; Wencel-Delord, J.; Glorius, F. *Angew. Chem., Int. Ed.* **2012**, *51*, 10236. (d) Choy, P. Y.; Lau, C. P.; Kwong, F. Y. *J. Org. Chem.* **2011**, *76*, 80. (e) Mutule, I.; Suna, E.; Olofsson, K.; Peleman, B. *J. Org. Chem.* **2009**, *74*, 7195. (f) Wang, G.-W.; Yuan, T.-T.; Wu, X.-L. *J. Org. Chem.* **2008**, *73*, 4717. (g) Yoneyama, T.; Crabtree, R. H. *J. Mol. Catal. A* **1996**, *108*, 35. (h) Davidson, J. M.; Triggs, C. *Chemistry & Industry* **1966**, 457. (i) Henry, P. M. *J. Org. Chem.* **1971**, *36*, 1886. (j) Jintoku, T.; Takaki, K.; Fujiwara, Y.; Fuchita, Y.; Hiraki, K. *B. Chem. Soc. Jpn.* **1990**, *63*, 438. (k) Jintoku, T.; Taniguchi, H.; Fujiwara, Y. *Chem. Lett.* **1987**, 1865. (l) Muehlhofer, M.; Strassner, T.; Herrmann, W. A. *Angew. Chem., Int. Ed.* **2002**, *41*, 1745. (m) Shibahara, F.; Kinoshita, S.; Nozaki, K. *Org. Lett.* **2004**, *6*, 2437. (n) Stock, L. M.; Tse, K.; Vorvick, L. J.; Walstrum,

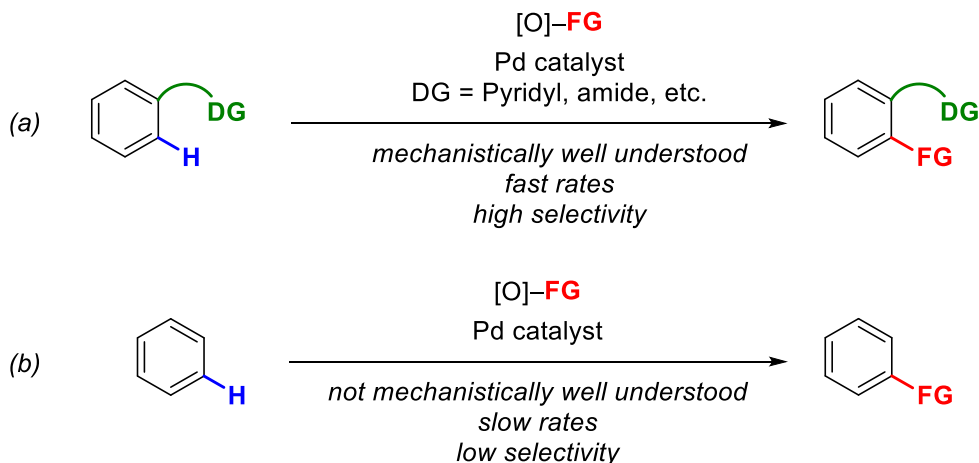
- S. A. *J. Org. Chem.* **1981**, *46*, 1757. (o) Burton, H. A.; Kozhevnikov, I. V. *J. Mol. Catal. A* **2002**, *185*, 285. (p) Liu, Y.; Murata, K.; Inaba, M. *J. Mol. Catal. A* **2006**, *256*, 247. (q) Ebersson, L.; Jonsson, E. *Acta Chem. Scand. B* **1974**, *28*, 771. (r) Ebersson, L.; Jonsson, L. *J. Chem. Soc., Chem. Comm.* **1974**, 885. (s) Ebersson, L.; Jonsson, L. *Acta Chem. Scand. B* **1976**, *30*, 361. (t) Ebersson, L.; Jonsson, L. *Justus Liebigs Annal. Chem.* **1977**, 233. (u) Deprez, N. R.; Kalyani, D.; Krause, A.; Sanford, M. S. *J. Am. Chem. Soc.* **2006**, *128*, 4972. (v) Emmert, M. H.; Gary, J. B.; Villalobos, J. M.; Sanford, M. S. *Angew. Chem., Int. Ed.* **2010**, *49*, 5884. (w) Hickman, A. J.; Sanford, M. S. *ACS Catalysis* **2011**, *1*, 170. (x) Lyons, T. W.; Hull, K. L.; Sanford, M. S. *J. Am. Chem. Soc.* **2011**, *133*, 4455.
- (4) Passoni, L. C.; Cruz, A. T.; Buffon, R.; Schuchardt, U. *J. Mol. Catal. A* **1997**, *120*, 117.
- (5) Price is calculated based upon the price of the largest quantity sold by Sigma Aldrich in July, 2015. PhI(OAc)<sub>2</sub> (100 g for \$141 or \$454 per mol).
- (6) Price is calculated based upon the price of the largest quantity of K<sub>2</sub>S<sub>2</sub>O<sub>8</sub> sold by Sigma Aldrich in July, 2015: 500 g for \$74 or \$40 per mol.
- (7) Desai, L. V.; Malik, H. A.; Sanford, M. S. *Org. Lett.* **2006**, *8*, 1141.
- (8) (a) Izawa, Y.; Stahl, S. S. *Adv. Synth. Catal.* **2010**, *352*, 3223. (b) Wang, C.; Rakshit, S.; Glorius, F. *J. Am. Chem. Soc.* **2010**, *132*, 14006. (c) Zhang, Y.-H.; Shi, B.-F.; Yu, J.-Q. *J. Am. Chem. Soc.* **2009**, *131*, 5072.
- (9) (a) Ferreira, E. M.; Stoltz, B. M. *J. Am. Chem. Soc.* **2003**, *125*, 9578. (b) Mikami, K.; Hatano, M.; Terada, M. *Chem. Lett.* **1999**, 55. (c) Stuart, D. R.; Fagnou, K. *Science* **2007**, *316*, 1172.
- (10) (a) Popp, B. V.; Stahl, S. S. *Chem. Eur. J.* **2009**, *15*, 2915. (b) Schultz, M. J.; Adler, R. S.; Zierkiewicz, W.; Privalov, T.; Sigman, M. S. *J. Am. Chem. Soc.* **2005**, *127*, 8499. (c) Steinhoff, B. A.; Guzei, I. A.; Stahl, S. S. *J. Am. Chem. Soc.* **2004**, *126*, 11268. (d) Steinhoff, B. A.; Stahl, S. S. *Org. Lett.* **2002**, *4*, 4179. (e) Trend, R. M.; Ramtohul, Y. K.; Stoltz, B. M. *J. Am. Chem. Soc.* **2005**, *127*, 17778. (f) Ye, X.; Liu, G.; Popp, B. V.; Stahl, S. S. *J. Org. Chem.* **2011**, *76*, 1031.
- (11) Zhdankin, V. V.; Stang, P. J. *Chem. Rev.* **2008**, *108*, 5299.
- (12) Leffler, J. E.; Story, L. J. *J. Am. Chem. Soc.* **1967**, *89*, 2333.
- (13) (a) Kholdeeva, O. A.; Kozhevnikov, I. V.; Sidel'nikov, V. N.; Utkin, V. A. *Russ. Chem. Bull.* **1989**, *38*, 1903. (b) Pande, C. S.; Jain, N. *Synth. Commun.* **1988**, *18*, 2123. (c) Santos, A. M.; Vindevoghel, P.; Graillat, C.; Guyot, A.; Guillot, J. *J Polym. Sci. Pol. Chem.* **1996**, *34*, 1271.
- (14) Hansch, C.; Leo, A.; Taft, R. W. *Chem. Rev.* **1991**, *91*, 165.
- (15) Etedgui, J.; Neumann, R. *J. Am. Chem. Soc.* **2009**, *131*, 4.
- (16) (a) Bar-Nahum, I.; Khenkin, A. M.; Neumann, R. *J. Am. Chem. Soc.* **2004**, *126*, 10236. (b) Etedgui, J.; Diskin-Posner, Y.; Weiner, L.; Neumann, R. *J. Am. Chem. Soc.* **2011**, *133*, 188.

# CHAPTER 3. ON THE MECHANISM OF THE PALLADIUM-CATALYZED ARENE C–H ACETOXYLATION: A COMPARISON OF CATALYSTS AND LIGAND EFFECTS<sup>1</sup>

## 3.1 INTRODUCTION

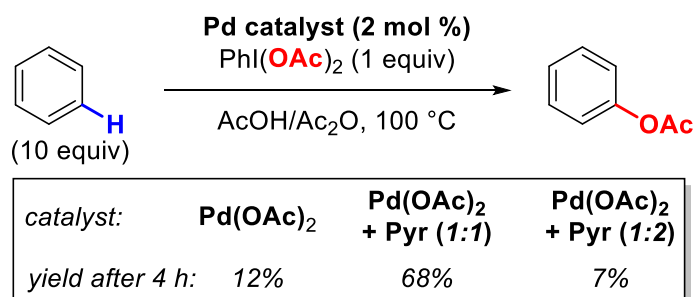
Over the past 15 years, there have been major advances in the field of Pd-catalyzed C–H functionalization.<sup>2</sup> Palladium catalysis enables the introduction of a diverse array of functional groups, often in the context of complex organic molecules.<sup>3</sup> However, the vast majority of synthetic<sup>2,3</sup> and mechanistic<sup>4</sup> efforts in this area have focused on substrates bearing directing groups (DG). These directing groups render the reactions kinetically fast as well as highly site-selective for C–H functionalization proximal to the DG (Scheme 3.1a).<sup>4p,5</sup> In contrast, analogous non-directed Pd-catalyzed C–H functionalization processes have been much less developed in terms of both synthetic applications<sup>6</sup> and mechanistic analysis<sup>4f,7</sup> (Scheme 3.1b). The identification of efficient and selective catalysts for non-directed C–H functionalization is of particular importance,<sup>8</sup> because many synthetic targets do not contain directing groups.

**Scheme 3.1.** Comparison of directed and non-directed C–H functionalization



Over the past several years, our group has focused on developing Pd catalysts for the non-directed C–H acetoxylation of arenes.<sup>9</sup> The Pd-catalyzed C–H acetoxylation of benzene was originally reported in the 1970's using simple Pd salts and oxidants such as  $K_2Cr_2O_7$  and  $K_2S_2O_8$ .<sup>10,11,12</sup> While these early studies provided proof-of-principle for the feasibility of this transformation, the catalyst turnover numbers were too low for practical utility (typically ranging between <1 and 7 turnovers). In 1996, Crabtree reported that the combination of  $Pd(OAc)_2$  (**1**) as the catalyst and  $PhI(OAc)_2$  as the oxidant afforded dramatically improved results, with up to 127 turnovers in the C–H acetoxylation of naphthalene.<sup>13</sup> More recently, our group has demonstrated that the rate and TON of Crabtree's reaction can be increased dramatically through the use of pyridine (pyr) as a supporting ligand.<sup>9c</sup> The ratio of  $Pd(OAc)_2$  to pyridine was critical in this system, with a 1:1 ratio proving optimal. This second generation catalyst system provided an approximately 10-fold increase in reaction rate versus  $Pd(OAc)_2$ , and TONs of >4500 were achieved (Scheme 3.2). In addition, the site selectivity of this transformation could be tuned through modification of the pyridine ligand.<sup>9a</sup> Despite these advances, the mechanistic role of the pyridine ligand remains poorly understood. Notably, similar pyridine effects have been observed in related Pd-catalyzed C–H functionalization<sup>14</sup> and oxidation reactions,<sup>15</sup> underscoring the significance of mechanistic understanding of ligand effects in these transformations.

**Scheme 3.2.** Pyridine ligand effects in the Pd-catalyzed C–H acetoxylation of benzene



This chapter describes a detailed mechanistic investigation focused on elucidating the impact of pyridine ligands on Pd-catalyzed benzene C–H acetoxylation. We compare three catalyst systems,  $Pd(OAc)_2$ ,  $Pd(OAc)_2$ /pyridine (1:1), and  $Pd(OAc)_2$ /pyridine (1:2), using a combination of mechanistic tools, including rate and order studies, Hammett analysis, detailed characterization of catalyst resting states, and isotope effects. These

investigations provide insights into the similarities and differences between the three catalyst systems that explain their dramatically different reactivities.

## 3.2 RESULTS AND DISCUSSION

**Mechanistic Investigation of the Pd(OAc)<sub>2</sub>-Catalyzed C–H Acetoxylation of Benzene.** We first assessed the order in Pd for the Pd(OAc)<sub>2</sub> catalyst system. In Crabtree's original study, a half order kinetic dependence on Pd was observed.<sup>13a</sup> This result was rationalized based on a resting state dimer, [Pd(OAc)<sub>2</sub>]<sub>2</sub> (**1a**), that breaks up into monomeric Pd(OAc)<sub>2</sub> (**1b**) to effect catalysis. However, the conditions developed in our lab are somewhat different than those reported by Crabtree (e.g., different concentration of benzene, different solvent system). Thus, we needed to establish whether the same kinetic dependence on Pd is observed in our system.

The method of initial rates was used to determine the rate of product formation as a function of Pd concentration over a concentration range of 0.28-56 mM. The reactions were monitored using GC-FID and were run to approximately 10% conversion. Hexafluorobenzene was employed as a co-solvent in order to mitigate changes in the polarity of the reaction medium upon varying the concentration of benzene (during benzene order studies, *vide infra*). Under our reaction conditions, the Pd(OAc)<sub>2</sub>-catalyzed C–H acetoxylation of benzene showed a half order dependence on Pd ( $0.49 \pm 0.06$ ), analogous to that observed by Crabtree (Figure 3.1). This is consistent with the Pd resting as a dimer in our system.

To further probe the impact of Pd aggregation state, we examined the kinetic order in Pd using Pd(OTFA)<sub>2</sub> (OTFA = trifluoroacetate) as the catalyst. In contrast to Pd(OAc)<sub>2</sub>, Pd(OTFA)<sub>2</sub> is known to exist as a monomer in organic solvents.<sup>16</sup> Thus, we predicted that a first order dependence on [Pd] should be observed with this catalyst. Indeed, under otherwise analogous conditions, the Pd(OTFA)<sub>2</sub>-catalyzed C–H acetoxylation of benzene was first order in [Pd] ( $1.0 \pm 0.1$ ; Figure 3.2). Notably, at 5.6 mM [Pd], the rate of C–H acetoxylation using Pd(OTFA)<sub>2</sub> is almost 4-times faster than with Pd(OAc)<sub>2</sub> ( $\Delta[\text{PhOAc}]/\Delta t = 6.5 \text{ mM/h}$  for Pd(OTFA)<sub>2</sub> and  $\Delta[\text{PhOAc}]/\Delta t = 1.7 \text{ mM/h}$  for Pd(OAc)<sub>2</sub>).

**Figure 3.1.** Order in Pd(OAc)<sub>2</sub>

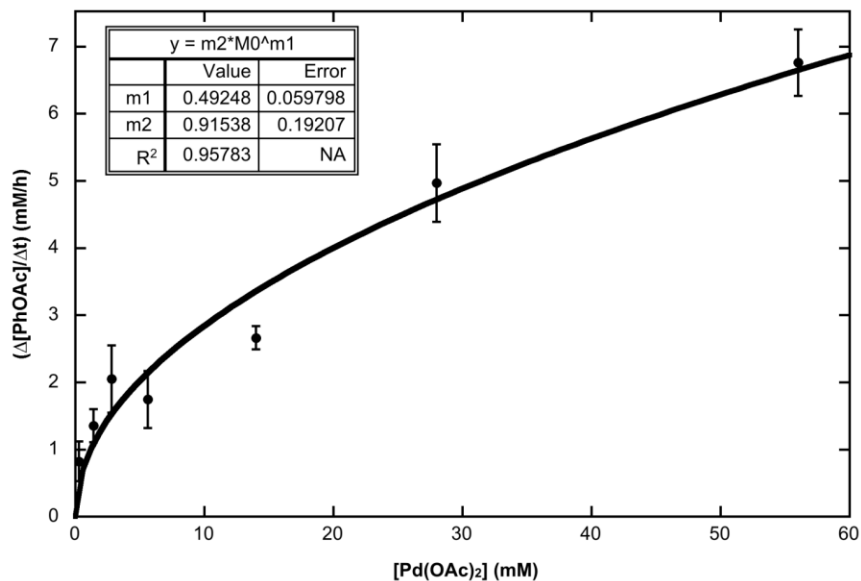
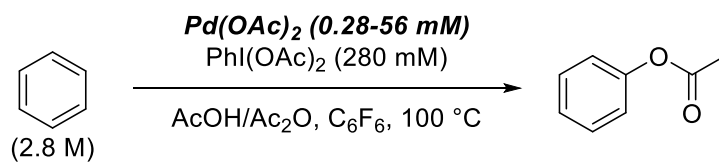
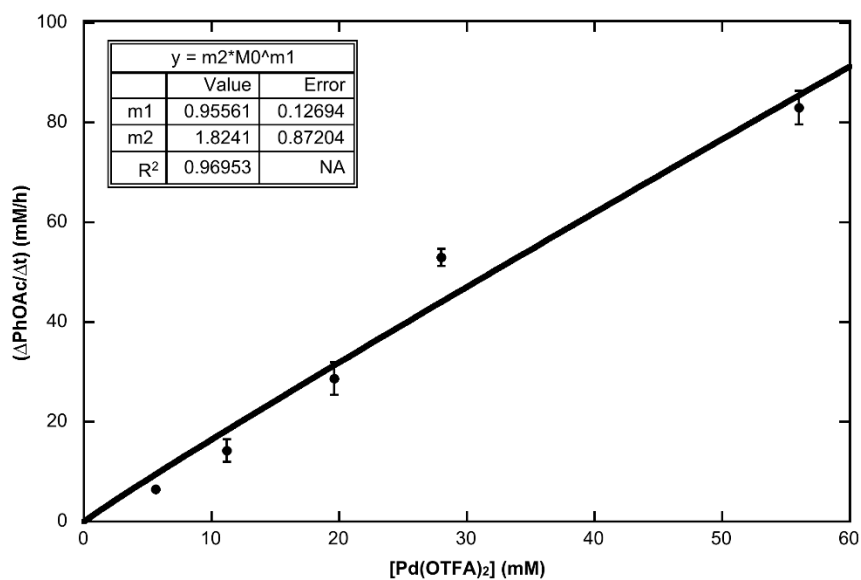
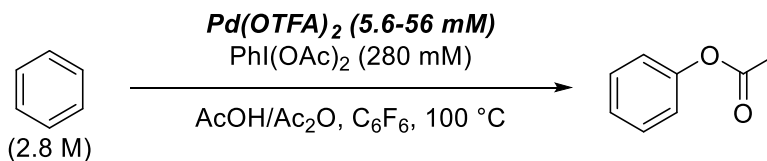
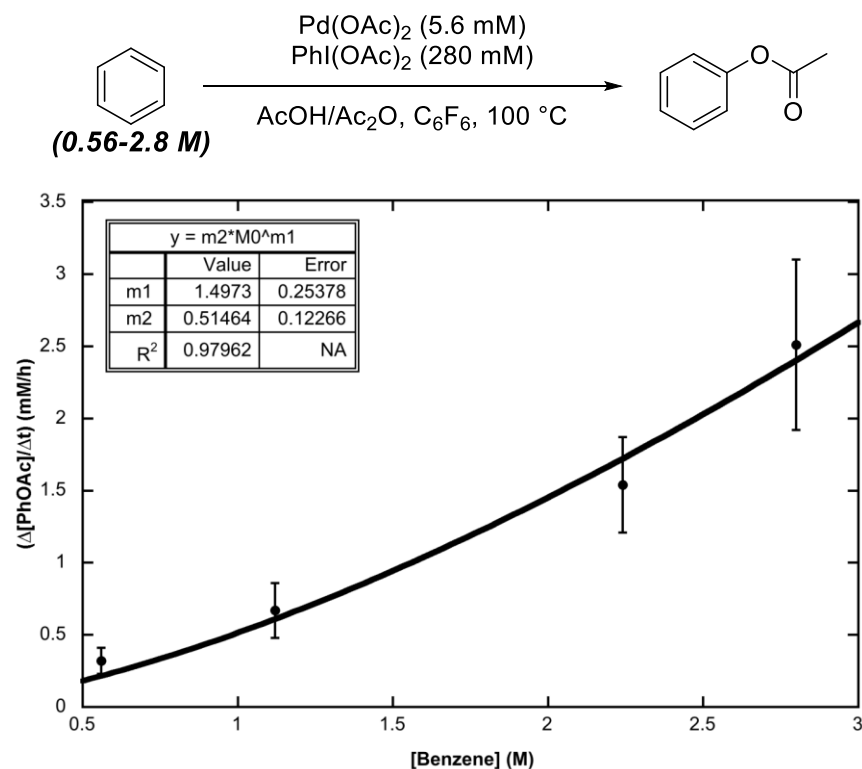


**Figure 3.2.** Order in Pd(OTFA)<sub>2</sub>



We next assessed the kinetic order of the Pd(OAc)<sub>2</sub>-catalyzed reaction in benzene and PhI(OAc)<sub>2</sub>. The order in benzene was determined by varying the concentration of benzene from 0.56-2.8 M. Hexafluorobenzene was used as a co-solvent, and the sum of the volumes of C<sub>6</sub>H<sub>6</sub> and C<sub>6</sub>F<sub>6</sub> was held constant during these experiments in order to minimize solvent effects on the observed rates. The order in PhI(OAc)<sub>2</sub> was determined by varying the concentration of PhI(OAc)<sub>2</sub> from 140-840 mM. Under these conditions, the reaction is approximately first order in benzene (1.5 ± 0.3) and zero order (0.1 ± 0.1) in PhI(OAc)<sub>2</sub> (Figure 3.3 and Figure 3.4).

**Figure 3.3.** Order in benzene using Pd(OAc)<sub>2</sub> as the catalyst



Finally, the kinetic isotope effect was determined by comparing the initial reaction rate with C<sub>6</sub>H<sub>6</sub> to that with C<sub>6</sub>D<sub>6</sub>. A KIE ( $k_{\text{H}}/k_{\text{D}}$ ) of  $4.5 \pm 0.4$  was obtained from these experiments (Figure 3.5). This value is similar to that observed under Crabtree's conditions ( $k_{\text{H}}/k_{\text{D}} = 4.1$ )<sup>13a</sup> and is consistent with a 1<sup>o</sup> isotope effect.<sup>17</sup>

**Figure 3.4.** Order in  $\text{PhI}(\text{OAc})_2$  using  $\text{Pd}(\text{OAc})_2$  as the catalyst

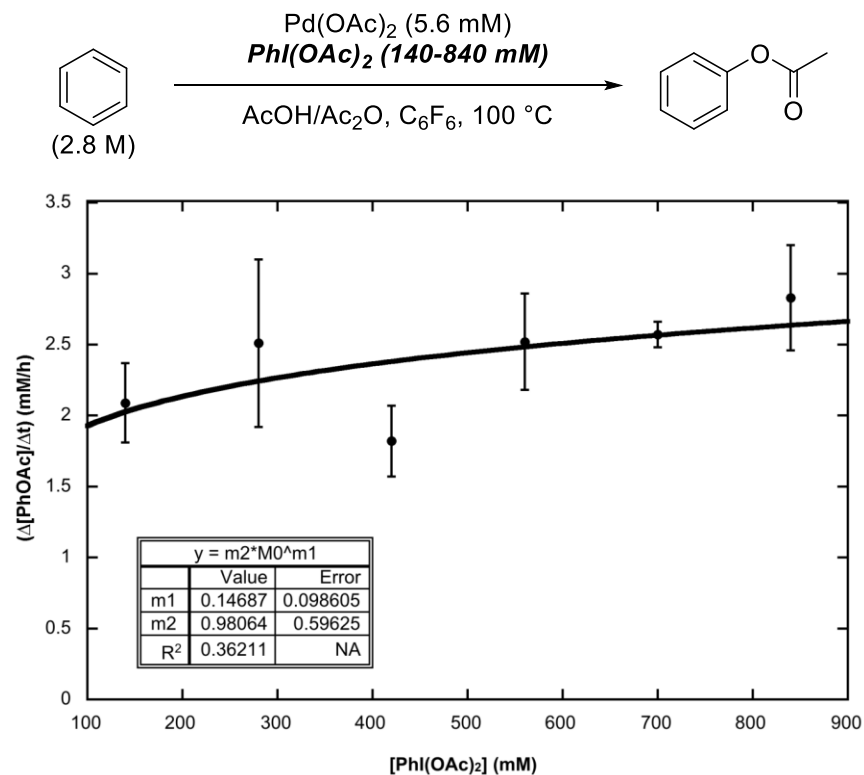
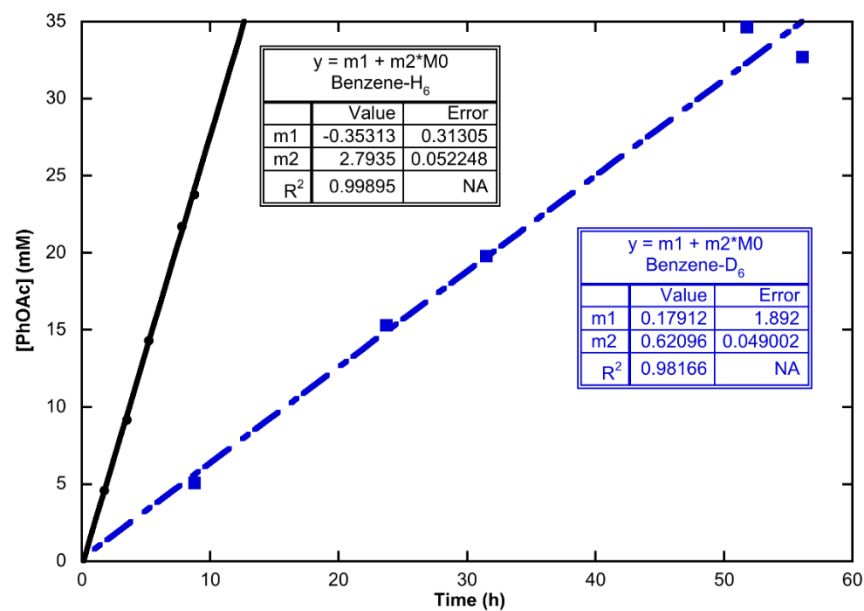


**Figure 3.5.** H/D kinetic isotope effect for benzene using  $\text{Pd}(\text{OAc})_2$  as the catalyst

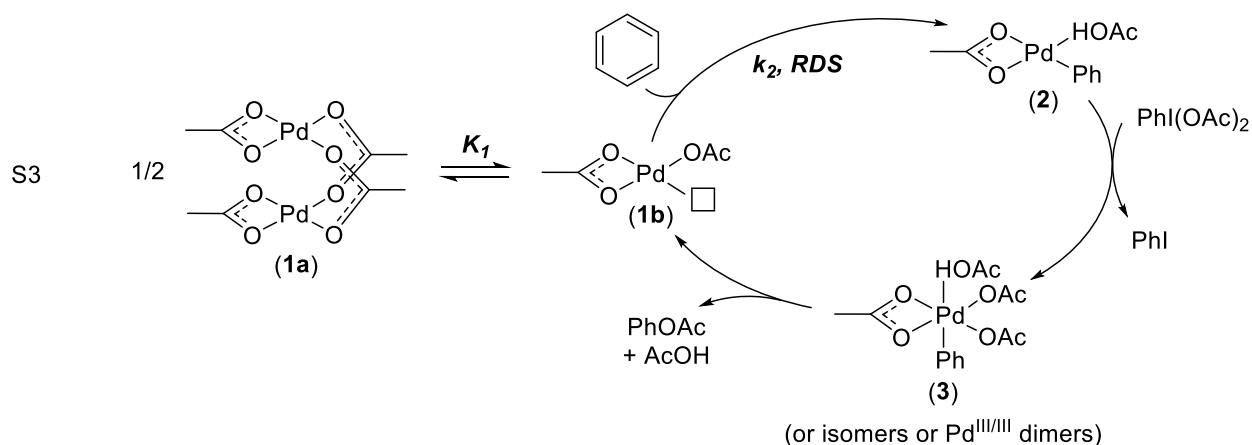


On the basis of all of the data presented above, we propose the catalytic cycle in Scheme 3.3 for the  $\text{Pd}(\text{OAc})_2$ -catalyzed C–H acetoxylation of benzene. The mechanism



begins with a dimeric Pd<sup>II</sup> precatalyst, [Pd(OAc)<sub>2</sub>]<sub>2</sub> (**1a**) as the resting state. Complex **1a** undergoes reversible dissociation into the monomer **1b**, which lies on the catalytic cycle. C–H activation of benzene at **1b** is the rate-determining step (RDS) and forms the Pd<sup>II</sup>-aryl intermediate **2**. This complex is then oxidized by PhI(OAc)<sub>2</sub> to form a high-valent Pd intermediate **3**, which undergoes reductive elimination to release PhOAc<sup>18</sup> and regenerate **1b**.

**Scheme 3.3.** Proposed mechanism of the Pd(OAc)<sub>2</sub>-catalyzed C–H acetoxylation of benzene



The rate expression for this mechanism can be derived as shown below in eqs. 1-3. This rate expression is fully consistent with the experimental data, as it predicts a half order dependence on Pd, a first order dependence on benzene, and a zero order dependence on PhI(OAc)<sub>2</sub>. Additionally, since C–H activation is the rate-determining step, a 1<sup>o</sup> kinetic isotope effect is expected.

$$\text{Rate} = \frac{d(\text{PhOAc})}{dt} = k_2[\mathbf{1b}][\text{benzene}] \quad (1)$$

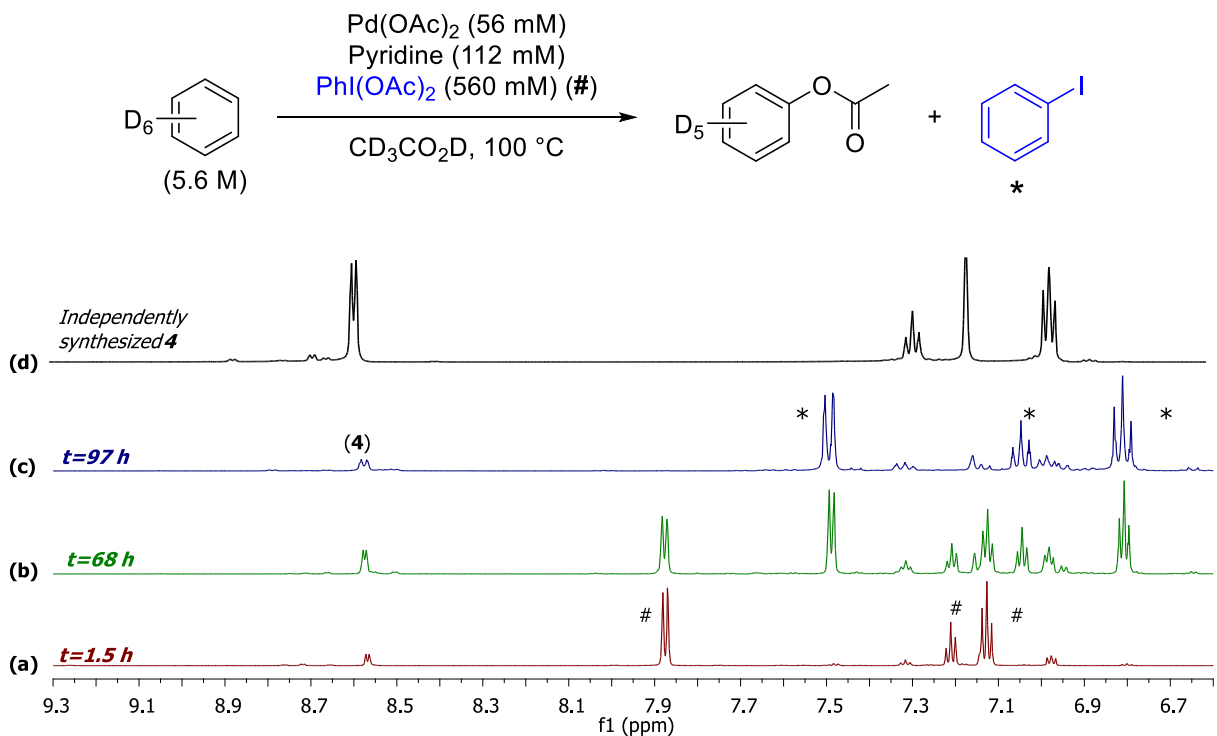
$$K_1 = \frac{[\mathbf{1b}]}{[\mathbf{1a}]^{1/2}} \quad (2)$$

$$\text{Rate} = K_1 k_2 [\mathbf{1a}]^{1/2} [\text{benzene}] \quad (3)$$

**Mechanistic Investigation of the Pd(OAc)<sub>2</sub>/Pyr (1:2)-Catalyzed C–H Acetoxylation of Benzene.** We next studied the catalyst generated upon combining a 1:2 ratio of Pd(OAc)<sub>2</sub> to pyridine (pyr). To assess the resting state of Pd during catalysis, the reaction was monitored by <sup>1</sup>H NMR spectroscopy. The only Pd species observed at

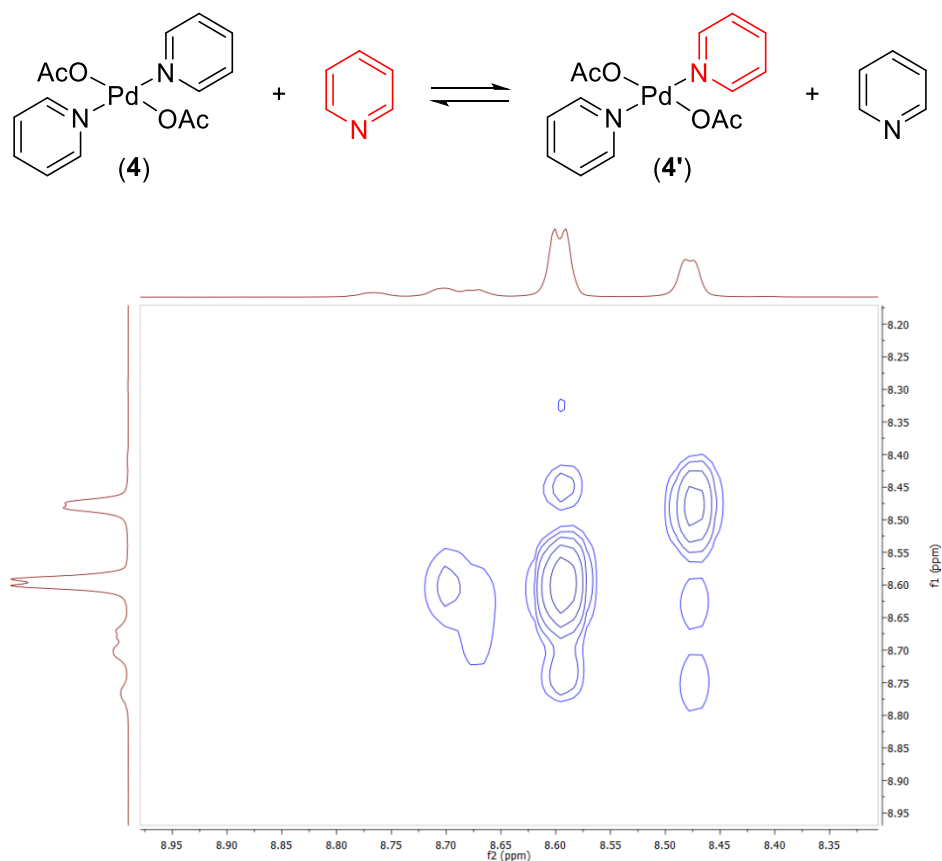
the beginning (Figure 3.6a), middle (Figure 3.6b), and end (Figure 3.6c) of the C–H acetoxylation reaction is  $(\text{pyr})_2\text{Pd}(\text{OAc})_2$  (**4**). The identity of **4** was verified via independent synthesis of this complex (Figure 3.6d).<sup>19</sup> These data implicate monomeric complex **4** as the catalyst resting state in this system.

**Figure 3.6.** C–H acetoxylation of benzene monitored by  $^1\text{H}$  NMR spectroscopy (aromatic region shown) using  $\text{Pd}(\text{OAc})_2/\text{pyr}$  (1:2) as catalyst



The lability of the pyridine ligands in complex **4** was assessed using Rotating Frame Nuclear Overhauser Effect NMR Spectroscopy (ROESY). As shown in Figure 3.7, exchange between free and bound pyridine is observed at  $80\text{ }^\circ\text{C}$  ( $20\text{ }^\circ\text{C}$  below the temperature used for catalytic C–H acetoxylation). This demonstrates the feasibility of pyridine ligand dissociation/exchange during catalysis.

**Figure 3.7.**  $^1\text{H}$ - $^1\text{H}$  ROESY NMR experiment showing exchange between free (8.48 ppm) and bound (8.59 ppm) pyridine. Spectrum acquired in  $\text{C}_6\text{D}_6/\text{CD}_3\text{CO}_2\text{D}$  (1:1) at  $80\text{ }^\circ\text{C}$



Using the method of initial rates, we next determined the order of the reaction in each reagent using GC-FID. Importantly, all of these experiments were conducted with a Pd:pyr ratio of 1:2 (i.e., no extra pyridine was added to the reactions); this will be referred to as *Regime 1*. Interestingly, this reaction showed a half order dependence on [Pd] ( $0.53 \pm 0.07$ ; Figure 3.8), despite the fact that the catalyst resting state appears to be a monomer. In addition, a first order dependence on [benzene] ( $1.01 \pm 0.07$ ; Figure 3.9) and a zero order dependence on  $[\text{PhI}(\text{OAc})_2]$  ( $-0.08 \pm 0.04$ ; Figure 3.10) were observed. The value of  $k_{\text{H}}/k_{\text{D}}$  for  $\text{C}_6\text{H}_6/\text{C}_6\text{D}_6$  was  $3.6 \pm 0.3$  with this catalyst system (Figure 3.11). Finally, a Hammett plot was constructed by examining the initial reaction rate with a series of 3- and 4-substituted pyridine derivatives. As shown in Figure 3.12, a Hammett  $\rho$  value of  $+0.64$  was obtained, indicative of increasing reaction rate with more electron deficient pyridine derivatives.

**Figure 3.8.** Order in [Pd] with the (pyr)<sub>2</sub>Pd(OAc)<sub>2</sub> catalyst in *Regime 1*

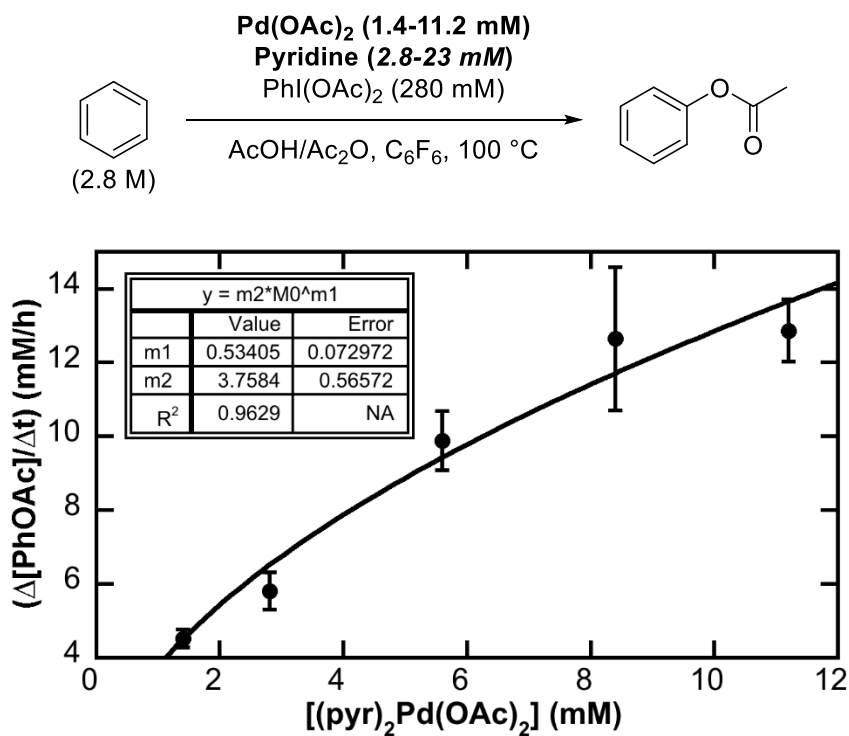


**Figure 3.9.** Order in benzene with (pyr)<sub>2</sub>Pd(OAc)<sub>2</sub> catalyst in *Regime 1*

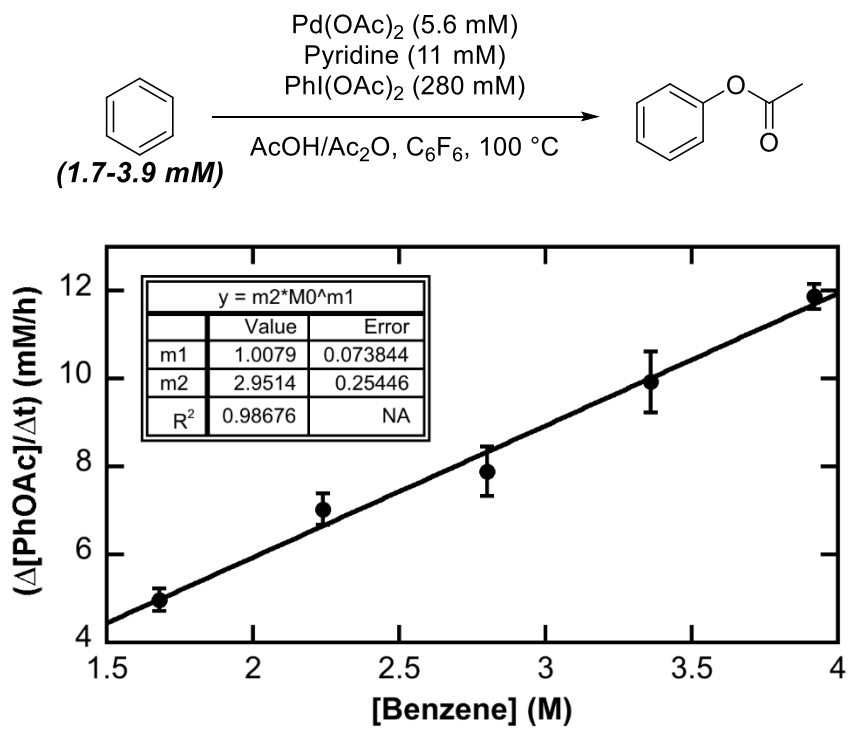
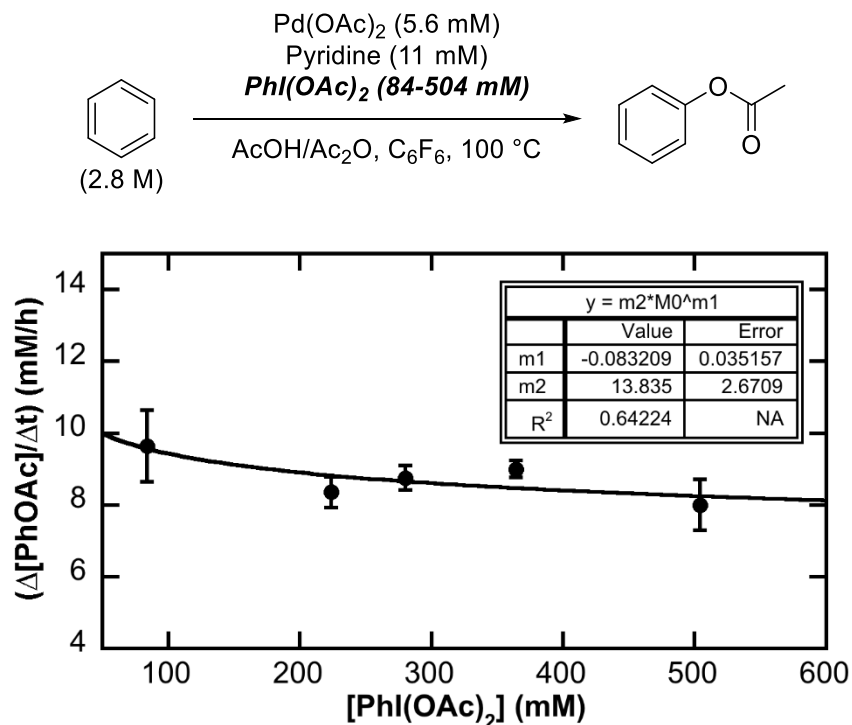


**Figure 3.10.** Order in  $\text{PhI}(\text{OAc})_2$  with  $(\text{pyr})_2\text{Pd}(\text{OAc})_2$  as catalyst in *Regime 1*



Based on the data discussed above, we propose the mechanism outlined in Scheme 3.4 for the  $\text{Pd}(\text{OAc})_2/\text{pyr}$  (1:2) catalyst system. The NMR data in Figure 3.6 implicate monomeric complex **4** as the catalyst resting state. This complex then undergoes reversible pyridine dissociation to generate mono-pyridine complex **5**. The ROESY experiment in Figure 3.7 supports the feasibility of this step. The positive Hammett value is also consistent, as more electron deficient pyridine ligands should provide a more favorable equilibrium towards the on-cycle intermediate **5**. C–H activation at **5** to generate **6** is then the rate-determining step. The observation of a first order dependence on benzene and a  $1^\circ$  kinetic isotope effect are further consistent with this proposal. Finally,  $2e^-$  oxidation of **6** would form **7** (or an isomer thereof) and C–O bond-forming reductive elimination would release PhOAc and regenerate **5**.

**Figure 3.11.** H/D kinetic isotope effect for benzene using  $(\text{pyr})_2\text{Pd}(\text{OAc})_2$  as catalyst in *Regime 1*

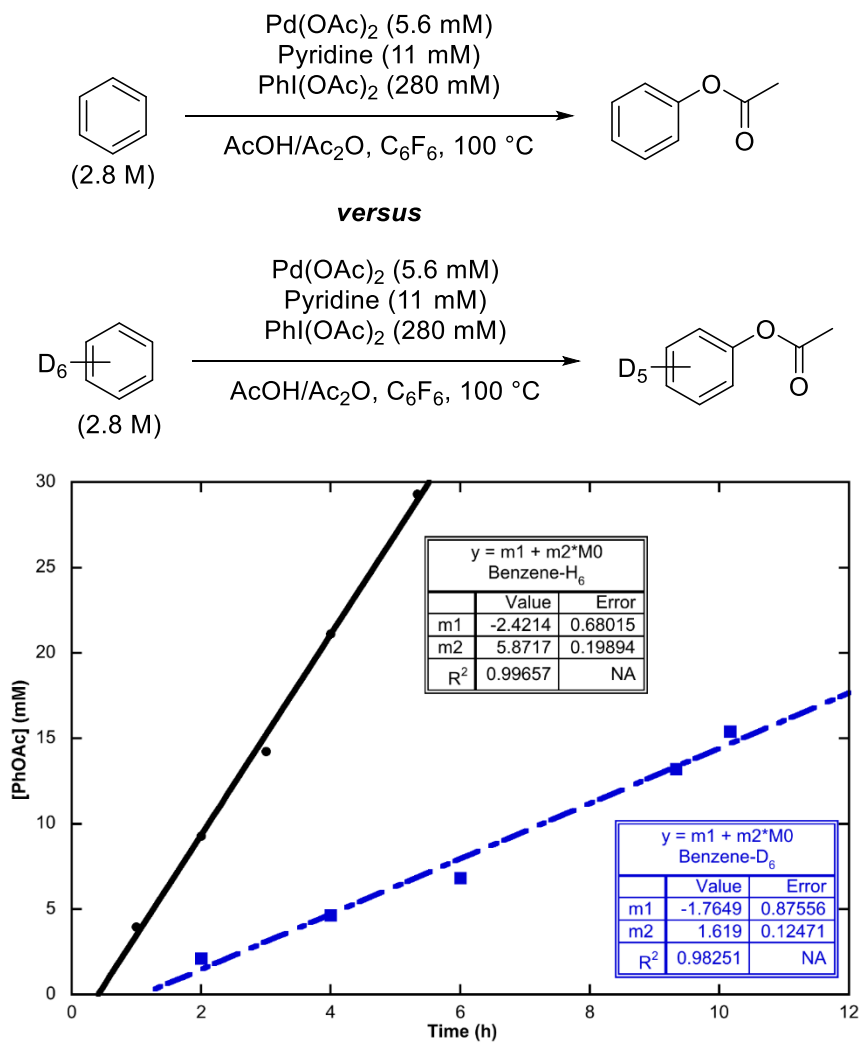
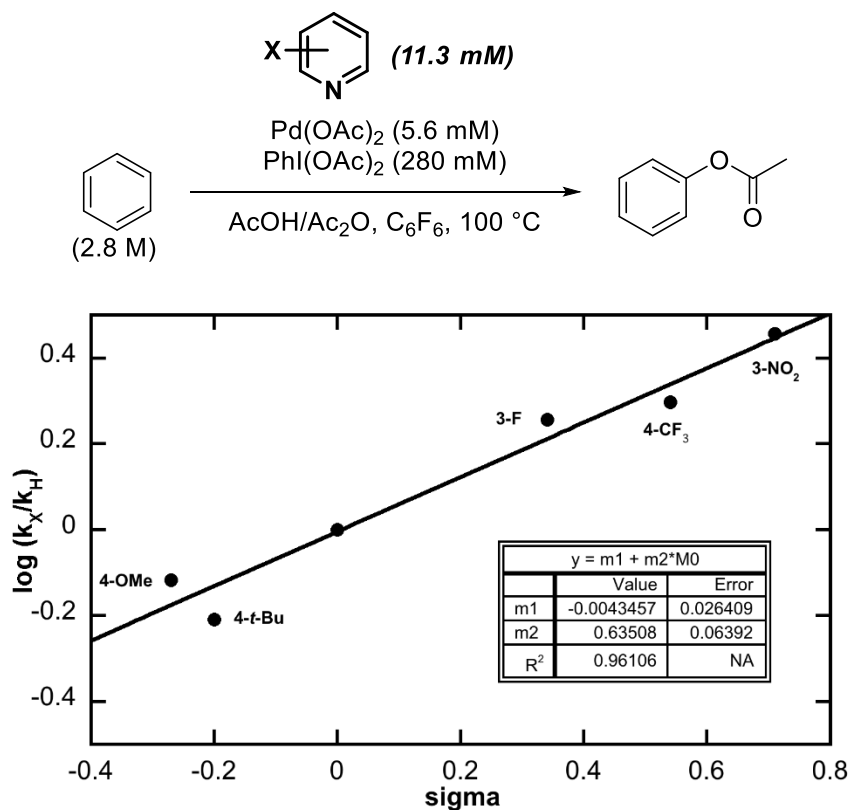
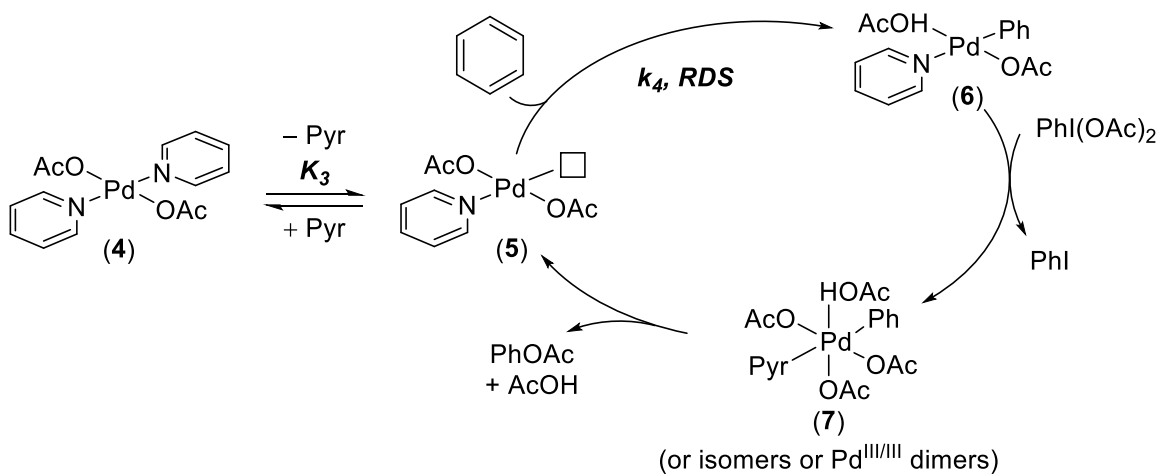


**Figure 3.12.** Hammett plot showing the effect of pyridine electronics for (pyr)<sub>2</sub>Pd(OAc)<sub>2</sub> catalyst in *Regime 1*



**Scheme 3.4.** Proposed mechanism for the (pyr)<sub>2</sub>Pd(OAc)<sub>2</sub>-catalyzed C–H acetoxylation of benzene



The rate expression for this sequence is shown in eq. 4:

$$\text{Rate} = \frac{d(\text{PhOAc})}{dt} = k_4[\mathbf{5}][\text{benzene}] \quad (4)$$

Using the equilibrium constant for the dissociation of pyridine from **4** provides eq. 5, which can be rearranged to eq. 6. Substitution for **[5]** then provides eq. 7.

$$K_3 = \frac{[\mathbf{5}][\text{pyr}]}{[\mathbf{4}]} \quad (5)$$

$$[\mathbf{5}] = \frac{K_3[\mathbf{4}]}{[\text{pyr}]} \quad (6)$$

$$\text{Rate} = \frac{k_4 K_3 [\mathbf{4}][\text{benzene}]}{[\text{pyr}]} \quad (7)$$

On the basis of the expression in eq. 7, we would initially anticipate a first order dependence on [Pd]. However, since all of the kinetic orders were determined under conditions where no exogenous pyridine is added (*Regime 1*), we can approximate that  $[\text{pyr}] = [\mathbf{5}]$ , and hence reduce eq. 5 to eq. 8. Using this approximation, the rate expression reduces to eq. 9, which predicts a half order dependence on [Pd], first order dependence on benzene, and zero order dependence on  $\text{PhI}(\text{OAc})_2$ , which are all in line with experimental observations.

$$K_3 = \frac{[\mathbf{5}]^2}{[\mathbf{4}]}; [\mathbf{5}] = K_3^{1/2}[\mathbf{4}]^{1/2} \quad (8)$$

$$\text{Rate} = k_4 K_3^{1/2} [\mathbf{4}]^{1/2} [\text{benzene}] \quad (9)$$

The approximation that  $[\text{pyr}] = [\mathbf{5}]$  (*Regime 1*) will not hold true under conditions where exogenous pyridine is added to the catalytic reaction. When  $[\text{pyr}] \gg [\mathbf{5}]$  (referred to as *Regime 2* for the remaining discussion), the rate expression in eq. 7 should be in operation. Here, a first order dependence on [Pd], first order dependence on benzene, and inverse first order dependence on pyridine are expected.

We next sought to experimentally determine the kinetic orders in [Pd], benzene, and pyr in the presence of added pyridine (*Regime 2*). However, with catalyst **4**, the addition of pyridine resulted in reaction rates that were too slow to measure accurately and reliably, even at elevated temperatures. To address this issue, we moved to the analogous 3-nitropyridine-containing catalyst **4-NO<sub>2</sub>**. In *Regime 1*, this catalyst reacts approximately 3-times faster than its pyr analogue (Figure 3.12), and we hypothesized that this would translate to enhanced reactivity and more reproducible rates in *Regime 2*.



The **4-NO<sub>2</sub>**-catalyzed conversion of benzene to phenyl acetate was first examined under *Regime 1* to compare the catalyst resting state and orders in [Pd], benzene, and PhI(OAc)<sub>2</sub> to those obtained with catalyst **4**. As shown using NMR spectroscopy, in Figure 3.13, the bis-pyridine complex (3-NO<sub>2</sub>pyr)<sub>2</sub>Pd(OAc)<sub>2</sub> (**4-NO<sub>2</sub>**) was the only Pd-containing species detected during catalysis, consistent with this complex as the catalyst resting state. Using GC-FID, in the absence of added ligand (*Regime 1*), we observed an approximately half order dependence on [Pd] ( $0.67 \pm 0.03$ ; Figure 3.14), approximately first order dependence on benzene ( $1.4 \pm 0.2$ ; Figure 3.15), and zero order dependence on PhI(OAc)<sub>2</sub> ( $-0.06 \pm 0.05$ ; Figure 3.16). These results are closely analogous to those obtained with catalyst **4**, and thus implicate similar mechanisms for **4** and **4-NO<sub>2</sub>** in *Regime 1*.

**Figure 3.13.** C–H acetoxylation of benzene monitored by <sup>1</sup>H NMR spectroscopy (aromatic region shown) using **4-NO<sub>2</sub>** as the catalyst

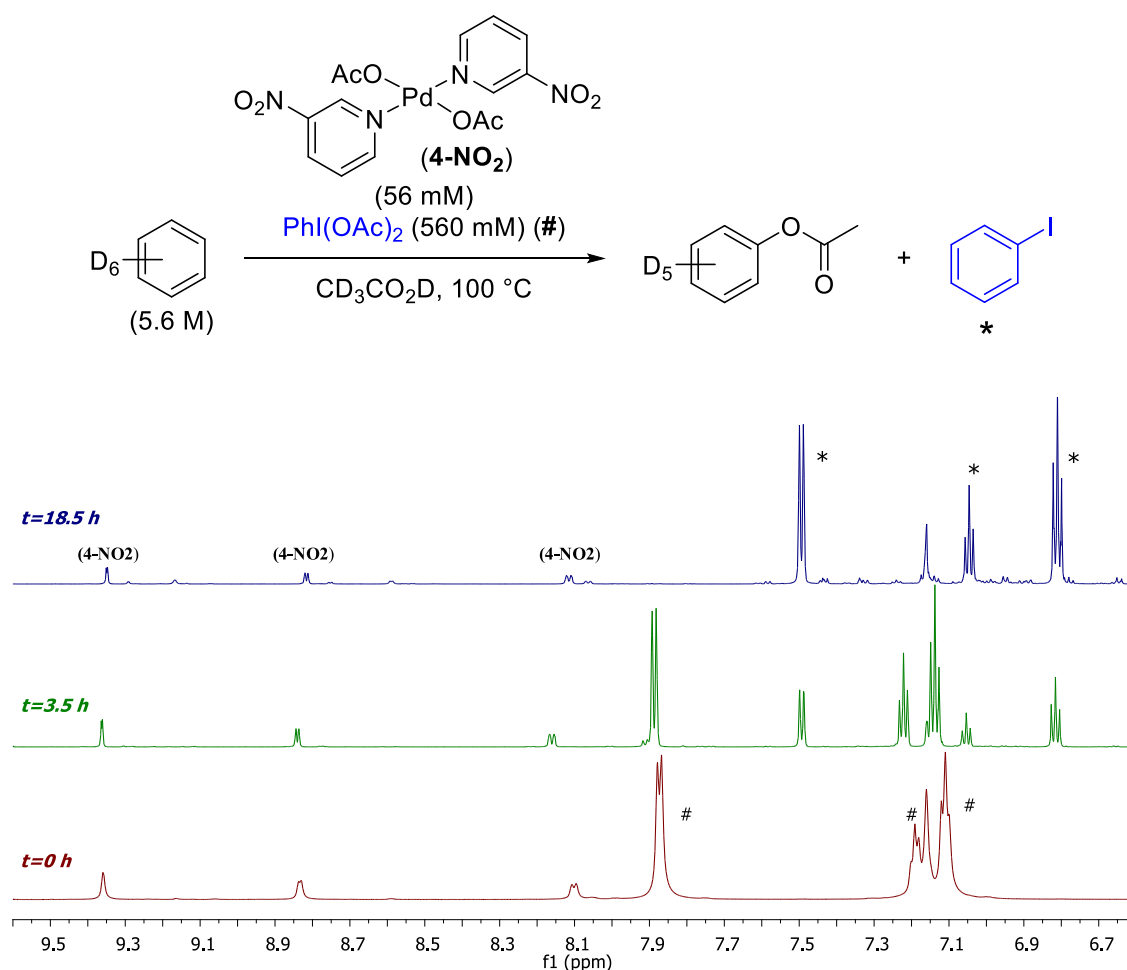


**Figure 3.14.** Order in [Pd] for the 4-NO<sub>2</sub> catalyst in *Regime 1*

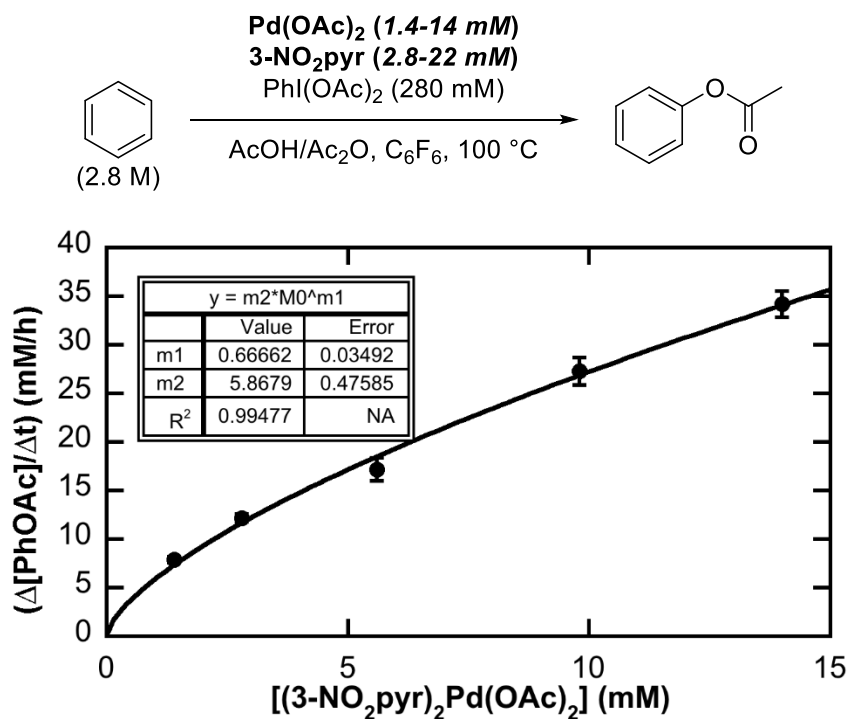


**Figure 3.15.** Order in benzene for the 4-NO<sub>2</sub> catalyst in *Regime 1*

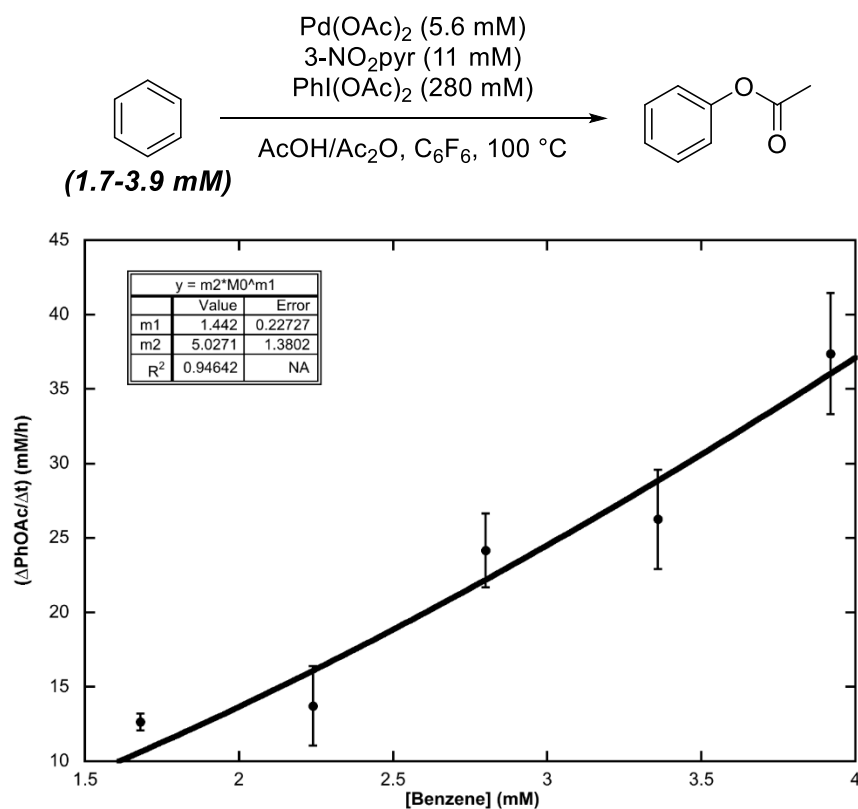
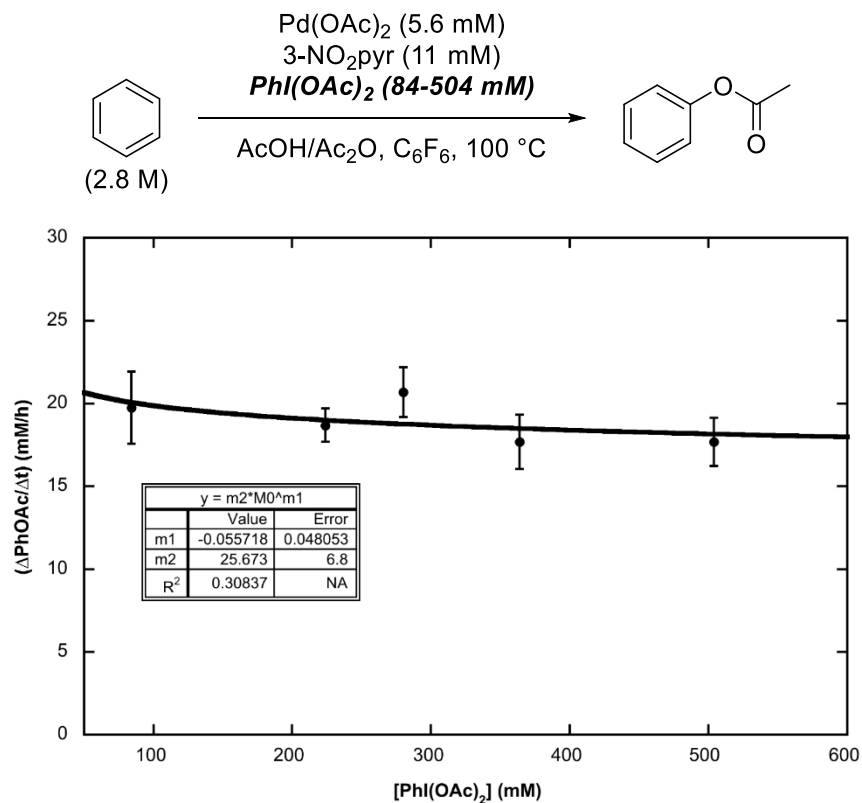


**Figure 3.16.** Order in  $\text{PhI}(\text{OAc})_2$  for the 4- $\text{NO}_2$  catalyst in *Regime 1*



We next evaluated catalyst **4- $\text{NO}_2$**  in the presence of exogenous 3-nitropyridine (28 mM). These conditions correspond to *Regime 2*; thus the rate expression in eq. 7 is expected to be operative. Indeed, an approximately first order dependence on  $[\text{Pd}]$  ( $1.2 \pm 0.1$ ; Figure 3.17), approximately inverse first order dependence on 3-nitropyridine ( $-1.4 \pm 0.1$ ; Figure 3.18), first order dependence on benzene ( $1.0 \pm 0.1$ ; Figure 3.19), and zero order dependence on  $\text{PhI}(\text{OAc})_2$  ( $0.05 \pm 0.08$ ; Figure 3.20) were observed. These results are consistent with the mechanism shown in Scheme 3.4 as well as the rate expression in eq. 7. Notably, these results are analogous to work by Stahl<sup>20</sup> and Hartwig,<sup>21</sup> in which half order in catalyst was obtained from a regime in which ligand dissociation occurs prior to the RDS; upon addition of exogenous ligand, the catalysts no longer show half order dependencies.

Figure 3.17. Order in [Pd] for the 4-NO<sub>2</sub> catalyst in *Regime 2*

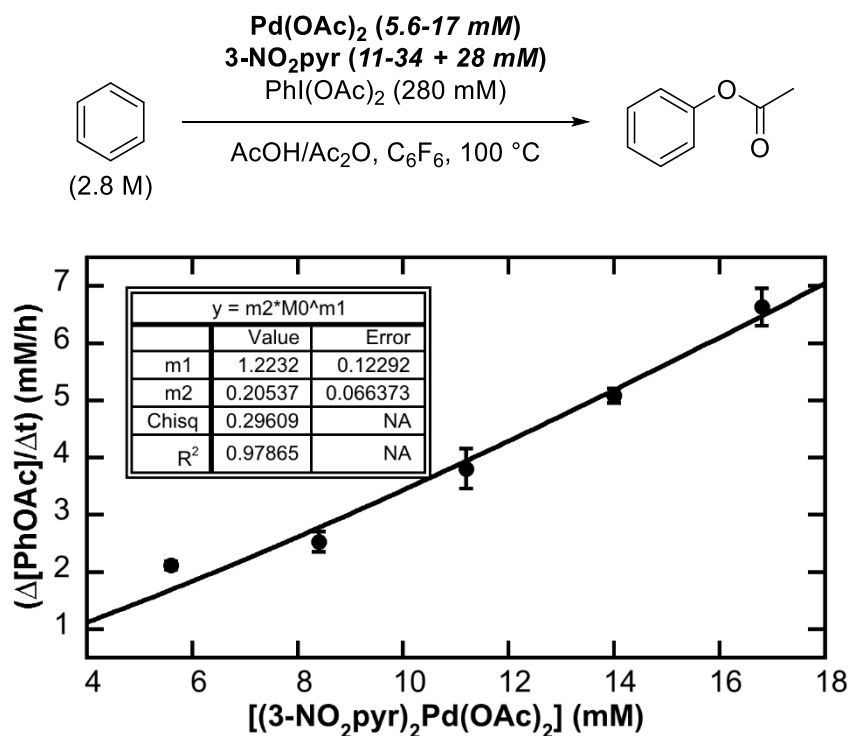
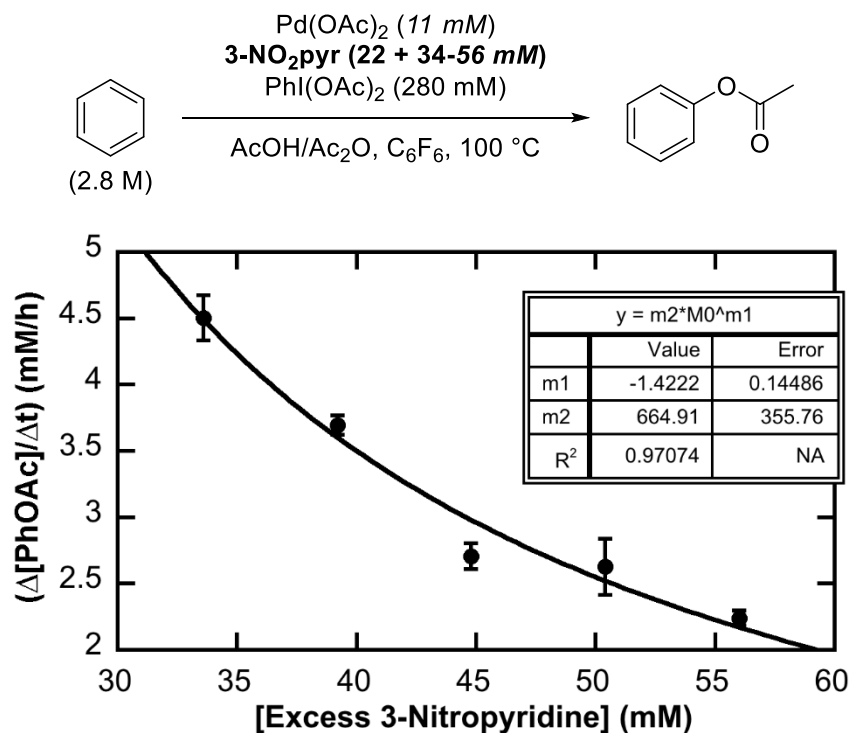
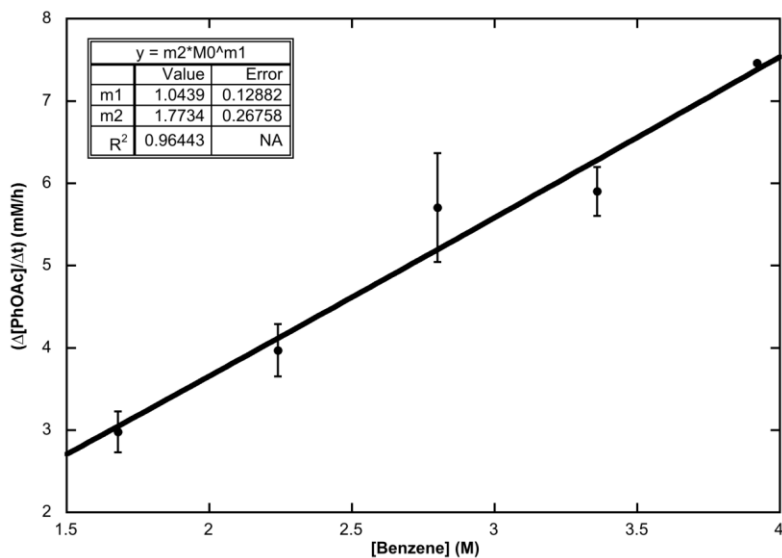
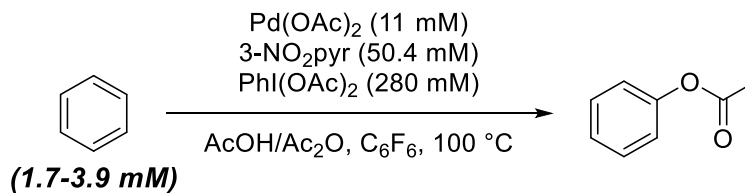


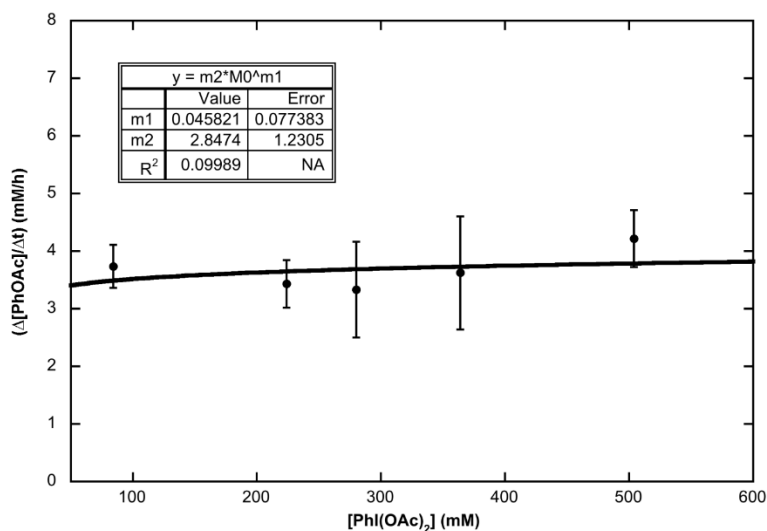
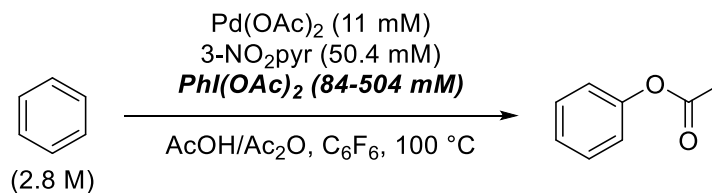
Figure 3.18. Order in (excess) 3-NO<sub>2</sub>Pyr for the 4-NO<sub>2</sub> catalyst in *Regime 2*



**Figure 3.19.** Order in benzene for the **4-NO<sub>2</sub>** catalyst in *Regime 2*



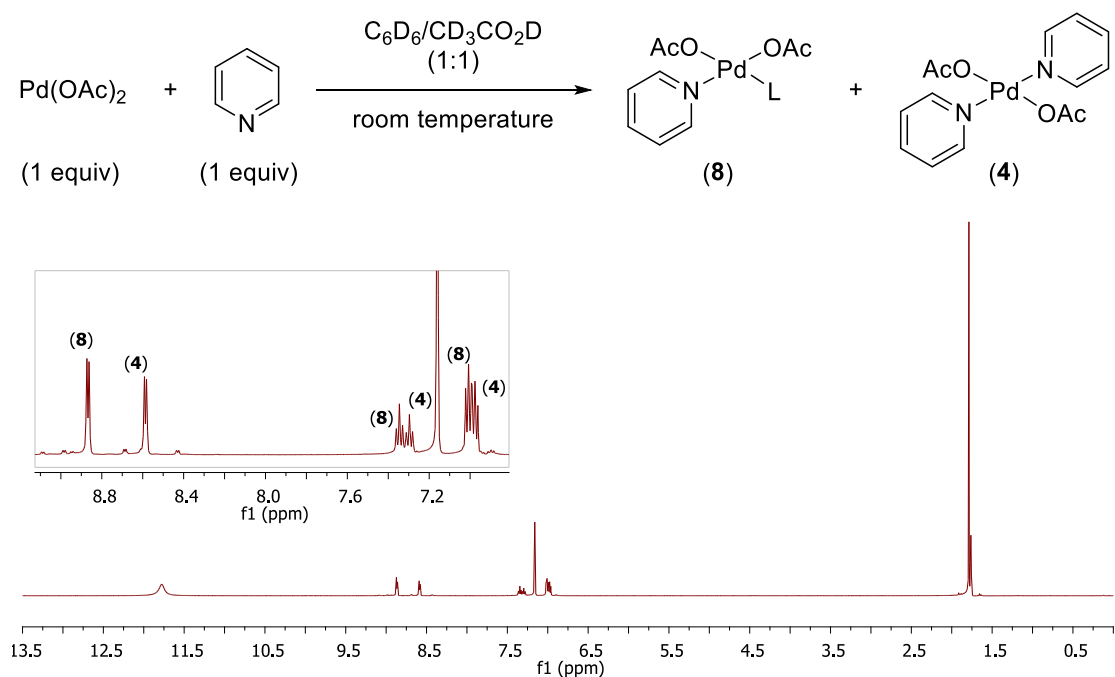
**Figure 3.20.** Order in  $\text{PhI(OAc)}_2$  for the **4-NO<sub>2</sub>** catalyst in *Regime 2*



### Mechanistic Investigation of the Pd(OAc)<sub>2</sub>/Pyridine (1:1) Catalyst System.

Finally, we conducted a detailed investigation of the most active catalyst system, which is generated by combining a 1:1 ratio of Pd(OAc)<sub>2</sub> to pyridine. To assess the catalyst resting state under these conditions, we combined equimolar quantities of pyridine and Pd(OAc)<sub>2</sub> in C<sub>6</sub>D<sub>6</sub>/CD<sub>3</sub>CO<sub>2</sub>D. <sup>1</sup>H NMR spectroscopic analysis at room temperature showed a mixture of two Pd-pyridine adducts: complex **4** [(pyr)<sub>2</sub>Pd(OAc)<sub>2</sub>] along with a second species of unknown structure (**8**) (Figure 3.21). As shown in Figure 3.22, both complexes **4** and **8** are observed throughout the catalytic reaction. Since the reaction rate under these conditions is significantly higher than that with **4** alone, we propose that **8** is likely the predominant active catalyst (or resting state of the active catalyst) in this system.

**Figure 3.21.** New species (**8**) observed by <sup>1</sup>H NMR spectroscopy along with **4** when combining a 1:1 ratio of Pd(OAc)<sub>2</sub>:pyr



#### Possible structures of 8:

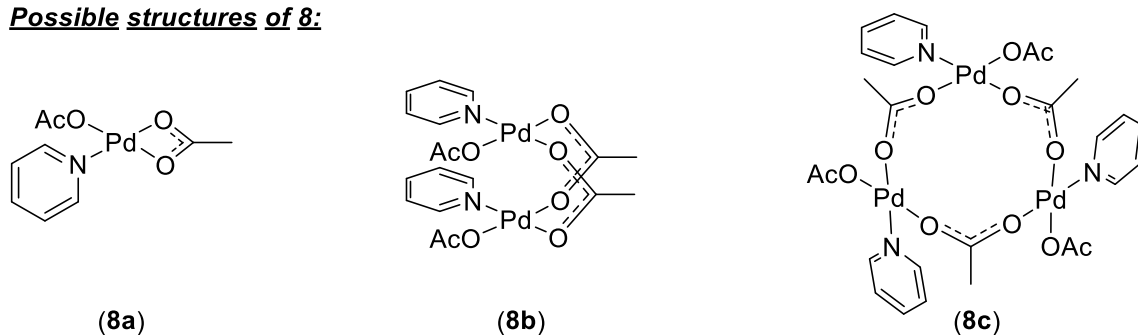
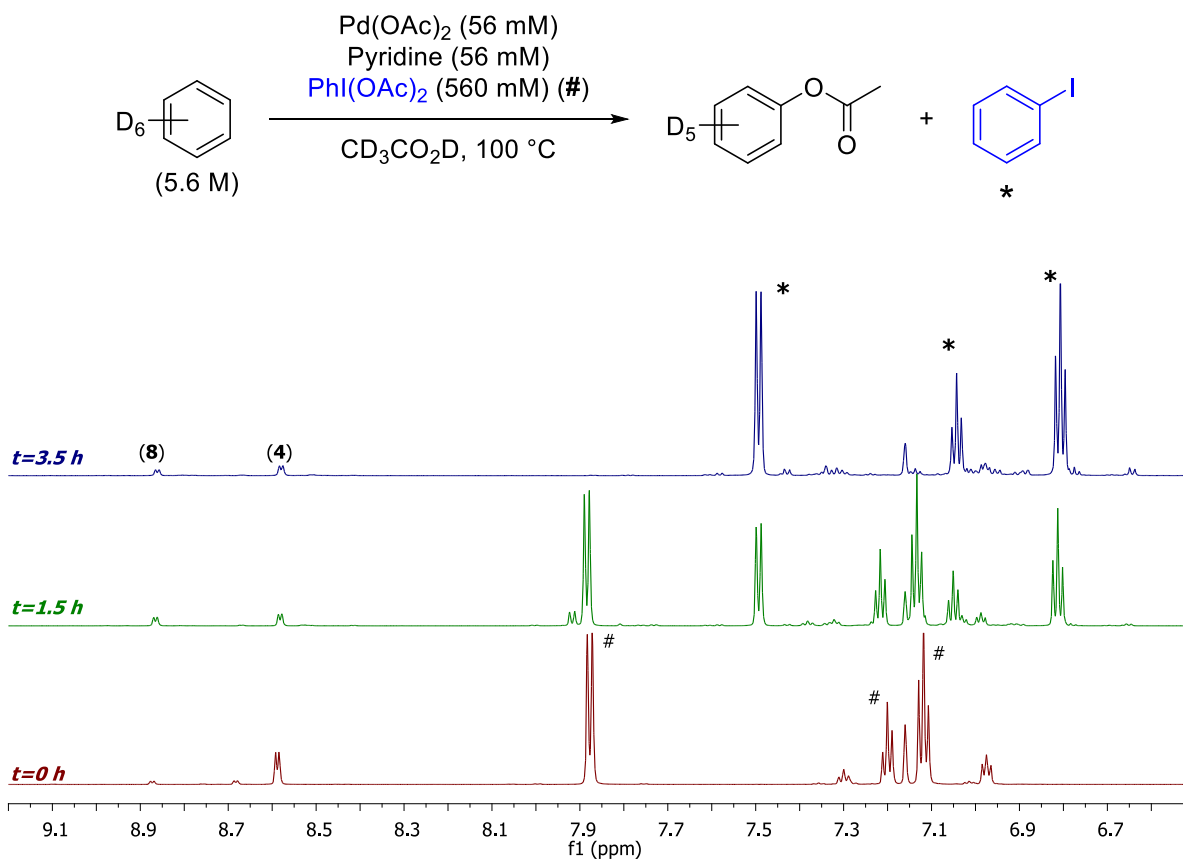


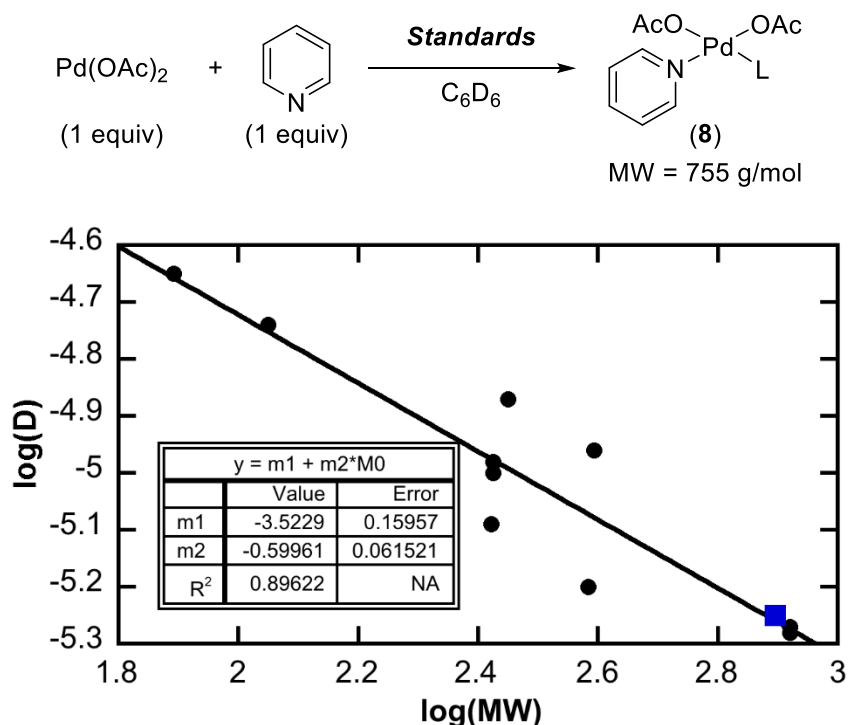
**Figure 3.22.** C–H acetoxylation of benzene monitored by  $^1\text{H}$  NMR spectroscopy (aromatic region shown) using a  $\text{Pd}(\text{OAc})_2$ :pyr ratio of 1:1



As shown in Figure 3.21, complex **8** could be a monomer (**8a**), dimer (**8b**), trimer (**8c**), or a larger oligomeric structure with a Pd:pyr stoichiometry of 1:1. A Diffusion Ordered Spectroscopy (DOSY) NMR experiment was performed to obtain the approximate molecular weight of **8** and thus to preliminarily differentiate between these possibilities.<sup>22</sup> This experiment involves generating **8** *in situ* in the presence of a series of different molecules that serve as molecular weight standards. These standards (which include small organic molecules and large Pd complexes; Table 3.1) were selected based on three criteria: (i) they represent a wide range of molecular weights (MW), (ii) they are all expected to be unreactive with **8** and with each other, and (3) they have distinct  $^1\text{H}$  NMR signals. The DOSY NMR spectrum of this mixture was then obtained at  $25\text{ }^\circ\text{C}$  in  $\text{C}_6\text{D}_6/\text{CD}_3\text{CO}_2\text{D}$  (1:1). The plot of  $\log(\text{MW})$  versus  $\log(D)$  ( $D$  = diffusion coefficient) is shown Figure 3.23. On the basis of these data, the molecular weight of **8** is calculated to be 755 g/mol (blue data point in Figure 3.23). This value is in between that of the dimer

**8b** (607 g/mol) and the trimer **8c** (911 g/mol). Importantly, the DOSY experiment requires assumptions about the size and shape of the standards compared to **8**; therefore the calculated MW is only an approximation. Nonetheless, we believe that these data suggest that complex **8** is unlikely to be a monomer (**8a**).

**Figure 3.23.** DOSY data used to approximate the molecular weight of **8** (blue data point) in solution

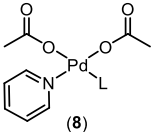
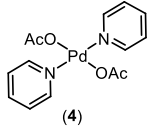
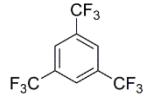
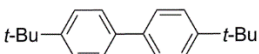
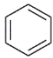
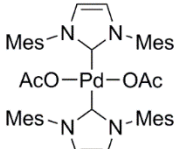
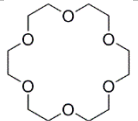
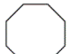
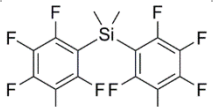


To gain further insights into the structure of **8**, we performed an NMR experiment using 1 equiv of  $\text{Pd}(\text{OAc})_2$  and 0.5 equiv each of two distinct pyridine derivatives (X and Y). If **8** is a monomer (**8a**), two different complexes should be formed in a 1:1 ratio:  $(\text{X})\text{Pd}(\text{OAc})_2$  and  $(\text{Y})\text{Pd}(\text{OAc})_2$ . If **8** is a dimer (**8b**), three compounds are expected in a 1:2:1 ratio:  $[(\text{X})\text{Pd}(\text{OAc})_2]_2$ ,  $[(\text{Y})\text{Pd}(\text{OAc})_2]_2$ , and  $(\text{X})(\text{Y})\text{Pd}_2(\text{OAc})_4$ . Finally, if **8** is a trimer (**8c**), four compounds are expected in a 1:1:3:3 ratio:  $[(\text{X})\text{Pd}(\text{OAc})_2]_3$ ,  $[(\text{Y})\text{Pd}(\text{OAc})_2]_3$ ,  $(\text{X})_2(\text{Y})\text{Pd}_3(\text{OAc})_6$  and  $(\text{X})(\text{Y})_2\text{Pd}_3(\text{OAc})_6$ .<sup>23</sup> We chose 4-methoxypyridine and 4-*tert*-butylpyridine for X and Y since they are expected to have similar binding affinities to  $\text{Pd}(\text{OAc})_2$  yet their <sup>1</sup>H NMR chemical shifts are well resolved. Upon mixing, the <sup>1</sup>H NMR spectrum shown in Figure 3.24c was obtained (only the signals associated with the 2-position of the pyr derivatives are shown). Both  $[(4\text{-OMe-pyr})\text{Pd}(\text{OAc})_2]_n$  (see Figure 3.24a



(green) for independently acquired  $^1\text{H}$  NMR spectrum) and  $[(4\text{-}t\text{Bu-pyr})\text{Pd}(\text{OAc})_2]_n$  (see Figure 3.24b (blue) for independently acquired  $^1\text{H}$  NMR spectrum) are observed along with signals associated with at least one additional compound.

**Table 3.1.** Results from DOSY experiment and internal standards used

Entry	Standard	MW	Chemical shifts used, $\delta$ (ppm)	Diffusion unit (D)
1	 (8)	unknown	8.88	$5.64 \times 10^{-6}$
2	 (4)	383	8.61	$6.32 \times 10^{-6}$
3	 1,3,5-tris(trifluoromethyl)benzene	282	7.89	$1.36 \times 10^{-5}$
4	 4,4'-di- <i>tert</i> -butyl-1,1'-biphenyl	266	7.48	$1.05 \times 10^{-5}$
5			1.23	$1.01 \times 10^{-5}$
6	 Benzene	78	7.16	$2.23 \times 10^{-5}$
7	 (IMes) $_2$ Pd(OAc) $_2$	833	6.86	$5.31 \times 10^{-6}$
8			6.36	$5.35 \times 10^{-6}$
9			2.32	$5.30 \times 10^{-6}$
10			1.91	$5.34 \times 10^{-6}$
11			1.38	$5.35 \times 10^{-6}$
12	 18-crown-6	264	3.48	$8.20 \times 10^{-6}$
13	 Cyclooctane	112	1.43	$1.80 \times 10^{-5}$
14	 (C $_6$ F $_5$ )Si(CH $_3$ ) $_2$	392	0.62	$1.09 \times 10^{-5}$

Since >2 distinct species are detected, monomer **8a** can be eliminated as a possible structure. Two new signals, labeled as **11**, are observed in a 1:1 ratio. This is inconsistent with the formation of **8c** (mixed trimers). The integral ratios also support formation of a dimer: two new signals labeled as **11** are observed in a 1:1 ratio; since the integral ratio of [(4-*t*-Bu-pyr)Pd(OAc)<sub>2</sub>]<sub>2</sub> and [(4-OMe-pyr)Pd(OAc)<sub>2</sub>]<sub>2</sub> is twice that of the mixed compound (4-*t*-Bu-pyr)(4-OMe-pyr)Pd<sub>2</sub>(OAc)<sub>4</sub>, the new complexes are formed in a 1:1:2 ratio (**9:10:11**) and this is consistent with the formation of **8b** (dimer). On the basis of these data, we propose that the resting state of the catalyst is the dimer [(pyr)Pd(OAc)<sub>2</sub>]<sub>2</sub> (**8b**).

Rate studies were next conducted using GC-FID to assess the order in each reaction component with Pd(OAc)<sub>2</sub>/pyridine (1:1) as the catalyst. Under these conditions, the reaction shows a half order dependence on Pd ( $0.55 \pm 0.02$ ; Figure 3.25), a first order dependence on benzene ( $0.94 \pm 0.06$ ; Figure 3.26) and a zero order dependence on PhI(OAc)<sub>2</sub> ( $0.00 \pm 0.06$ ; Figure 3.27). In addition, a relatively large primary kinetic isotope effect ( $k_H/k_D = 3.9 \pm 0.2$ ) with C<sub>6</sub>H<sub>6</sub>/C<sub>6</sub>D<sub>6</sub> is observed (Figure 3.28). These data are consistent with a mechanism in which a dimeric precatalyst (**8b**) enters the catalytic cycle by dissociation to a monomer (**5**) (Scheme 3.5). Rate-limiting C–H activation of benzene at **5** would then form the aryl complex **6**, and fast oxidation and reductive elimination steps would release the product and regenerate the catalyst. The rate expression for the mechanism proposed in Scheme 3.5 can be derived as shown in eqs. 10-13. It is in full accord with the experimental data.

**Figure 3.24.** Mixed pyridines experiment. (a)  $^1\text{H}$  NMR spectrum when  $\text{Pd}(\text{OAc})_2$  and OMe-pyr (1:1) are mixed. (b)  $^1\text{H}$  NMR spectrum when  $\text{Pd}(\text{OAc})_2$  and *t*-Bu-pyr (1:1) are mixed. (c)  $^1\text{H}$  NMR spectrum when  $\text{Pd}(\text{OAc})_2$ , *t*-Bu-pyr, and OMe-pyr (1:0.5:0.5) are mixed. Two new peaks are observed. (Spectra shown are the region corresponding to the signals of the 2-position of the mono-pyridine complexes.)

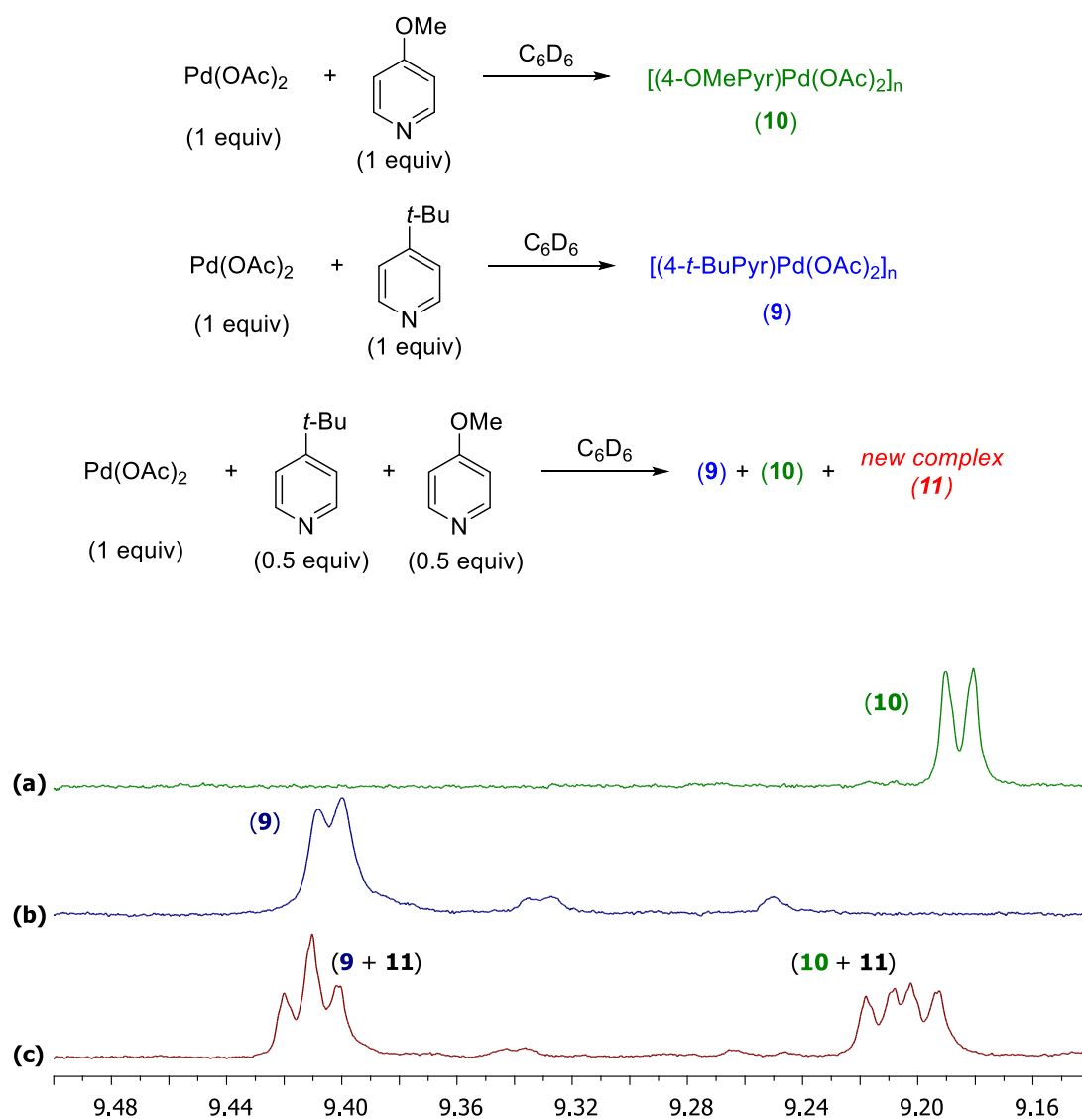


Figure 3.25. Order in [Pd] with Pd(OAc)<sub>2</sub>/pyr (1:1) as catalyst

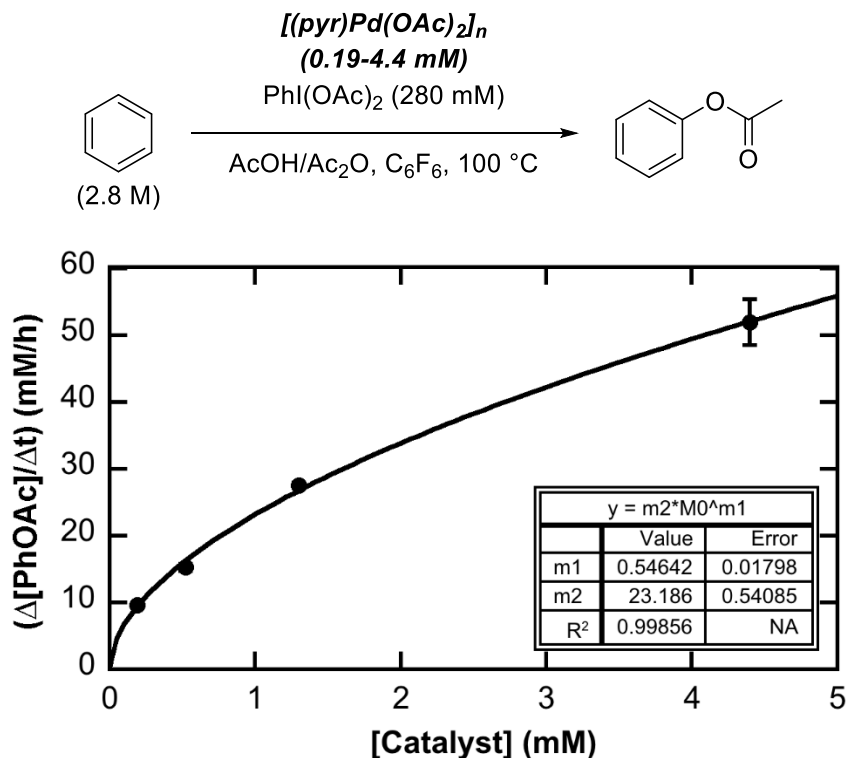
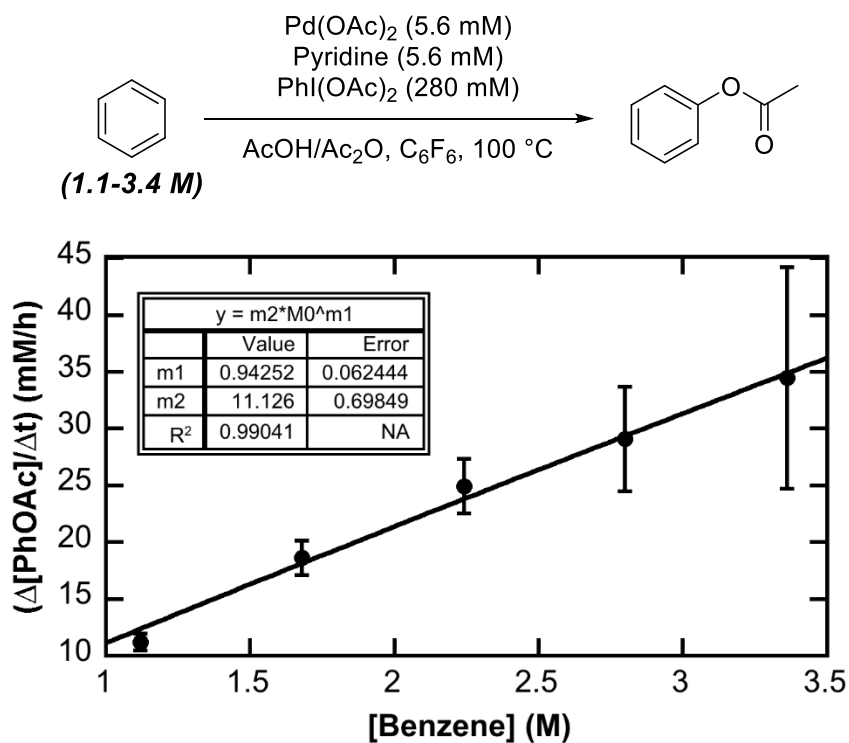
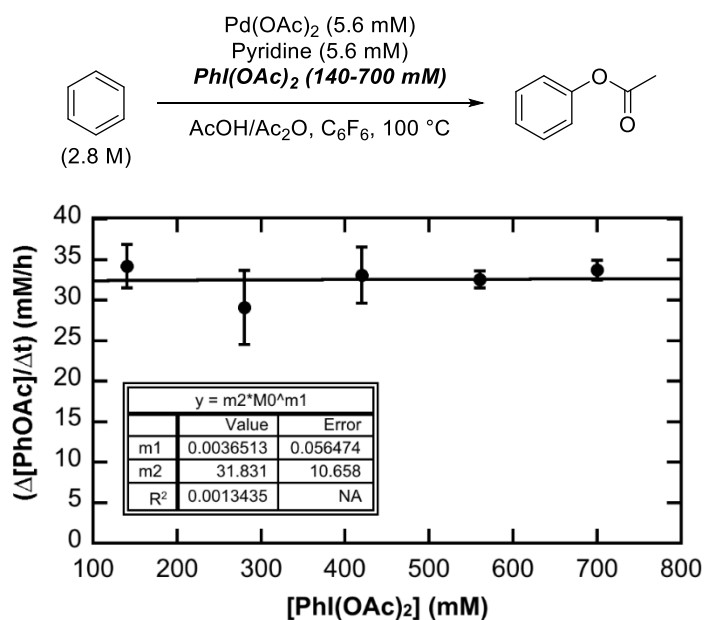


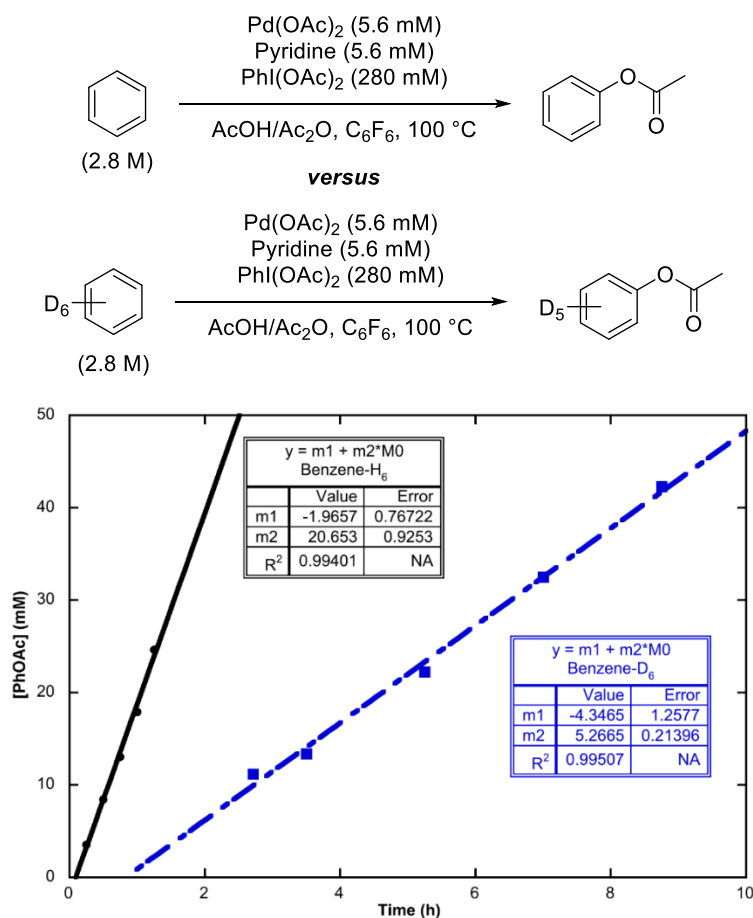
Figure 3.26. Order in benzene with Pd(OAc)<sub>2</sub>/pyr (1:1) as catalyst



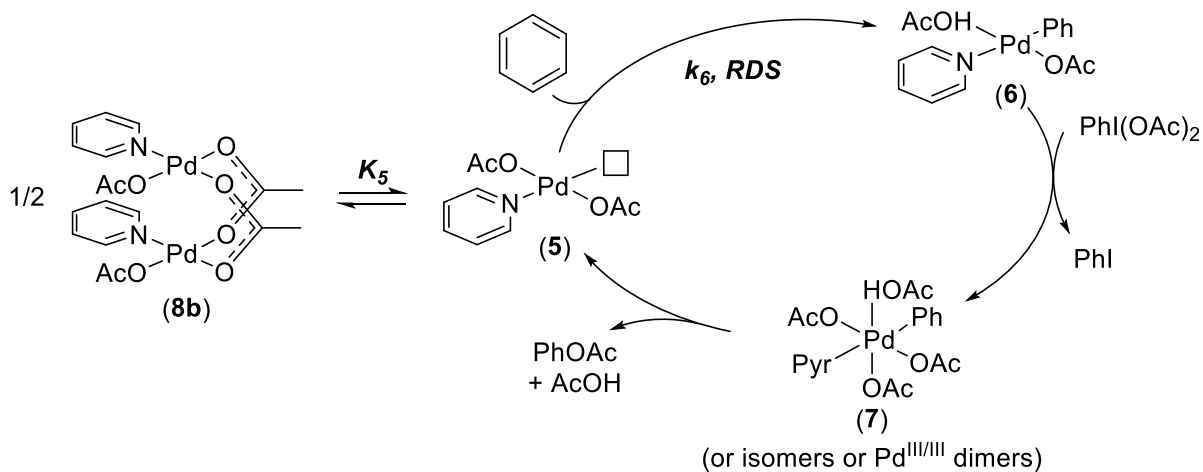
**Figure 3.27.** Order in  $\text{PhI}(\text{OAc})_2$  with  $\text{Pd}(\text{OAc})_2/\text{pyr}$  (1:1) as catalyst



**Figure 3.28.** H/D kinetic isotope effect for benzene using  $\text{Pd}(\text{OAc})_2/\text{pyr}$  (1:1) as catalyst



**Scheme 3.5.** Proposed mechanism with Pd(OAc)<sub>2</sub>/pyr (1:1) as catalyst



$$\text{Rate} = \frac{d(\text{PhOAc})}{dt} = k_6[\text{benzene}][\mathbf{5}] \quad (10)$$

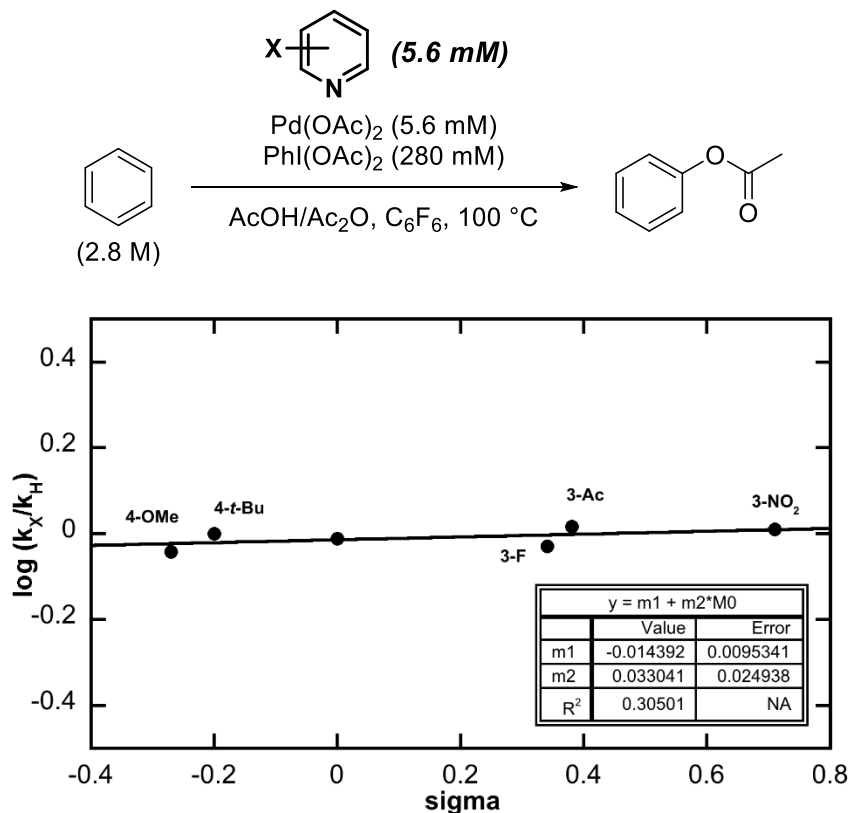
$$K_5 = \frac{[\mathbf{5}]}{[\mathbf{8b}]^{1/2}} \quad (11)$$

$$[\mathbf{5}] = K_5[\mathbf{8b}]^{1/2} \quad (12)$$

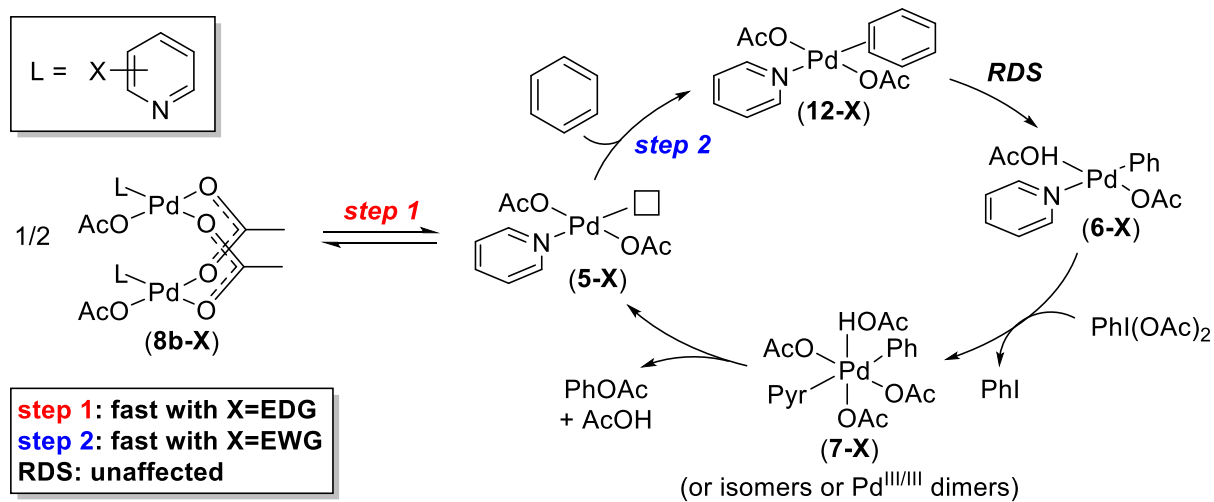
$$\text{Rate} = k_6 K_5 [\text{benzene}][\mathbf{8b}]^{1/2} \quad (13)$$

We next probed the impact of substituted pyridine ligands on the rate of the Pd(OAc)<sub>2</sub>/pyridine (1:1)-catalyzed C–H acetoxylation of benzene. As shown in the Hammett plot in Figure 3.29, substitution of the pyridine ligand had a negligible impact on the overall reaction rate ( $\rho \sim 0$ ). This result can be rationalized based on counterbalancing electronic effects of pyridine substituents on the dissociation of dimer **8b-X** to monomer **5-X** (Scheme 3.6, step 1) and the coordination of benzene to form the  $\eta^2$ -benzene intermediate **12-X** (Scheme 3.6, step 2). Step 1 is expected to be accelerated by electron-rich pyridine ligands<sup>24</sup> (e.g., 4-methoxypyridine), while step 2 is expected to be fastest with electron-deficient pyridines, such as 3-nitropyridine.<sup>25</sup> Rate-determining C–H activation would then occur at intermediate **12-X**. Literature precedent strongly suggests that this step proceeds via a concerted, acetate-assisted metalation-deprotonation transition state.<sup>5</sup> This transition state is cyclic and minimal charge is accumulated. As such, we anticipate that substitution on the pyridine ligand would have minimal impact on the energy of this transition state. Overall, the observed Hammett value of  $\sim 0$  is consistent with the electronic effects on steps 1 and 2 essentially cancelling one another.

**Figure 3.29.** Hammett plot showing the effect of pyridine electronics with Pd(OAc)<sub>2</sub>/pyr (1:1) as catalyst



**Scheme 3.6.** Explanation for lack of pyridine electronic effect with catalyst **8b**



### 3.3 CONCLUSIONS

This chapter describes a detailed exploration of differences between three catalysts  $\text{Pd}(\text{OAc})_2$ ,  $[(\text{pyr})\text{Pd}(\text{OAc})_2]_2$  and  $(\text{pyr})_2\text{Pd}(\text{OAc})_2$  for the C–H acetoxylation of benzene. With all three catalyst systems, the reaction appears to involve rate-limiting C–H bond cleavage. NMR and kinetic studies suggest that the most active catalyst (**8**) rests as a dimer in solution. A comparison of the mechanisms with bis-pyridine complex **4** and mono-pyridine complex **8** implicate C–H activation occurring at same intermediate **5**. The difference in reactivity between the bis- and mono-ligated catalysts, therefore, lies in how they enter into the catalytic cycle. Bis-pyridine complex **4** dissociates a pyridine ligand, while the dimeric mono-pyridine complex **8a** breaks up into a monomer. This study provides valuable insights into the chemistry of  $\text{Pd}(\text{OAc})_2/\text{pyr}$ -based catalyst systems for C–H bond acetoxylation. Additionally, they have broader implications in catalysis, since Pd/pyr catalysts are employed for a variety of transformations including alcohol oxidation,<sup>15a,d</sup> alkene amination,<sup>15b</sup> indole arylation,<sup>14c</sup> and the Fujiwara-Moritani reaction.<sup>14a,b</sup>

### 3.4 PERSPECTIVE AND OUTLOOK

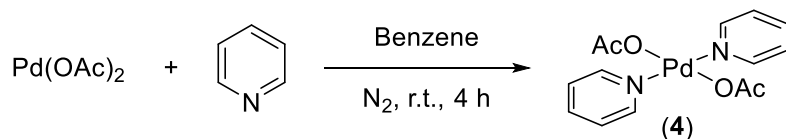
Much insight has been elucidated for the three catalysts systems detailed in this chapter. However, the use of this knowledge towards the development of more active catalysts is lacking, and therein lies the future work of this project. It is noted that, in both  $[(\text{pyr})\text{Pd}(\text{OAc})_2]_2$  and  $(\text{pyr})_2\text{Pd}(\text{OAc})_2$  precatalysts, one pyridine and one acetate ligand are spectators throughout the catalytic cycle. Development of ligands that exploit this would be desirable. Additionally, knowing that the highly active catalyst  $[(\text{pyr})\text{Pd}(\text{OAc})_2]_2$  must dissociate from a dimer to a monomer, tuning the steric environment of the pyridine and the acetate groups might increase the rate and equilibrium of monomer formation, and therefore increase the rate of catalysis. With the hypothesis that  $[(\text{pyr})\text{Pd}(\text{OAc})_2]_2$  readily forms an open coordination site, the application of this precatalyst to diverse transformations is desirable. The Pd:Pyr ratio has been shown to be important in other reactions using different types of substrates and solvents,<sup>14,15</sup> and whether the complex



$[(\text{pyr})\text{Pd}(\text{OAc})_2]_2$  is formed during these catalytic reactions is an interesting avenue of exploration.

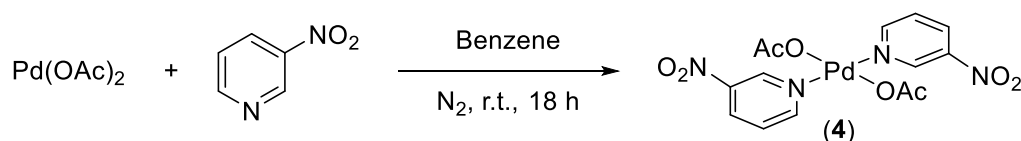
### 3.5 EXPERIMENTAL

#### Synthesis of $(\text{pyr})_2\text{Pd}(\text{OAc})_2$ (**4**)



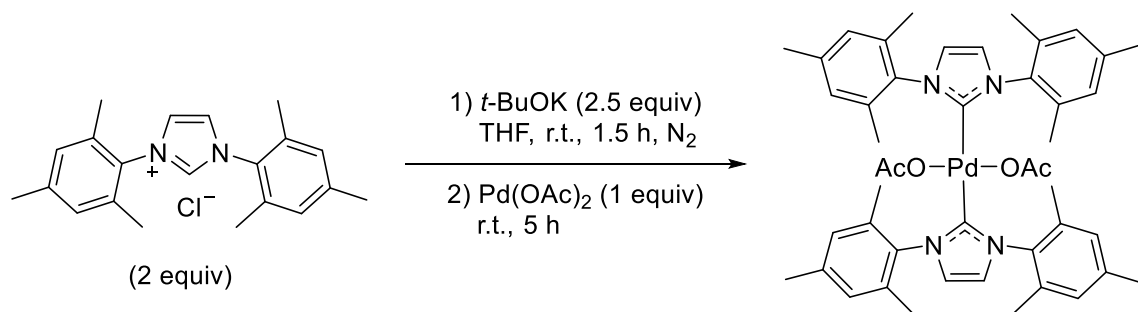
$(\text{Pyr})_2\text{Pd}(\text{OAc})_2$  (**4**) was prepared using a modified literature procedure.<sup>26</sup>  $\text{Pd}(\text{OAc})_2$  (100 mg, 0.45 mmol, 1.0 equiv) was weighed into a 10 mL Schlenk flask. The flask was placed under a  $\text{N}_2$  atmosphere and then benzene (6 mL) and pyridine (72  $\mu\text{L}$ , 0.89 mmol, 2.0 equiv) were added sequentially. This mixture was stirred at room temperature for 4 h. Benzene was removed under vacuum, giving **4** as a yellow-orange solid (52 mg, 31% yield). The characterization spectra match those reported in the literature.<sup>27</sup>

#### Synthesis of $(3\text{-NO}_2\text{pyr})_2\text{Pd}(\text{OAc})_2$ (**4-NO}\_2**)



$(3\text{-Nitropyridine})_2\text{Pd}(\text{OAc})_2$  (**4-NO}\_2**) was prepared using a modified literature procedure.<sup>26</sup>  $\text{Pd}(\text{OAc})_2$  (91 mg, 0.40 mmol, 1.0 equiv) was weighed out into a 10 mL Schlenk flask. The flask was placed under a  $\text{N}_2$  atmosphere and then benzene (5 mL) and 3-nitropyridine (100 mg, 0.81 mmol, 2.0 equiv) were added sequentially. This mixture was stirred at room temperature for 18 h. The precipitate that formed was collected, giving **4-NO}\_2** as a yellow-orange solid (109 mg, 58% yield).

## Synthesis of (IMes)<sub>2</sub>Pd(OAc)<sub>2</sub>



(IMes)<sub>2</sub>Pd(OAc)<sub>2</sub> was prepared using a modified literature procedure.<sup>28</sup> To a 50 mL Schlenk flask equipped with a Teflon-coated stirbar under a N<sub>2</sub> atmosphere was added 1,3-bis(2,4,6-trimethylphenyl)imidazolium chloride (0.46 g, 1.3 mmol, 2.0 equiv) and THF (24 mL). KO<sup>t</sup>Bu (1 M solution in THF; 1.7 mL, 1.7 mmol, 2.5 equiv) was then added drop-wise. This mixture was stirred for 1.5 h at room temperature. Pd(OAc)<sub>2</sub> (150 mg, 0.67 mmol, 1.0 equiv) was added, and the reaction was stirred at room temperature for 5 h. The reaction was filtered through Celite, and the filtrate was poured into hexanes (90 mL). The resulting solution was cooled to -30 °C to allow solids to form. The solids were removed by filtration, and the filtrate was concentrated to afford an orange solid. This solid was recrystallized from EtOAc to afford the product as a pale yellow solid (118 mg, 32% yield). The NMR spectral data match that reported in the literature.<sup>28</sup>

## General Procedure for Monitoring Reactions by <sup>1</sup>H NMR

To a screw-cap <sup>1</sup>H NMR tube was added PhI(OAc)<sub>2</sub> (91 mg, 0.28 mmol, 1.0 equiv, 560 mM), Pd(OAc)<sub>2</sub> (6.3 mg, 0.028 mmol, 0.1 equiv, 56 mM), and ligand. Benzene-d<sub>6</sub> (0.25 mL, 2.8 mmol, 10 equiv, 5.6 M), and CD<sub>3</sub>CO<sub>2</sub>D (0.25 mL) were added via disposable plastic syringe. This mixture was sonicated for 1 min and then a <sup>1</sup>H NMR spectrum was recorded (t = 0). The NMR tube was heated to 100 °C in an oil bath. The NMR tube was periodically removed from heating to record <sup>1</sup>H NMR spectra at ambient temperature (the resting state was also independently observed at 80 °C in the NMR spectrometer during the course of the reaction (data not shown)). Progress was monitored by disappearance of PhI(OAc)<sub>2</sub> and appearance of PhI (since the C-H acetoxylation product is deuterated).

## General Procedure for Kinetics Using Pd(OAc)<sub>2</sub> (No Ligand)

$\text{Pd}(\text{OAc})_2$  was measured from a 0.0445 M stock solution (100 mg  $\text{Pd}(\text{OAc})_2$  dissolved in 10.0 mL DCM) using a Hamilton gastight syringe into a 1-dram vial equipped with a Teflon-coated stirbar. This aliquot was stirred open to air at room temperature for ~2 h to allow the solvent to evaporate to dryness. To the vial containing the resulting solid  $\text{Pd}(\text{OAc})_2$ ,  $\text{PhI}(\text{OAc})_2$  was added, followed by  $\text{C}_6\text{F}_6$  (measured by plastic, disposable syringe), benzene or benzene- $\text{d}_6$  (measured by plastic, disposable syringe), AcOH (0.18 mL; measured by plastic, disposable syringe), and  $\text{Ac}_2\text{O}$  (20  $\mu\text{L}$ ; measured by Hamilton gastight syringe). The vial was tightly sealed with a Teflon-lined screw cap and heated to 100 °C in a preheated, aluminum heating block. After the desired reaction time (measured precisely by a timer), the reaction was flash-cooled in a liquid nitrogen bath until frozen solid (about 45 s). The reaction was then allowed to warm back up to room temperature and 10  $\mu\text{L}$  PhCl (GC internal standard) were added using a 25  $\mu\text{L}$  Hamilton gastight syringe. The reaction mixture was diluted with EtOAc (1 mL) and transferred to a 20 mL scintillation vial containing 2 mL of a 4 M aqueous  $\text{K}_2\text{CO}_3$  solution. After gas formation ceased, the organic layer was separated via pipet and filtered through a plug of Celite. The filtrate was analyzed by GC-FID. Yields and concentrations of PhOAc are reported as averages of two independent vial reactions. The concentrations of PhOAc were used to obtain initial rates and standard error using the program Kaleidagraph. The rates and standard error were then plotted as a function of concentration of the varied reagent, which was fit to a curve using a non-linear least squares fit for the function  $y = a \cdot x^b$ , where  $y$  = initial rate of reaction input,  $a = k_{\text{obs}}$  output,  $x$  = [varied reagent] input, and  $b$  = order in varied reagent output.

### **General Procedure for Kinetics Using $\text{Pd}(\text{OAc})_2$ :Ligand (1:1)**

$\text{Pd}(\text{OAc})_2$  was measured from a 0.0445 M stock solution (100 mg  $\text{Pd}(\text{OAc})_2$  dissolved in 10.0 mL DCM) using a Hamilton gastight syringe into a 1-dram vial equipped with a Teflon-coated stirbar. This aliquot was stirred open to air at room temperature for at least 2 h to allow the solvent to evaporate to dryness. To the vial containing the resulting solid  $\text{Pd}(\text{OAc})_2$ ,  $\text{PhI}(\text{OAc})_2$  was added, followed by  $\text{C}_6\text{F}_6$  (measured by plastic, disposable syringe), benzene or benzene- $\text{d}_6$  (measured by plastic, disposable syringe), and  $\text{Ac}_2\text{O}$  (20  $\mu\text{L}$ ; measured by Hamilton gastight syringe). Pyridine derivatives were added as stock solutions in AcOH (0.18 mL; measured by plastic, disposable syringe). The vial was tightly

sealed with a Teflon-lined screw cap and heated to 100 °C in a preheated, aluminum heating block. After the desired reaction time (measured precisely by a timer), the reaction was flash-cooled in a liquid nitrogen bath until frozen solid (about 45 s). The reaction was then allowed to warm back up to room temperature, and 10  $\mu$ L PhCl (GC internal standard) were added using a 25  $\mu$ L Hamilton gastight syringe. The reaction mixture was diluted with EtOAc (1 mL) and transferred to a 20 mL scintillation vial containing 2 mL of a 4 M aqueous  $K_2CO_3$  solution. After gas formation ceased, the organic layer was separated via pipet and filtered through a plug of Celite. The filtrate was analyzed by GC-FID. Yields and concentrations of PhOAc are reported as averages of two independent vial reactions and are calculated using a calibration curve. These concentrations of PhOAc were used to obtain the initial rates and standard error using the program Kaleidagraph. The initial rates and standard error were then plotted as a function of concentration of the varied reagent, which was fit to a curve using a non-linear least squares fit for the function  $y = a \cdot x^b$ , where  $y$  = rate of reaction input,  $a = k_{obs}$  output,  $x$  = [varied reagent] input, and  $b$  = order in varied reagent output.

### **General Procedure for Kinetics Using Pd(OAc)<sub>2</sub>:Ligand (1:2)**

Pd(OAc)<sub>2</sub> and pyridine were measured from a 0.0445 M in Pd/0.0896 M in ligand stock solution in DCM (100 mg/0.445 mmol Pd(OAc)<sub>2</sub> + 0.896 mmol pyridine dissolved in 10.0 mL DCM) using a Hamilton gastight syringe into a 1-dram vial equipped with a Teflon-coated stirbar. This aliquot was stirred open to air at room temperature for at least 2 h to allow the solvent to evaporate to dryness. To the vial containing the resulting solid Pd(OAc)<sub>2</sub>, PhI(OAc)<sub>2</sub> was added, followed by C<sub>6</sub>F<sub>6</sub> (measured by plastic, disposable syringe), benzene or benzene-d<sub>6</sub> (measured by plastic, disposable syringe), AcOH (0.18 mL; measured by plastic, disposable syringe), and Ac<sub>2</sub>O (20  $\mu$ L; measured by Hamilton gastight syringe). The vial was tightly sealed with a Teflon-lined screw cap and heated to 100 °C in a preheated, aluminum heating block. After the desired reaction time (measured precisely by a timer), the reaction was flash-cooled in a liquid nitrogen bath until frozen solid (about 45 s). The reaction was then allowed to warm back up to room temperature, and 10  $\mu$ L PhCl (GC internal standard) were added using a 25  $\mu$ L Hamilton gastight syringe. The reaction mixture was diluted with EtOAc (1 mL) and transferred to a 20 mL scintillation vial containing 2 mL of a 4 M aqueous  $K_2CO_3$  solution. After gas formation

ceased, the organic layer was separated via pipet and filtered through a plug of Celite. The filtrate was analyzed by GC-FID. Yields and concentrations of PhOAc are reported as averages of two independent vial reactions and are calculated using a calibration curve. These concentrations of PhOAc were used to obtain the initial rates and standard error using the program Kaleidagraph. The initial rates and standard error were then plotted as a function of concentration of the varied reagent, which was fit to a curve using non-linear least squares fit for the function  $y = a * x^b$ , where  $y$  = rate of reaction input,  $a = k_{obs}$  output,  $x$  = [varied reagent] input, and  $b$  = order in varied reagent output.

### **Procedure for Molecular Weight Determination by Internal Reference Diffusion-Ordered NMR Spectroscopy (DOSY)**

To an NMR tube was added Pd(OAc)<sub>2</sub> (6.3 mg, 28 μmol, 1.0 equiv), pyridine (2.3 μL, 28 μmol, 1.0 equiv), 18-crown-6 (0.3 mg, 1.1 μmol, 0.04 equiv), cyclooctane (0.2 μL, 1.7 μmol, 0.060 equiv), (IMes)<sub>2</sub>Pd(OAc)<sub>2</sub> (2.3 mg, 28 μmol, 1.0 equiv), 1,3,5-tris(trifluoromethyl)benzene (1.6 μL, 8.5 μmol, 0.30 equiv), 4,4'-di-*tert*-butyl-1,1'-biphenyl (1.9 mg, 7.1 μmol, 0.25 equiv), (C<sub>6</sub>F<sub>5</sub>)<sub>2</sub>Si(CH<sub>3</sub>)<sub>2</sub> (1.3 μL, 4.8 μmol, 0.17 equiv), C<sub>6</sub>D<sub>6</sub> (0.2 mL), and CD<sub>3</sub>CO<sub>2</sub>D (0.2 mL). The equivalents of standards added were chosen to regulate the intensity of the peaks in the NMR spectra. The DOSY spectrum was then recorded at 25.0 °C using a Varian vnmrs 500 (500.10 MHz for <sup>1</sup>H) using the following parameters: 1 s relaxation delay, 8 scans, 1 ms diffusion gradient, and 200 ms diffusion delay.

The diffusion coefficient ( $D$ ) and molecular weight ( $MW$ ) are related by the equation:

$$\log(D) = A * \log(MW) + B$$

$A$  and  $B$  are coefficients that depend on reaction conditions such as temperature, density, and solvent viscosity. Using a set of standards,  $A$  and  $B$  can be solved for under the NMR reaction conditions as the slope and intercept of a plot of  $\log(MW)$  versus  $\log(D)$ .

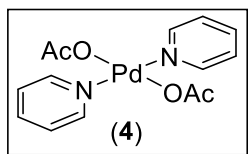
### **Procedure for the Mixed Pyridines Experiment**

Pd(OAc)<sub>2</sub> (5.0 mg, 22 μmol, 1.0 equiv) was weighed into 5 different NMR tubes. 4-*tert*-Butylpyridine and/or 4-methoxypyridine (see Table 3.2 for amounts) were added to each tube, followed by C<sub>6</sub>D<sub>6</sub> (0.4 mL). Each tube was capped and sonicated for 5 min. <sup>1</sup>H NMR spectra were recorded on a Varian vnmrs 700 (699.76 MHz for <sup>1</sup>H).

**Table 3.2.** Amounts of pyridine derivatives for the mixed pyridines experiment

Entry	Tube	Pyridine Derivative used
1	A	4- <i>tert</i> -Butylpyridine
2	B	4- <i>tert</i> -Butylpyridine (6.5 $\mu$ L, 45 $\mu$ mol, 2.0 equiv)
3	C	4- <i>tert</i> -Butylpyridine (3.3 $\mu$ L, 22 $\mu$ mol, 1.0 equiv)
4	D	4- <i>tert</i> -Butylpyridine (3.3 $\mu$ L, 22 $\mu$ mol, 1.0 equiv) + 4-Methoxypyridine (2.3 $\mu$ L, 22 $\mu$ mol, 1.0 equiv)
5	E	4-Methoxypyridine (2.3 $\mu$ L, 22 $\mu$ mol, 1.0 equiv)
6	F	4-Methoxypyridine (4.5 $\mu$ L, 45 $\mu$ mol, 2.0 equiv)
7	G	4-Methoxypyridine

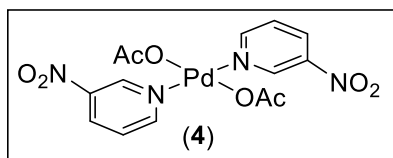
### 3.6 CHARACTERIZATION



$^1\text{H}$  NMR ( $\text{CD}_3\text{CO}_2\text{D}$ , 500 MHz):  $\delta$  8.67 (dd,  $J$  = 6.5, 1.5 Hz, 4 H), 7.95 (tt,  $J$  = 7.7, 1.5 Hz, 2H), 7.50 (dd,  $J$  = 7.7, 6.5 Hz, 4H), 2.09 (s, 6 H).

$^{13}\text{C}$  NMR ( $\text{CD}_3\text{CO}_2\text{D}$ , 178 MHz):  $\delta$  151.96, 139.98, 125.86, 20.13.

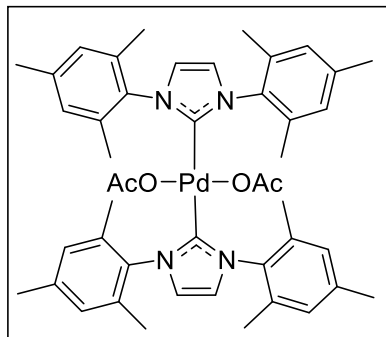
(C=O resonance of **4** is underneath C=O resonance of solvent).



Elemental analysis: calculated for  $\text{C}_{14}\text{H}_{14}\text{N}_4\text{O}_8\text{Pd}$ , C: 35.57, H: 2.99, N: 11.85, found C: 35.64, H: 2.97, N: 11.72.

IR (ATR):  $\nu$ =3058 (w), 2029 (w), 2000 (w), 1594 (m), 1573 (m), 1593 (m), 1436 (w), 1354 (m), 1318 (m), 1291 (m), 1194 (w), 1118 (w), 1054 (w), 1023 (w), 927 (w), 867 (m), 832 (m), 728 (m), 697 (m), 684 (m)  $\text{cm}^{-1}$ .

$^1\text{H}$  NMR ( $\text{C}_6\text{D}_6/\text{CD}_3\text{CO}_2\text{D}$  (1:1), 400 MHz):  $\delta$  9.36 (d,  $J = 2.3$  Hz, 2 H), 8.83 (dd,  $J = 5.6$ ,



1.2 Hz, 2H), 8.08 (ddd,  $J = 8.5, 2.3, 1.2$  Hz, 2 H), 7.13 (dd,  $J = 8.5, 5.6$  Hz, 1 H), 1.78 (s, 6 H).

$^{13}\text{C}$  NMR ( $\text{C}_6\text{D}_6/\text{CD}_3\text{CO}_2\text{D}$  (1:1), 178 MHz):  $\delta$  177.98, 156.27, 147.21, 145.00, 134.20, 125.73, 20.12.

$^1\text{H}$  NMR ( $\text{CDCl}_3$ , 500 MHz):  $\delta$  6.92 (s, 8 H), 6.75 (s, 4H), 2.45 (s, 12 H), 1.97 (s, 24 H), 1.25 (s, 6 H).

$^{13}\text{C}$  NMR ( $\text{CDCl}_3$ , 178 MHz):  $\delta$  174.84, 170.04, 137.48, 136.16, 136.14, 128.85, 122.28, 22.89, 21.30, 18.56.

### 3.7 REFERENCES

- (1) Adapted with permission from Cook, A. K.; Sanford, M. S. *J. Am. Chem. Soc.*, **2015**, *137*, pp 3109. © American Chemical Society.
- (2) (a) Lyons, T. W.; Sanford, M. S. *Chem. Rev.* **2010**, *110*, 1147. (b) Muniz, K. *Angew. Chem. Int. Ed.* **2009**, *48*, 9412.
- (3) (a) Noisier, A. F. M.; Brimble, M. A. *Chem. Rev.* **2014**, *114*, 8775. (b) Yamaguchi, J.; Yamaguchi, A. D.; Itami, K. *Angew. Chem. Int. Ed.* **2014**, *51*, 8960. (c) Wencel-Delord, J.; Glorius, F. *Nat. Chem.* **2013**, *5*, 369. (d) Chen, D. Y.-K.; Youn, S. W. *Chem. Eur. J.* **2012**, *18*, 9452. (e) Gutkunst, W. R.; Baran, P. S. *Chem. Soc. Rev.* **2011**, *40*, 1976. (f) McMurray, L.; O'Hara, F.; Gaunt, M. J. *Chem. Soc. Rev.* **2011**, *40*, 1885. (g) Godula, K.; Sames, D. *Science* **2006**, *312*, 67.
- (4) For examples of mechanistic studies of ligand-directed Pd-catalyzed C(sp<sup>2</sup>)-H functionalization, see: (a) Yang, Y.-F.; Cheng, G.-J.; Liu, P.; Leow, D.; Sun, T.-Y.; Chen, P.; Zhang, X.; Yu, J.-Q.; Wu, Y.-D.; Houk, K. N. *J. Am. Chem. Soc.* **2014**, *136*, 344. (b) Baxter, R. D.; Sale, D.; Engle, K. M.; Yu, J.-Q.; Blackmond, D. G. *J. Am. Chem. Soc.* **2012**, *134*, 4600. (c) Iglesias, Á.; Álvarez, R.; de Lera, Á. R.; Muñoz, K. *Angew. Chem. Int. Ed.* **2012**, *51*, 2225. (d) Powers, D. C.; Ritter, T. *Acc. Chem. Res.* **2012**, *45*, 840. (e) Ackermann, L. *Chem. Rev.* **2011**, *111*, 1315. (f) Lyons, T. W.; Hull, K. L.; Sanford, M. S. *J. Am. Chem. Soc.* **2011**, *133*, 4455. (g) Engle, K. M.; Wang, D.-H.; Yu, J.-Q. *J. Am. Chem. Soc.* **2010**, *132*, 14137. (h) Powers, D. C.; Xiao, D. Y.; Geibel, M. A.; Ritter, T. *J. Am. Chem. Soc.* **2010**, *132*, 14530. (i) Deprez, N. R.; Sanford, M. S. *J. Am. Chem. Soc.* **2009**, *131*, 11234. (j) Powers, D. C.; Ritter, T. *Nat. Chem.* **2009**, *1*, 302. (k) Stowers, K. J.; Sanford, M. S. *Org. Lett.* **2009**, *11*, 4584. (l) Desai, L. V.; Stowers, K. J.; Sanford, M. S. *J. Am. Chem. Soc.* **2008**, *130*, 13285. (m) Li, J.-J.; Giri, R.; Yu, J.-Q. *Tetrahedron* **2008**, *64*, 6979. (n) Hull, K. L.; Lanni, E. L.; Sanford, M. S. *J. Am. Chem. Soc.* **2006**, *128*, 14047. (o) Yu, J.-Q.; Giri, R.; Chen, X. *Org. Biomol. Chem.* **2006**, *4*, 4041. (p) Kalyani, D.; Deprez, N. R.; Desai, L. V.; Sanford, M. S. *J. Am. Chem. Soc.* **2005**, *127*, 7330.
- (5) For reviews of computational studies on the mechanism of CMD-type C-H activation, see: (a) Balcells, D.; Clot, E.; Eisenstein, O. *Chem. Rev.* **2010**, *110*, 749. (b) Lapointe, D.; Fagnou, K. *Chem. Lett.* **2010**, *39*, 1118. (c) Boutadla, Y.; Davies, D. L.; Macgregor, S. A.; Poblador-Bahamonde, A. I. *Dalton Trans.* **2009**, 5820.
- (6) For a review on methodological studies of C-H activation/functionalization with substrates that do not bear directing groups, see: (a) Kuhl, N.; Hopkinson, M. N.; Wencel-Delord, J.; Glorius, F. *Angew. Chem. Int. Ed.* **2012**, *51*, 10236. For a subsequent report of C-H amination with substrates that do not bear directing groups, see: (b) Shrestha, R.; Mukherjee, P.; Tan, Y.; Litman, Z. C.; Hartwig, J. F. *J. Am. Chem. Soc.* **2013**, *135*, 8480. For subsequent reports on C-H arylation with substrates that do not bear directing groups, see: (c) Durak, L. J.; Lewis, J. C. *Organometallics* **2014**, *33*, 620. (d) Storr,

- T. E.; Namata, F.; Greaney, M. F. *Chem. Commun.* **2014**, 50, 13275. (e) Wang, S.; Liu, W.; Cen, J.; Liao, J.; Huang, J.; Zhan, H. *Tetrahedron Lett.* **2014**, 55, 1589. (f) Yan, T.; Zhao, L.; He, M.; Soulé, J.-F.; Bruneau, C.; Doucet, H. *Adv. Synth. Catal.* **2014**, 356, 1586. (g) Zhao, L.; Yan, T.; Bruneau, C.; Doucet, H. *Catal. Sci. Technol.* **2014**, 4, 352. (h) Cambeiro, X. C.; Boorman, T. C.; Lu, P.; Larrosa, I. *Angew. Chem. Int. Ed.* **2013**, 52, 1781. (i) Wagner, A. M.; Sanford, M. S. *J. Am. Chem. Soc.* **2013**, 135, 15110. (j) Ren, X.; Wen, P.; Shi, X.; Wang, Y.; Li, J.; Yang, S.; Yan, H.; Huang, G. *Org. Lett.* **2013**, 15, 5194. (k) Storr, T. E.; Greaney, M. F. *Org. Lett.* **2013**, 15, 1410. (l) Wencel-Delord, J.; Nimphius, C.; Wang, H.; Glorius, F. *Angew. Chem. Int. Ed.* **2012**, 51, 13001. (m) Zhou, L.; Lu, W. *Organometallics*, **2012**, 31, 2124. For subsequent reports on C–H olefination with substrates that do not bear directing groups, see: (n) Gigant, N.; Bäckvall, J.-E. *Org. Lett.* **2014**, 16, 4432. (o) Gigant, N.; Bäckvall, J.-E. *Org. Lett.* **2014**, 16, 1664. (p) Jin, W.; Wong, W.-T.; Law, G.-L. *Chem. Cat. Chem.* **2014**, 6, 1599. (q) Pham, M. V.; Cramer, N. *Angew. Chem. Int. Ed.* **2014**, 53, 3484. (r) Vora, H. U.; Silvestri, A. P.; Engelin, C. J.; Yu, J.-Q. *Angew. Chem. Int. Ed.* **2014**, 53, 2683. (s) Ying, C.-H.; Yan, S.-B.; Duan, W.-L. *Org. Lett.* **2014**, 16, 500. (t) Zhou, L.; Lu, W. *Chem. Eur. J.* **2014**, 20, 634. (u) Min, M.; Choe, H.; Hong, S. *Asian J. Org. Chem.* **2012**, 1, 47. (v) Wencel-Delord, J.; Nimphius, C.; Patureau, F. W.; Glorius, F. *Chem. Asian J.* **2012**, 7, 1208. For a subsequent report on C–H carboxylation with substrates that do not bear directing groups, see: (w) Suga, T.; Mizuno, H.; Takaya, J.; Iwasawa, N. *Chem. Commun.* **2014**, 50, 14360.
- (7) For mechanistic studies on C–H activation/functionalization with substrates that do not bear directing groups, see: (a) Cheng, C.; Hartwig, J. F. *J. Am. Chem. Soc.* **2014**, 136, 12064. (b) Wang, D.; Izawa, Y.; Stahl, S. S. *J. Am. Chem. Soc.* **2014**, 136, 9914. (c) Sanhueza, I. A.; Wagner, A. M.; Sanford, M. S.; Schoenebeck, F. *Chem. Sci.* **2013**, 4, 2767. (d) Wagner, A. M.; Hickman, A. J.; Sanford, M. S. *J. Am. Chem. Soc.* **2013**, 135, 15710. (e) Lyons, T. W.; Hull, K. L.; Sanford, M. S. *J. Am. Chem. Soc.* **2011**, 133, 4455. (f) Tan, Y.; Hartwig, J. F. *J. Am. Chem. Soc.* **2011**, 133, 3308. (g) Zhang, S.; Shi, L.; Ding, Y. *J. Am. Chem. Soc.* **2011**, 133, 20218. (h) Hull, K. L.; Sanford, M. S. *J. Am. Chem. Soc.* **2009**, 131, 9651. (i) Biswas, B.; Sugimoto, M.; Sakaki, S. *Organometallics* **2000**, 19, 3895.
- (8) For reviews summarizing various approaches to non-directed C–H functionalization, see: (a) Ref. 5a. (a) Neufeldt, S. R.; Sanford, M. S. *Acc. Chem. Res.* **2012**, 45, 936. (b) Brückl, T.; Baxter, R. D.; Ishihara, Y.; Baran, P. S. *Acc. Chem. Res.* **2012**, 45, 826. (b) Newhouse, T.; Baran, P. S. *Angew. Chem. Int. Ed.* **2011**, 50, 3362. (c) Shul'pin, G. *Org. Biomol. Chem.* **2010**, 8, 4217. (c) Ref. 2g. (d) Dick, A. R.; Sanford, M. S. *Tetrahedron* **2006**, 62, 2439. For a perspective on the role of ligands in C–H activation, see: (e) Engle, K. M.; Yu, J.-Q. *J. Org. Chem.* **2013**, 78, 8927.
- (9) (a) Cook, A. K.; Emmert, M. H.; Sanford, M. S. *Org. Lett.* **2013**, 15, 5428. (b) Gary, J. B.; Cook, A. K.; Sanford, M. S. *ACS Catal.* **2013**, 3, 700. (c) Emmert, M. H.; Cook, A. K.; Xie, Y. J.; Sanford, M. S. *Angew. Chem. Int. Ed.* **2011**, 50, 9409. (d) Emmert, M. H.; Gary, J. B.; Villalobos, J. M.; Sanford, M. S. *Angew. Chem. Int. Ed.* **2010**, 49, 5884.
- (10) For Pd-catalyzed C–H acetoxylation of arenes using K<sub>2</sub>S<sub>2</sub>O<sub>8</sub> as oxidant, see: (a) Ebersson, L.; Jonsson, L. *Liebigs Ann. Chem.* **1977**, 233. (b) Ebersson, L.; Jonsson, L. *Acta Chem. Scand. B* **1976**, 30, 361. (c) Ebersson, L.; Jonsson, L. *Acta Chem. Scand. B* **1974**, 28, 771. (d) Ebersson, L.; Jonsson, L. *J. Chem. Soc., Chem. Commun.* **1974**, 885.
- (11) For Pd-catalyzed C–H acetoxylation of arenes using chromates, nitrogen oxides, and dioxygen as oxidants, see: Ref. 9a-c, (a) Ebersson, L.; Gomez-Gonzales, L. *J. Chem. Soc. D* **1971**, 263. (b) Stock, L. M.; Tse, K.; Vorvick, L. J.; Walstrum, S. A. *J. Org. Chem.* **1981**, 46, 1757. (c) Henry, P. M. *J. Org. Chem.* **1971**, 36, 1886. (d) Tissue, T.; Downs, W. J. *J. Chem. Soc. D.* **1969**, 410a. (e) Davidson, J. M.; Triggs, C. *J. Chem. Soc. A* **1968**, 1331.
- (12) For related work on Pd-catalyzed C–H hydroxylation of arenes, see: (a) Guo, H.; Chen, Z.; Mei, F.; Zhu, D.; Xiong, H.; Yin, G. *Chem. Asian J.* **2013**, 8, 888. (b) Liang, P.; Xiong, H.; Guo, H.; Yin, G. *Catal. Commun.* **2010**, 11, 560. (c) Lee, J. H.; Yoo, K. S.; Park, C. P.; Olsen, J. M.; Sakaguchi, S.; Prakash, G. K. S.; Mathew, T.; Jung, K. W. *Adv. Synth. Catal.* **2009**, 351, 563. (d) Liu, Y.; Murata, K.; Inaba, M. *J. Mol. Catal. A* **2006**, 256, 247. (e) Shibahara, F.; Kinoshita, S.; Nozaki, K. *Org. Lett.* **2004**, 6, 2437. (f) Passoni, L. C.; Cruz, A. T.; Buffon, R.; Schuchardt, U. *J. Mol. Catal. A* **1997**, 120, 117. (g) Jintoku, T.; Takaki, K.; Fujiwara, Y.; Fuchita, Y.; Hiraki, K. *Bull. Chem. Soc. Jpn.* **1990**, 63, 438. (h) Jintoku, T.; Taniguchi, H.; Fujiwara, Y. *Chem. Lett.* **1987**, 1865.
- (13) (a) Yoneyama, T.; Crabtree, R. H. *J. Mol. Catal. A* **1996**, 108, 35. For subsequent work on Pd-catalyzed C–H acetoxylation using PhI(OAc)<sub>2</sub>, see: (b) Tato, F.; García-Domínguez, A.; Cárdenas, D. J.



- 
- Organometallics* **2013**, 32, 7487. (c) Wang, N.; McCormick, T. M.; Ko, S.-B.; Wang, S. *Eur. J. Inorg. Chem.* **2012**, 4463.
- (14) (a) Kubota, A.; Emmert, M. H.; Sanford, M. S. *Org. Lett.* **2012**, 14, 1760. (b) Zhang, Y.-H.; Shi, B.-F.; Yu, J.-Q. *J. Am. Chem. Soc.* **2009**, 131, 5072. For an additional report in which a mono-pyridine/Pd complex is implied as an intermediate, see: (c) Stuart, D. R.; Fagnou, K. *Science* **2007**, 316, 1172.
- (15) (a) Steinhoff, B. A.; Stahl, S. S. *Org. Lett.* **2002**, 4, 4179. For additional reports in which mono-pyridine/Pd complexes are implied as intermediates, see: (b) Ye, X.; Liu, G.; Popp, B. V.; Stahl, S. S. *J. Org. Chem.* **2011**, 76, 1031. (c) Popp, B. V.; Stahl, S. S. *Chem. Eur. J.* **2009**, 15, 2915. (d) Schultz, M. J.; Adler, R. S.; Zierkiewicz, W.; Privalov, T.; Sigman, M. S. *J. Am. Chem. Soc.* **2005**, 127, 8499.
- (16) Stephenson, T. A.; Morehouse, S. M.; Powell, A. R.; Heffer, J. P.; Wilkinson, G. *J. Chem. Soc.* **1965**, 3632.
- (17) Simmons, E. M.; Hartwig, J. F. *Angew. Chem. Int. Ed.* **2001**, 51, 3066.
- (18) Gary, J. B.; Sanford, M. S. *Organometallics* **2011**, 30, 6143.
- (19) Trend, R. M.; Ramtohul, Y. K.; Stoltz, B. M. *J. Am. Chem. Soc.* **2005**, 127, 17778.
- (20) (a) Steinhoff, B. A.; Guzei, I. A.; Stahl, S. S. *J. Am. Chem. Soc.* **2004**, 126, 11268. (b) King, A. E.; Ryland, B. L.; Brunold, T. C.; Stahl, S. S. *Organometallics* **2012**, 31, 7948.
- (21) Boller, T. M.; Murphy, J. M.; Hapke, M.; Ishiyama, T.; Miyaura, N.; Hartwig, J. F. *J. Am. Chem. Soc.* **2005**, 127, 14263.
- (22) (a) Macchioni, A.; Ciancaleoni, G.; Zuccaccia, C.; Zuccaccia, D. *Supramolec. Chem.: From Mol. to Nanomat.* **2012**, 1. (b) Li, D.; Keresztes, I.; Hopson, R.; Willard, P. G. *Acc. Chem. Res.* **2009**, 42, 270.
- (23) For a review on the method of continuous variations, a related technique used to quantify aggregation, see Renny, J. S.; Tomasevich, L.L.; Tallmadge, E. H.; Collum, D. B. *Angew. Chem. Int. Ed.* **2013**, 52, 11998.
- (24) For a study on the trans influence as a function of pyridine substituents, see: Woods, C.; Daffron, C. *Inorg. Chim. Acta* **1985**, 101, 13.
- (25) Appleton, T.G.; Clark, H. C.; Manzer, L. E. *Coord. Chem. Rev.* **1973**, 10, 335.
- (26) Trend, R. M.; Ramtohul, Y. K.; Stoltz, B. M. *J. Am. Chem. Soc.* **2005**, 127, 17778.
- (27) Powers, D. C.; Benitez, D.; Tkatchouk, E.; Goddard III, W. A.; Ritter, T. *J. Am. Chem. Soc.* **2010**, 132, 14092.
- (28) Konnick, M. M.; Guzei, I. A.; Stahl, S. S. *J. Am. Chem. Soc.* **2004**, 126, 10212.

# CHAPTER 4. STERIC CONTROL OF SITE SELECTIVITY IN THE Pd-CATALYZED C–H ACETOXYLATION OF SIMPLE ARENES<sup>1</sup>

## 4.1 INTRODUCTION

The ability to oxidatively transform carbon–hydrogen bonds into carbon–heteroatom bonds is highly desirable for the late-stage derivatization of complex molecules. Such transformations have the potential to greatly expedite the discovery and optimization of biologically active molecules including pharmaceuticals and agrochemicals.<sup>2</sup> However, the full potential of this strategy has not yet been realized, in large part due to the difficulty of controlling site-selectivity.<sup>3</sup> While many advances have been made in Pd-catalyzed ligand-directed C–H oxidation,<sup>1-4</sup> analogous non-chelate-assisted transformations remain relatively poorly developed.<sup>2-5</sup> For example, the Pd-catalyzed C–H oxygenation of simple arenes is typically characterized by the formation of complex mixtures of isomers.<sup>5,6</sup> In many of these systems, the selectivity is governed by electronic factors, with C–H oxidation occurring preferentially at the more electron rich site(s) in the substrate.<sup>5,6</sup>

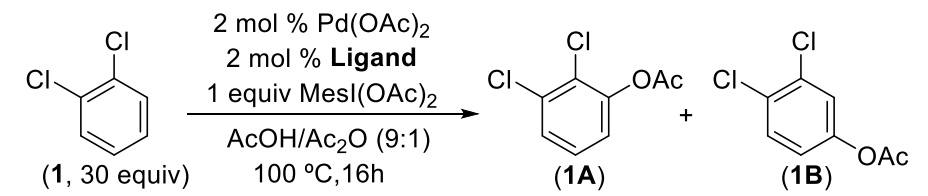
We recently reported that pyridine dramatically accelerates the Pd(OAc)<sub>2</sub>-catalyzed C–H acetoxylation of simple arenes.<sup>7,8,9</sup> Pyridine is believed to serve as a ligand for Pd during this process, and the ratio of pyridine: Pd was found to be critical to high rates and yields (an approximately 1:1 ratio was optimal). We hypothesized that, in addition to accelerating the rate of C–H acetoxylation, the ancillary ligand could also be used to influence the site selectivity of the reaction. Such ligand-modulated selectivity would provide opportunities for accessing different isomeric products by simply changing the catalyst structure.<sup>3</sup> Herein we report the realization of this strategy in the development of pyridine-based ligands that impart sterically-controlled selectivity<sup>10,11</sup> in Pd-catalyzed C–H acetoxylation.

## 4.2 RESULTS AND DISCUSSION

Our initial studies probed the effect of a series of pyridine-based ligands on the selectivity of the C–H acetoxylation of 1,2-dichlorobenzene (**1**) with  $\text{MeI}(\text{OAc})_2$ .<sup>12</sup> Pyridine and its derivatives are highly attractive ligands for this chemistry because: (1) they are generally not susceptible to oxidation with hypervalent iodine reagents, (2) they are known to increase the rate of C–H acetoxylation,<sup>7b</sup> and (3) they possess highly modular structures. The test substrate **1** was selected because it has two inequivalent arene C–H bonds that are electronically similar, but sterically dissimilar. Furthermore, electron-deficient arenes like **1** are traditionally difficult to functionalize via Pd-catalyzed C–H acetoxylation.<sup>6,7b,13</sup>

In the absence of added ligand, the  $\text{Pd}(\text{OAc})_2$ -catalyzed reaction of **1** with  $\text{MeI}(\text{OAc})_2$  proceeded in low yield (19%) after 16 h at 100 °C (Table 4.1, entry 1). Acetoxylation at the less sterically-hindered B-position was weakly preferred under these ligand-free conditions (**1A:1B**=29:71). A similar yield and selectivity were obtained in the presence of 2 mol % of 2,6-di-*tert*-butylpyridine (entry 2), suggesting that the very sterically hindered nitrogen atom does not bind to the Pd center. In contrast, pyridine and its derivatives including lutidine, picoline, quinoline, 2-methylquinoline, 3-fluoropyridine, pyridine, 4-methoxypyridine, and acridine (entries 3-10) all afforded large increases in yield and enhancements in selectivity for acetoxylation at the sterically less hindered B-position. Pyridine, 4-methoxypyridine, and 3-fluoropyridine afforded identical selectivity, suggesting that there is minimal ligand electronic effect on this reaction. Under these conditions, the best selectivity was obtained with acridine as the ligand (**1A:1B**=5:95, entry 10).

**Table 4.1.** Effect of pyridine ligands on site selectivity and yield for the C–H acetoxylation of 1,2-dichlorobenzene

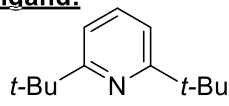


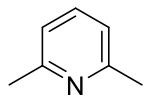
$2 \text{ mol } \% \text{ Pd(OAc)}_2$   
 $2 \text{ mol } \% \text{ Ligand}$   
 $1 \text{ equiv MesI(OAc)}_2$   
 $\text{AcOH/Ac}_2\text{O (9:1)}$   
 $100 \text{ }^\circ\text{C, 16h}$

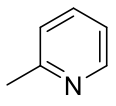
(1, 30 equiv)      (1A)      (1B)

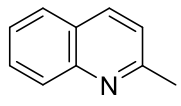
---

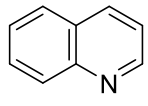
**Ligand:**

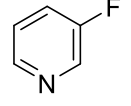
  
2,6-*t*-Bu<sub>2</sub>-pyr

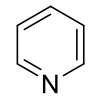
  
2,6-lutidine

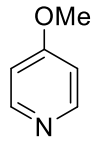
  
2-picoline

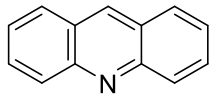
  
2-Me-quinoline

  
quinoline

  
3-F-pyr

  
pyridine

  
4-OMe-pyr

  
acridine

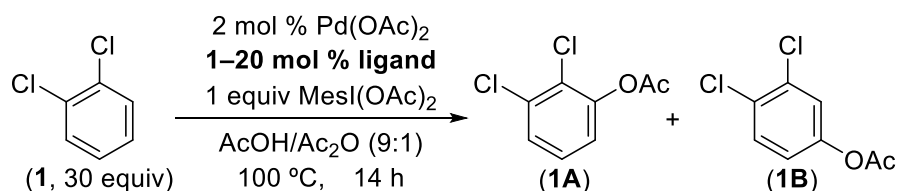
Entry	Ligand	Yield (%) <sup>a</sup>	Selectivity (1A:B)
1	none	19	29:71
2	2,6- <i>t</i> -Bu <sub>2</sub> -pyr	28	27:73
3	2,6-lutidine	76	11:89
4	2-picoline	84	8:82
5	quinoline	82	7:93
6	2-Me-quinoline	77	7:93
7	3-F-pyr	55	6:94
8	pyridine	71	6:94
9	4-OMe-pyr	59	6:94
10	acridine	78	5:95

<sup>a</sup>Yield and selectivity were determined by GC using a calibration curve based on PhCl as a standard.

We next evaluated the influence of the acridine: Pd ratio on the reaction yield and site selectivity. As shown in Table 4.2, the addition of up to 6 mol % of acridine (3 equivalents relative to Pd) led to further enhancements in selectivity (**1A:1B**=2:98) with minimal deleterious effect on the overall reaction yield (entry 4). Further increases in acridine loading resulted in even better selectivity (>1:99 at 20 mol % acridine, entry 7); however, the product yield was significantly lower under these conditions. Notably, the results with acridine stand in striking contrast to the effects observed upon increasing the loading of pyridine. As shown in entries 8-11, increasing the pyridine loading to 6 mol %

led to a precipitous drop-off in yield. Overall, an acridine:Pd ratio of 3:1 provided the best balance of reactivity and selectivity, and was thus used in all further experiments exploring the substrate scope.

**Table 4.2.** Optimization of Pd(OAc)<sub>2</sub>/acridine-catalyzed C–H acetoxylation of 1,2-dichlorobenzene



Entry	Ligand	Ligand loading (mol %)	Yield <sup>a</sup> (%)	Selectivity (1A:1B)
1	acridine	1	79	10:90
2	acridine	2	78	5:95
3	acridine	3	78	5:95
4	acridine	6	76	2:98
5	acridine	8	68	1:99
6	acridine	10	66	1:99
7	acridine	20	29	<1:99
8	pyridine	1	62	9:91
9	pyridine	2	71	6:94
10	pyridine	3	56	7:93
11	pyridine	6	3	--- <sup>b</sup>

<sup>a</sup>Yield and selectivity were determined by GC using a calibration curve based on PhCl as a standard. <sup>b</sup>The yield was too low for accurate determination of the selectivity.

Further studies revealed that the site selectivity of Pd(OAc)<sub>2</sub>/acridine catalyzed C–H acetoxylation was substantially influenced by the nature of the oxidant (Table 4.3).<sup>7b,12</sup> For instance, a significant erosion in selectivity was observed when MesI(OAc)<sub>2</sub> was replaced with PhI(OAc)<sub>2</sub>. With 2 mol % of acridine and 2 mol % of Pd(OAc)<sub>2</sub>, the A:B selectivity was 5:95 with MesI(OAc)<sub>2</sub> (entry 2) and 19:81 with PhI(OAc)<sub>2</sub> (entry 1) as oxidant. These results suggest a synergistic effect between the hypervalent iodine oxidant and the ligand. Similar effects were seen with pyridine as the ligand (entries 3 and 4) and with no ligand added (entries 5 and 6). For example, with 2 mol % Pd(OAc)<sub>2</sub> and 2 mol %

pyridine, the selectivity (**1A:1B**) using substrate **1** was 19:81 with PhI(OAc)<sub>2</sub> and 6:94 with MesI(OAc)<sub>2</sub>.

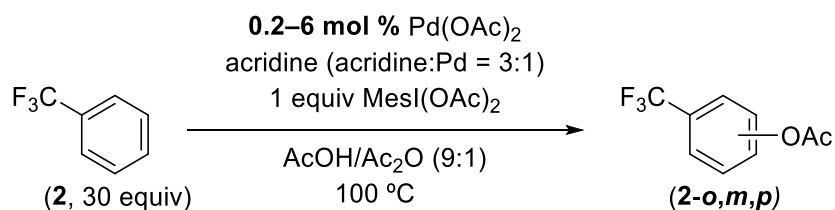
**Table 4.3.** Effect of the oxidant on site selectivity for the C–H acetoxylation of 1,2-dichlorobenzene

Reaction scheme showing the C–H acetoxylation of 1,2-dichlorobenzene (**1**, 30 equiv) using 2 mol % Pd(OAc)<sub>2</sub>, 2 mol % ligand, and 1 equiv ArI(OAc)<sub>2</sub> in AcOH/Ac<sub>2</sub>O (9:1) at 100 °C for 14 h. The products are 1-acetoxy-2,3-dichlorobenzene (**1A**) and 1-acetoxy-2,6-dichlorobenzene (**1B**).

Entry	Ligand	Oxidant	Yield (%) <sup>a</sup>	Selectivity ( <b>1A:1B</b> )
1	Acridine	PhI(OAc) <sub>2</sub>	73	19:81
2	Acridine	MesI(OAc) <sub>2</sub>	78	5:95
3	Pyridine	PhI(OAc) <sub>2</sub>	70	19:81
4	Pyridine	MesI(OAc) <sub>2</sub>	71	6:94
5	None	PhI(OAc) <sub>2</sub>	14	39:61
6	None	MesI(OAc) <sub>2</sub>	19	29:71

<sup>a</sup>Yield and selectivity were determined by GC using a calibration curve based on PhCl as a standard.

We next optimized the catalyst loading using trifluorotoluene (**2**). This substrate was selected because it is a challenging one that typically shows low reactivity in Pd-catalyzed C–H oxidations.<sup>7b,8,9</sup> Thus, we anticipated that the trends observed in this system should be transferrable to a wide variety of other substrates. Varying the catalyst loading from 6 to 0.2 mol % Pd(OAc)<sub>2</sub> while keeping the acridine: Pd ratio constant at 3:1 revealed that the reaction yield is highest at 0.5 mol % Pd (44% yield, corresponding to a TON of 88; Table 4.4, entry 5). As such, this catalyst loading was selected for subsequent experiments.

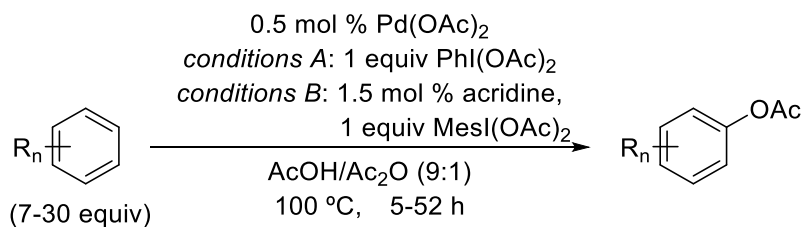
**Table 4.4.** Optimization of catalyst loading

Entry	mol % Pd	Yield (%) <sup>a</sup>	TON
1 <sup>b</sup>	6	21	3.5
2 <sup>b</sup>	4	30	7.4
3 <sup>c</sup>	2	35	18
4 <sup>b</sup>	1	36	36
5 <sup>d</sup>	0.5	44	88
6 <sup>e</sup>	0.2	38	188

<sup>a</sup>Yields determined by GC using a calibration curve based on PhCl as a standard. In all cases, the *o*:*m*:*p* selectivity was 1:76:23. Reactions were generally stopped upon observation of Pd black, as our previous studies<sup>7,8</sup> have shown that this is indicative of the reaction cessation. <sup>b</sup>22 h. <sup>c</sup>21 h. <sup>d</sup>49 h. <sup>e</sup>120 h.

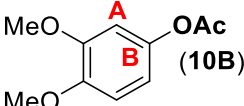
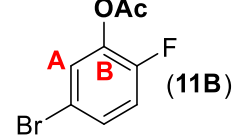
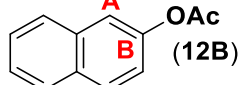
With these optimized conditions in hand, we next explored the C–H acetoxylation of a variety of mono-, di- and tri-substituted arene substrates (Table 4.5 and Table 4.6). For each substrate we compared the ligand-free conditions with PhI(OAc)<sub>2</sub> as the oxidant (*conditions A*) to the conditions with acridine as the ligand and MesI(OAc)<sub>2</sub> as the oxidant (*conditions B*). In general, *conditions A* provided modest yields and poor site selectivities. With a few exceptions, the selectivity under *conditions A* was dominated by electronic factors, with preferential functionalization at the most electron rich sites in the molecule. In contrast, *conditions B* generally provided higher product yields. Furthermore, the selectivity was typically enhanced in favor of acetoxylation at the least sterically hindered C–H bond. In many cases (e.g., **4-9** and **12**), a reversal in the favored isomer was observed upon moving from *conditions A* to *conditions B*. For example, the C–H bond at the A-position of **8** is electronically activated, and acetoxylation is favored at this site in the absence of acridine (**8A:8B**=87:13, *conditions A* of Table 4.5). This electronic bias is overridden with the Pd/acridine system, and the major product is the B-functionalized isomer (**8A:8B**=28:72, *conditions B* of Table 4.5).

**Table 4.5.** Pd(OAc)<sub>2</sub>/acridine-catalyzed C–H acetoxylation of tri- and di-substituted arenes



Product ( <b>B</b> Shown)	Yield <sup>a</sup> ( <b>A</b> : <b>B</b> Selectivity): <i>Conditions A</i>	Yield <sup>a</sup> ( <b>A</b> : <b>B</b> Selectivity): <i>Conditions B</i>	Isolated Yield ( <b>A</b> : <b>B</b> Selectivity): <i>Conditions B</i>
 ( <b>3B</b> )	44% (47:53)	64% (17:83)	55% (19:81)
 ( <b>4B</b> )	42% (65:35)	71% (22:78)	60% (5:95)
 ( <b>5B</b> )	42% (59:41)	55% (24:76)	28% (22:78)
 ( <b>6B</b> )	36% (81:19)	38% (39:61)	25% (41:59)
 ( <b>7B</b> )	29% (61:39)	49% (8:92)	53% (2:98)
 ( <b>8B</b> )	26% (87:13)	42% (28:72)	38% (<1:99)
 ( <b>9B</b> )	17% (83:17)	56% (17:83)	42% (<1:99)
 ( <b>1B</b> )	16% (44:56)	82% (4:96)	64% (2:98)



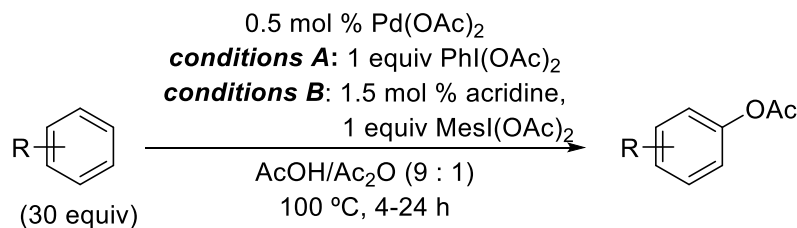
 (10B)	35% (17:83)	66% (4:96)	62% (<1:99)
 (11B)	51% (16:84)	82% (5:95)	38% (2:98)
 (12B)	69% (53:47)	88% (20:80)	60% (19:81)

<sup>a</sup>Yields and selectivities in columns 2 and 3 were determined by calibrated GC using PhCl or PhCH<sub>2</sub>C(CH<sub>3</sub>)<sub>3</sub> as a standard. **Conditions A:** 0.5 mol % Pd(OAc)<sub>2</sub>, 1 equiv PhI(OAc)<sub>2</sub>. **Conditions B:** 0.5 mol % Pd(OAc)<sub>2</sub>, 1.5 mol % acridine, 1 equiv MesI(OAc)<sub>2</sub>.

Although the product ratios using Pd/acridine/MesI(OAc)<sub>2</sub> typically reflect a preference for acetoxylation at the least hindered site, this catalyst system does not effectively distinguish between the *meta*- and *para*-positions of mono-substituted arenes. For example, *ortho*-acetoxylation of anisole (**14**) and chlorobenzene (**16**) was dramatically suppressed under *conditions B*, but a nearly 1:1 ratio of *meta* and *para* substituted products was formed (Table 4.6).

### 4.3 CONCLUSIONS

This chapter demonstrates the use of acridine as an ancillary ligand to control site selectivity in the Pd(OAc)<sub>2</sub>-catalyzed C–H acetoxylation of simple arenes. In combination with MesI(OAc)<sub>2</sub> as the terminal oxidant, the Pd(OAc)<sub>2</sub>/acridine system overrides the substrate electronic bias that dominates the site selectivity observed using ligand-free Pd(OAc)<sub>2</sub> as catalyst and PhI(OAc)<sub>2</sub> as oxidant. Instead, the site selectivity of acetoxylation using the Pd(OAc)<sub>2</sub>/acridine/MesI(OAc)<sub>2</sub> system is primarily dictated by sterics for a variety of different substrates.

**Table 4.6.** Pd(OAc)<sub>2</sub>/acridine-catalyzed C–H acetoxylation of mono-substituted arenes

Major Product	Yield <sup>a</sup> ( <i>o:m:p</i> Selectivity): Conditions A	Yield <sup>a</sup> ( <i>o:m:p</i> Selectivity): Conditions B	Isolated Yield ( <i>o:m:p</i> Selectivity): Conditions B
 (13)	12%	94%	38%
 (14p)	54% (46:6:51)	94% (12:40:48)	61% (13:24:63)
 (15m)	51% (0:16:84)	99% (0:62:38)	68% (0:60:40)
 (16m)	18% (26:27:47)	77% (5:52:43)	54% (3:49:48)
 (2m)	5% (3:74:23)	65% (3:75:22)	50% (<1:77:23)

<sup>a</sup>Yields and selectivities in columns 2 and 3 were determined by calibrated GC using PhCl or PhCH<sub>2</sub>C(CH<sub>3</sub>)<sub>3</sub> as a standard. *Conditions A:* 0.5 mol % Pd(OAc)<sub>2</sub>, 1 equiv PhI(OAc)<sub>2</sub>. *Conditions B:* 0.5 mol % Pd(OAc)<sub>2</sub>, 1.5 mol % acridine, 1 equiv MesI(OAc)<sub>2</sub>.

#### 4.4 PERSPECTIVE AND OUTLOOK

Catalyst-controlled selectivity through the use of ancillary ligands provides exciting new prospects for the field of Pd-catalyzed C–H oxidation. In this chapter, the use of MesI(OAc)<sub>2</sub> as the oxidant gave an increase in the site-selectivity, as compared to the less sterically encumbered oxidant, PhI(OAc)<sub>2</sub>. This phenomenon is unexpected, based on the mechanism of benzene acetoxylation detailed in Chapter 3, since the oxidant is not involved in the rate-limiting step nor the selectivity-determining step. It is possible that a change in mechanism or rate-limiting step has occurred under these site-selective conditions. Elucidating the role the oxidant (as well as the ligand, acridine) plays in

catalysis would be a valuable and significant contribution in the effort for further improvements in site-selectivity.

## 4.5 EXPERIMENTAL

### General procedure for the optimization of the acetoxylation of arenes

$\text{Pd}(\text{OAc})_2$  was measured from a 0.045 M stock solution into a 2 dram vial equipped with a Teflon-coated stirbar. This aliquot was stirred openly at room temperature for at least 2 h to allow the solvent to evaporate to dryness. To a vial containing the resulting solid  $\text{Pd}(\text{OAc})_2$ , the oxidant,  $\text{MesI}(\text{OAc})_2$  or  $\text{PhI}(\text{OAc})_2$ , (0.224 mmol, 1.00 equiv) was added. Then, the arene was added into the vial using a 1 mL plastic syringe.  $\text{Ac}_2\text{O}$  (20  $\mu\text{L}$ ) was then added via a 100  $\mu\text{L}$  Hamilton gastight syringe. The indicated ligand was added as a stock solution in  $\text{AcOH}$  using a 1 mL plastic syringe. The vial was sealed tightly with a Teflon-lined screw cap and heated to 100 °C for the desired time on a preheated vial plate. The reaction was cooled to room temperature and 10  $\mu\text{L}$  PhCl were added via a 25  $\mu\text{L}$  Hamilton gastight syringe as a GC standard. The reaction mixture was diluted with  $\text{EtOAc}$  (1.5 mL) and 2 mL of a 4 M aqueous  $\text{K}_2\text{CO}_3$  solution was added slowly. After gas formation ceased, an aliquot was taken from the organic layer, filtered through Celite, and analyzed by GC.

### General procedure for *conditions A* for the substrate scope

$\text{Pd}(\text{OAc})_2$  (1.26 mg, 5.61  $\mu\text{mol}$ , 0.00500 equiv) was measured from a 0.0560 M stock solution (100  $\mu\text{L}$  of a solution prepared with 126 mg  $\text{Pd}(\text{OAc})_2$  in 10.0 mL DCM) into a 20 mL scintillation vial equipped with a Teflon-coated stirbar. This aliquot was stirred at room temperature for at least 2 h to allow the DCM to evaporate to dryness.  $\text{PhI}(\text{OAc})_2$  (361 mg, 1.12 mmol, 1.0 equiv) was weighed into the vial; then the arene (11.2–33.6 mmol, 10.0–30.0 equiv) was added into the vial using a 5 mL, plastic syringe.  $\text{Ac}_2\text{O}$  (0.1 mL) and  $\text{AcOH}$  (0.9 mL) were added using 1 mL plastic syringes. The vial was sealed with a Teflon-lined screw cap and heated at 100 °C for 4–52 h on a preheated vial plate. The reactions were cooled to room temperature and 20  $\mu\text{L}$  PhCl or neopentylbenzene (GC standard) was added via a 25  $\mu\text{L}$  Hamilton gastight syringe. The reaction mixture was diluted with  $\text{EtOAc}$  (3 mL). 5 mL of a 4 M aqueous  $\text{K}_2\text{CO}_3$  solution was added slowly,

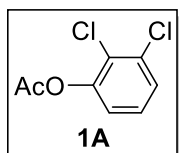
and then after gas formation ceased, an aliquot was taken from the organic layer, filtered through Celite, and analyzed by GC.

### **General procedure for *conditions B* for the substrate scope**

Pd(OAc)<sub>2</sub> (1.26 mg, 5.61 μmol, 0.00500 equiv) was measured from a 0.0560 M stock solution (100 μL of a solution prepared with 126 mg Pd(OAc)<sub>2</sub> in 10.0 mL DCM) into a 20 mL scintillation vial equipped with a Teflon-coated stirbar. This aliquot was stirred at room temperature for at least 2 h to allow the DCM to evaporate. MesI(OAc)<sub>2</sub> (408 mg, 1.12 mmol, 1.00 equiv) was weighed into the vial; then the arene (11.2–33.6 mmol, 10.0–30.0 equiv) was added into the vial using a 5 mL plastic syringe. Ac<sub>2</sub>O (0.10 mL) was added via a 1 mL plastic syringe. Acridine (0.0168 mmol, 0.0150 equiv) was added as a stock solution in AcOH (0.90 mL of 0.019 M) using a 1 mL plastic syringe. The vial was sealed with a Teflon-lined screw cap and heated at 100 °C for 4–52 h on a preheated vial plate. Reactions were determined to be complete when the formation of Pd-black was observed. The reactions were cooled to room temperature, and 20 μL PhCl or neopentylbenzene (GC standard) were added using a 25 μL Hamilton gastight syringe. The reaction mixture was diluted with EtOAc (3 mL), 5 mL of a 4 M aqueous K<sub>2</sub>CO<sub>3</sub> solution was added slowly, and after gas formation ceased, an aliquot was taken from the organic layer, filtered through Celite, and analyzed by GC. The organic layer was separated, dried over MgSO<sub>4</sub>, and concentrated. The material was then purified via column chromatography.

## **4.6 CHARACTERIZATION**

Mixtures of isomers were compared to the independently synthesized compounds from their respective phenols in an analogy to a literature procedure.<sup>14</sup> The following compounds have been previously characterized in the literature: **6B**,<sup>15</sup> **8B**,<sup>16</sup> **9B**,<sup>17</sup> **10B**,<sup>18</sup> **12A**,<sup>19</sup> **12B**,<sup>20</sup> **14o**,<sup>21</sup> **14m**,<sup>22</sup> **14p**,<sup>20</sup> **16m**,<sup>23</sup> and **16p**.<sup>22</sup> **13** was compared to the commercially available material from Sigma Aldrich. Compounds **3A**, **6A**, **7A**, and **8A** were characterized as mixtures with their respective isomers from the acetoxylation reactions. All other compounds were characterized in full, as they have not been previously reported.



**1A: 2,3-dichlorophenyl acetate**

Pale yellow oil.

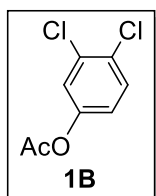
$R_f = 0.47$  in 80% hexanes/20% EtOAc.

$^1\text{H NMR}$  ( $\text{CDCl}_3$ , 700 MHz):  $\delta$  7.36 (d,  $J = 8.2$  Hz, 1H), 7.21 (app t,  $J = 8.2$  Hz, 1H), 7.07 (d,  $J = 8.2$  Hz, 1H), 2.35 (s, 3H).

$^{13}\text{C}\{^1\text{H}\}$  NMR ( $\text{CDCl}_3$ , 175 MHz):  $\delta$  168.26, 148.36, 133.96, 127.93, 127.53, 126.40, 122.06, 20.64.

IR (thin film,  $\text{CH}_2\text{Cl}_2$ ): 1772, 1577, 1449, 1368, 1181  $\text{cm}^{-1}$ .

HRMS EI (m/z):  $[\text{M}]^+$  calcd for  $\text{C}_8\text{H}_6\text{Cl}_2\text{O}_2$ : 203.9745; found: 203.9737.



**1B: 3,4-dichlorophenyl acetate**

Pale yellow oil.

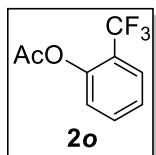
$R_f = 0.47$  in 80% hexanes/20% EtOAc.

$^1\text{H NMR}$  ( $\text{CDCl}_3$ , 700 MHz):  $\delta$  7.43 (d,  $J = 8.8$  Hz, 1H), 7.24 (d,  $J = 2.5$  Hz, 1H), 6.97 (dd,  $J = 2.5, 8.8$  Hz, 1H), 2.29 (s, 3H).

$^{13}\text{C}\{^1\text{H}\}$  NMR ( $\text{CDCl}_3$ , 175 MHz):  $\delta$  168.87, 149.36, 132.97, 130.78, 129.77, 123.97, 121.38, 21.05.

IR (thin film,  $\text{CH}_2\text{Cl}_2$ ): 3096, 1762, 1590, 1466, 1368, 1188  $\text{cm}^{-1}$ .

HRMS EI (m/z):  $[\text{M}]^+$  calcd for  $\text{C}_8\text{H}_6\text{Cl}_2\text{O}_2$ : 203.9745; found: 203.9744.



**2o: 2-(trifluoromethyl)phenyl acetate**

Yellow oil.

$R_f = 0.51$  in 80% hexanes/20% EtOAc.

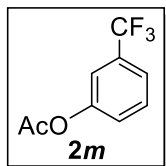
$^1\text{H NMR}$  ( $\text{CDCl}_3$ , 700 MHz):  $\delta$  7.67 (d,  $J = 7.9$  Hz, 1H), 7.57 (app t,  $J = 7.9$  Hz, 1H), 7.34 (app t,  $J = 7.9$  Hz, 1H), 7.23 (d,  $J = 7.9$  Hz, 1H), 2.33 (s, 3H).

$^{13}\text{C}\{^1\text{H}\}$  NMR ( $\text{CDCl}_3$ , 175 MHz):  $\delta$  168.99, 148.24 (q,  $^3J_{\text{C-F}} = 1.8$  Hz), 133.13, 127.03 (q,  $^3J_{\text{C-F}} = 4.9$  Hz), 126.08, 124.56, 123.08 (q,  $^1J_{\text{C-F}} = 272.5$  Hz), 123.03 (q,  $^2J_{\text{C-F}} = 31.4$  Hz), 20.83.

$^{19}\text{F NMR}$  ( $\text{CDCl}_3$ , 470 MHz):  $\delta$  -61.95 (s).

IR (thin film,  $\text{CH}_2\text{Cl}_2$ ): 2362, 1771 (C=O), 1614, 1494, 1456, 1372, 1319, 1188  $\text{cm}^{-1}$ .

HRMS EI (m/z): [M]<sup>+</sup> calcd for C<sub>9</sub>H<sub>7</sub>F<sub>3</sub>O<sub>2</sub>, 204.0398; found: 204.0401.



**2m: 3-(trifluoromethyl)phenyl acetate**

Yellow oil.

R<sub>f</sub> = 0.54 in 80% hexanes/20% EtOAc.

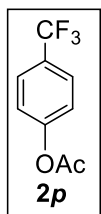
<sup>1</sup>H NMR (CDCl<sub>3</sub>, 700 MHz): δ 7.50 (app d, *J* = 4.0 Hz, 2H), 7.38 (s, 1H), 7.31-7.29 (m, 1H), 2.32 (s, 3H).

<sup>13</sup>C{<sup>1</sup>H} NMR (CDCl<sub>3</sub>, 175 MHz): δ 169.11, 150.84, 132.0 (q, <sup>2</sup>J<sub>C-F</sub> = 66.0 Hz), 130.11, 125.35, 123.60 (q, <sup>1</sup>J<sub>C-F</sub> = 272.4 Hz), 122.74 (q, <sup>3</sup>J<sub>C-F</sub> = 3.8 Hz), 119.02 (q, <sup>3</sup>J<sub>C-F</sub> = 3.8 Hz), 21.08.

<sup>19</sup>F NMR (CDCl<sub>3</sub>, 470 MHz): δ -62.77 (s).

IR (thin film, CH<sub>2</sub>Cl<sub>2</sub>): 3079, 1769 (C=O), 1598, 1450, 1326, 1221 cm<sup>-1</sup>.

HRMS EI (m/z): [M]<sup>+</sup> calcd for C<sub>9</sub>H<sub>7</sub>F<sub>3</sub>O<sub>2</sub>, 204.0398; found: 204.0397.



**2p: 4-(trifluoromethyl)phenyl acetate**

Colorless oil.

R<sub>f</sub> = 0.49 in 80% hexanes/20% EtOAc.

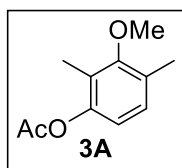
<sup>1</sup>H NMR (CDCl<sub>3</sub>, 700 MHz): δ 7.65 (d, *J* = 8.4 Hz, 2H), 7.22 (d, *J* = 8.4 Hz, 2H), 2.32 (s, 3H).

<sup>13</sup>C{<sup>1</sup>H} NMR (CDCl<sub>3</sub>, 175 MHz): δ 169.01, 153.27, 128.18 (q, <sup>2</sup>J<sub>C-F</sub> = 32.8 Hz), 126.88 (q, <sup>3</sup>J<sub>C-F</sub> = 3.7 Hz), 123.99 (q, <sup>1</sup>J<sub>C-F</sub> = 271.8 Hz), 122.21, 21.13.

<sup>19</sup>F NMR (CDCl<sub>3</sub>, 470 MHz): δ -62.32 (s).

IR (thin film, CH<sub>2</sub>Cl<sub>2</sub>): 2362, 1759 (C=O), 1614, 1514, 1372, 1321 cm<sup>-1</sup>.

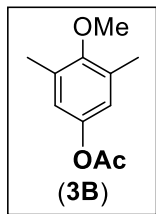
HRMS EI (m/z): [M]<sup>+</sup> calcd for C<sub>9</sub>H<sub>7</sub>F<sub>3</sub>O<sub>2</sub>, 204.0398; found: 204.0402.



**3A: 3-methoxy-2,4-dimethylphenyl acetate**

<sup>1</sup>H NMR (CD<sub>2</sub>Cl<sub>2</sub>, 700 MHz): δ 7.02 (d, *J* = 8.2 Hz, 1H), 6.71 (d, *J* = 8.2 Hz, 1H), 3.71 (s, 3H), 2.28 (s, 3H), 2.27 (s, 3H), 2.08 (s, 3H).

<sup>13</sup>C{<sup>1</sup>H} NMR (CD<sub>2</sub>Cl<sub>2</sub>, 175 MHz): δ 169.61, 157.95, 148.71, 129.02, 128.44, 124.23, 117.74, 60.27, 20.96, 16.02, 9.75.



**3B: 4-methoxy-2,4-dimethylphenyl acetate**

Colorless oil.

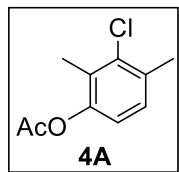
R<sub>f</sub> = 0.45 in 80% hexanes/20% EtOAc.

<sup>1</sup>H NMR (CDCl<sub>3</sub>, 700 MHz): δ 6.73 (s, 2H), 3.70 (s, 3H), 2.27 (s, 6H), 2.25 (s, 3H).

<sup>13</sup>C{<sup>1</sup>H} NMR (CDCl<sub>3</sub>, 175 MHz): δ 169.82, 154.54, 146.07, 131.97, 121.35, 59.68, 21.03, 16.15.

IR (thin film, CH<sub>2</sub>Cl<sub>2</sub>): 2938, 1757 (C=O), 1480, 1199, 1008, 901 cm<sup>-1</sup>.

HRMS ESI (m/z): [M+Na]<sup>+</sup> calcd for C<sub>11</sub>H<sub>14</sub>O<sub>3</sub>Na, 217.0835; found: 217.0841.

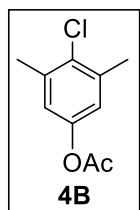


**4A: 3-chloro-2,4-dimethylphenyl acetate**

Colorless oil.

<sup>1</sup>H NMR (CD<sub>2</sub>Cl<sub>2</sub>, 700 MHz): δ 7.11 (d, *J* = 8.2 Hz, 1H), 6.86 (d, *J* = 8.2 Hz, 1H), 2.37 (s, 3H), 2.30 (s, 3H), 2.20 (s, 3H).

<sup>13</sup>C{<sup>1</sup>H} NMR (CD<sub>2</sub>Cl<sub>2</sub>, 175 MHz): δ 169.51, 148.24, 135.62, 134.52, 129.43, 121.82, 120.42, 20.94, 20.70, 14.12.



**4B: 4-chloro-3,5-dimethylphenyl acetate**

White solid.

Mp = 43-44 °C.

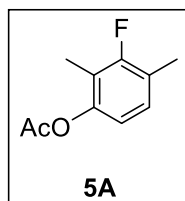
R<sub>f</sub> = 0.53 in 80% hexanes/20% EtOAc.

<sup>1</sup>H NMR (CDCl<sub>3</sub>, 700 MHz): δ 6.83 (s, 2H), 2.37 (s, 6H), 2.28 (s, 3H).

<sup>13</sup>C{<sup>1</sup>H} NMR (CDCl<sub>3</sub>, 175 MHz): δ 169.68, 148.35, 137.60, 131.86, 121.47, 21.18, 20.96.

IR (thin film, CH<sub>2</sub>Cl<sub>2</sub>): 2930, 1758 (C=O), 1199, 1144, 1028, 898 cm<sup>-1</sup>.

HRMS ESI (m/z): [M+H]<sup>+</sup> calcd for C<sub>10</sub>H<sub>12</sub>ClO<sub>2</sub>, 199.0520; found: 199.0515.



**5A: 3-fluoro-2,4-dimethylphenyl acetate**

Colorless oil.

R<sub>f</sub> = 0.54 in 80% hexanes/20% EtOAc.

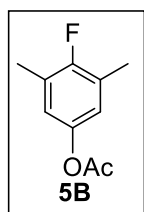
<sup>1</sup>H NMR (CD<sub>2</sub>Cl<sub>2</sub>, 700 MHz): δ 7.02 (app t, *J* = 8.3 Hz, 1H), 6.73 (d, *J* = 8.3 Hz, 1H), 2.29 (s, 3H), 2.25 (d, <sup>4</sup>*J*<sub>H-F</sub> = 1.8 Hz, 3H), 2.06 (d, <sup>4</sup>*J*<sub>H-F</sub> = 1.8 Hz, 3H).

$^{13}\text{C}\{^1\text{H}\}$  NMR ( $\text{CD}_2\text{Cl}_2$ , 175 MHz):  $\delta$  169.47, 160.14 (d,  $^1J_{\text{C-F}} = 243.9$  Hz), 148.54 (d,  $^3J_{\text{C-F}} = 6.9$  Hz), 128.33 (d,  $^3J_{\text{C-F}} = 6.4$  Hz), 122.57 (d,  $^2J_{\text{C-F}} = 18.5$  Hz), 118.33 (d,  $^2J_{\text{C-F}} = 20.4$  Hz), 117.41 (d,  $^4J_{\text{C-F}} = 3.8$  Hz), 20.90, 14.53 (d,  $^4J_{\text{C-F}} = 3.8$  Hz), 8.68 (d,  $^4J_{\text{C-F}} = 5$  Hz).

$^{19}\text{F}$  NMR ( $\text{CD}_2\text{Cl}_2$ , 470 MHz):  $\delta$  -118.99 (app s).

IR (thin film,  $\text{CH}_2\text{Cl}_2$ ): 2924, 2854, 1768 (C=O), 1488, 1465, 1215, 1200, 1073  $\text{cm}^{-1}$ .

HRMS EI (m/z):  $[\text{M}]^+$  calcd for  $\text{C}_{10}\text{H}_{11}\text{FO}_2$ , 182.0743; found: 182.0744.



**5B: 4-fluoro-3,5-dimethylphenyl acetate**

Colorless oil.

$R_f = 0.54$  in 80% hexanes/20% EtOAc.

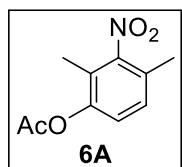
$^1\text{H}$  NMR ( $\text{CD}_2\text{Cl}_2$ , 700 MHz):  $\delta$  6.74 (d,  $^4J_{\text{H-F}} = 6.0$  Hz, 2H), 2.25 (d,  $^4J_{\text{H-F}} = 1.6$  Hz, 6H), 2.24 (s, 3H).

$^{13}\text{C}\{^1\text{H}\}$  NMR ( $\text{CD}_2\text{Cl}_2$ , 175 MHz):  $\delta$  170.01, 157.74 (d,  $^1J_{\text{C-F}} = 240.8$  Hz), 146.17 (d,  $^4J_{\text{C-F}} = 3.1$  Hz), 125.85 (d,  $^2J_{\text{C-F}} = 19.8$  Hz), 121.92 (d,  $^3J_{\text{C-F}} = 5.1$  Hz), 21.19, 14.82 (d,  $^4J_{\text{C-F}} = 4.1$  Hz).

$^{19}\text{F}$  NMR ( $\text{CD}_2\text{Cl}_2$ , 470 MHz):  $\delta$  -126.07 (app s).

IR (thin film,  $\text{CH}_2\text{Cl}_2$ ): 2926, 2853, 1762 (C=O), 1485, 1437, 1368, 1214, 1188  $\text{cm}^{-1}$ .

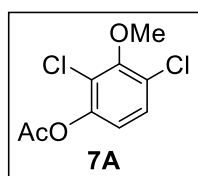
HRMS EI (m/z):  $[\text{M}]^+$  calcd for  $\text{C}_{10}\text{H}_{11}\text{FO}_2$ , 182.0743; found: 182.0740.



**6A: 2,4-dimethyl-3-nitrophenyl acetate**

$^1\text{H}$  NMR ( $\text{CD}_2\text{Cl}_2$ , 700 MHz):  $\delta$  7.18 (d,  $J = 8.3$  Hz, 1H), 7.10 (d,  $J = 8.3$  Hz, 1H), 2.32 (s, 3H), 2.29 (s, 3H), 2.09 (s, 3H).

$^{13}\text{C}\{^1\text{H}\}$  NMR ( $\text{CD}_2\text{Cl}_2$ , 175 MHz):  $\delta$  169.15, 152.82, 148.14, 129.50, 127.44, 124.40, 123.09, 20.86, 17.24, 11.55.

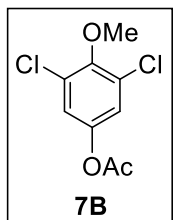


**7A: 2,4-dichloro-3-methoxyphenyl acetate**

$^1\text{H}$  NMR ( $\text{CD}_2\text{Cl}_2$ , 700 MHz):  $\delta$  7.34 (d,  $J = 8.8$  Hz, 1H), 6.93 (d,  $J = 8.8$  Hz, 1H), 3.91 (s, 3H), 2.33 (s, 3H).

$^{13}\text{C}\{^1\text{H}\}$  NMR ( $\text{CD}_2\text{Cl}_2$ , 175 MHz):  $\delta$  168.53, 153.75, 147.37, 128.45, 126.87, 123.59, 119.92, 61.17, 20.75.





**7B: 3,5-dichloro-4-methoxyphenyl acetate**

Pale yellow oil.

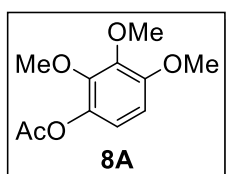
$R_f = 0.50$  in 80% hexanes/20% EtOAc.

$^1\text{H NMR}$  ( $\text{CDCl}_3$ , 700 MHz):  $\delta$  7.08 (s, 2H), 3.88 (s, 3H), 2.27 (s, 3H).

$^{13}\text{C}\{^1\text{H}\}$  NMR ( $\text{CDCl}_3$ , 175 MHz):  $\delta$  168.90, 150.41, 146.25, 129.56, 122.46, 60.86, 20.98.

IR (thin film,  $\text{CH}_2\text{Cl}_2$ ): 2936, 1766 (C=O), 1569, 1473, 1423, 1171  $\text{cm}^{-1}$ .

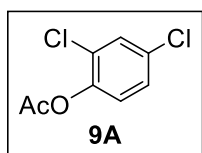
HRMS EI (m/z):  $[\text{M}]^+$  calcd for  $\text{C}_9\text{H}_8\text{Cl}_2\text{O}_3$ , 233.9850; found: 233.9855.



**8A: 2,3,4-trimethoxyphenyl acetate**

$^1\text{H NMR}$  ( $\text{CD}_2\text{Cl}_2$ , 700 MHz):  $\delta$  6.73 (d,  $J = 8.8$  Hz, 1H), 6.64 (d,  $J = 8.8$  Hz, 1H), 3.85 (s, 3H), 3.84 (s, 3H), 3.83 (s, 3H), 2.27 (s, 3H).

$^{13}\text{C}\{^1\text{H}\}$  NMR ( $\text{CD}_2\text{Cl}_2$ , 175 MHz):  $\delta$  169.81, 152.30, 143.53, 138.22, 117.00, 106.81, 61.36, 61.17, 56.52, 20.81.



**9A: 2,4-dichlorophenyl acetate**

Colorless oil.

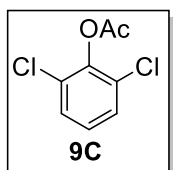
$R_f = 0.53$  in 80% hexanes/20% EtOAc.

$^1\text{H NMR}$  ( $\text{CDCl}_3$ , 700 MHz):  $\delta$  7.44 (d,  $J = 2.4$  Hz, 1H), 7.24 (dd,  $J = 8.7$ , 2.4 Hz, 1H), 7.06 (d,  $J = 8.7$  Hz, 1H), 2.33 (s, 3H).

$^{13}\text{C}\{^1\text{H}\}$  NMR ( $\text{CDCl}_3$ , 175 MHz):  $\delta$  168.33, 145.81, 131.99, 130.16, 128.02, 127.91, 124.65, 20.62.

IR (thin film,  $\text{CH}_2\text{Cl}_2$ ): 3095, 1765 (C=O), 1473, 1371, 1181, 1095  $\text{cm}^{-1}$ .

HRMS EI (m/z):  $[\text{M}]^+$  calcd for  $\text{C}_8\text{H}_6\text{Cl}_2\text{O}_2$ , 203.9745; found: 203.9741.



**9C: 2,6-dichlorophenyl acetate**

Pale yellow oil.

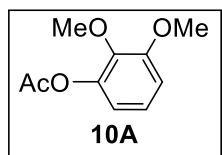
$R_f = 0.57$  in 80% hexanes/20% EtOAc.

$^1\text{H NMR}$  ( $\text{CD}_2\text{Cl}_2$ , 700 MHz):  $\delta$  7.39 (d,  $J = 8.1$  Hz, 2H), 7.17 (t,  $J = 8.1$  Hz, 1H), 2.38 (s, 3H).

$^{13}\text{C}\{^1\text{H}\}$  NMR ( $\text{CDCl}_3$ , 175 MHz):  $\delta$  168.39, 148.43, 128.04, 127.58, 122.11, 20.77.

IR (thin film, CH<sub>2</sub>Cl<sub>2</sub>): 3084, 1772 (C=O), 1576, 1445, 1368, 1176 cm<sup>-1</sup>.

HRMS EI (m/z): [M]<sup>+</sup> calcd for C<sub>8</sub>H<sub>6</sub>Cl<sub>2</sub>O<sub>2</sub>, 203.9745; found: 203.9749.



**10A: 2,3-dimethoxyphenyl acetate (authentic sample, synthesized from 2,3-dimethoxyphenol)**

Colorless oil.

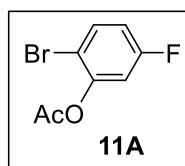
R<sub>f</sub> = 0.32 in 80% hexanes/20% EtOAc.

<sup>1</sup>H NMR (CDCl<sub>3</sub>, 700 MHz): δ 7.01 (app t, *J* = 8.3 Hz, 1H), 6.80 (d, *J* = 8.3 Hz, 1H), 6.67 (d, *J* = 8.3 Hz, 1H), 3.85 (s, 3H), 3.83 (s, 3H), 2.31 (s, 3H).

<sup>13</sup>C{<sup>1</sup>H} NMR (CDCl<sub>3</sub>, 175 MHz): δ 169.20, 153.75, 144.24, 141.09, 123.47, 115.04, 110.21, 60.67, 56.03, 20.72.

IR (thin film, CH<sub>2</sub>Cl<sub>2</sub>): 2944, 2838, 1767 (C=O), 1492, 1472, 1198 cm<sup>-1</sup>.

HRMS ESI (m/z): [M+H]<sup>+</sup> calcd for C<sub>10</sub>H<sub>13</sub>O<sub>4</sub>, 197.0808; found: 197.0805.



**11A: 2-bromo-5-fluorophenyl acetate (authentic sample, synthesized from 2-bromo-5-fluorophenol)**

Colorless oil.

R<sub>f</sub> = 0.57 in 80% hexanes/20% EtOAc.

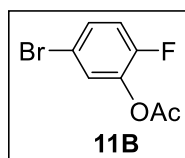
<sup>1</sup>H NMR (CDCl<sub>3</sub>, 700 MHz): δ 7.55 (dd, *J* = 8.7, 5.9 Hz, 1H), 6.92 (dd, *J* = 8.7, 2.9 Hz, 1H), 6.88 (dt, *J* = 8.7, 2.9 Hz, 1H), 2.34 (s, 3H).

<sup>13</sup>C{<sup>1</sup>H} NMR (CDCl<sub>3</sub>, 175 MHz): δ 168.10, 161.95 (d, <sup>1</sup>*J*<sub>C-F</sub> = 248.9 Hz), 148.98 (d, <sup>3</sup>*J*<sub>C-F</sub> = 11.0 Hz), 133.78 (d, <sup>3</sup>*J*<sub>C-F</sub> = 9.04 Hz), 114.73 (d, <sup>2</sup>*J*<sub>C-F</sub> = 22.3 Hz), 111.97 (d, <sup>2</sup>*J*<sub>C-F</sub> = 25.2 Hz), 110.93 (d <sup>4</sup>*J*<sub>C-F</sub> = 4.0 Hz), 20.76.

<sup>19</sup>F NMR (CDCl<sub>3</sub>, 376 MHz): δ -112.0 (dt, *J* = 5.9, 8.7 Hz).

IR (thin film, CH<sub>2</sub>Cl<sub>2</sub>): 1771 (C=O), 1590, 1474, 1183, 1142 cm<sup>-1</sup>.

HRMS EI (m/z): [M]<sup>+</sup> calcd for C<sub>8</sub>H<sub>6</sub>BrFO<sub>2</sub>, 231.9535; found: 231.9537.



**11B: 5-bromo-2-fluorophenyl acetate**

White solid.

Mp = 72-73 °C.

R<sub>f</sub> = 0.55 in 80% hexanes/20% EtOAc.

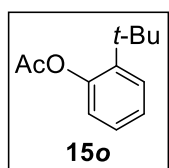
$^1\text{H}$  NMR ( $\text{CDCl}_3$ , 700 MHz):  $\delta$  7.34-7.32 (m, 1H), 7.30 (d,  $J = 6.7$ , 1H), 7.05 (app t,  $J = 9.7$ , 1H), 2.33 (s, 3H).

$^{13}\text{C}\{^1\text{H}\}$  NMR ( $\text{CDCl}_3$ , 175 MHz):  $\delta$  168.02, 153.57 (d,  $^1J_{\text{C-F}} = 249.9$  Hz), 138.89 (d,  $^2J_{\text{C-F}} = 14.1$  Hz), 130.16 (d,  $^3J_{\text{C-F}} = 7.03$  Hz), 127.18, 118.15 (d,  $^2J_{\text{C-F}} = 20.1$  Hz), 116.22 (d,  $^3J_{\text{C-F}} = 3.8$  Hz), 20.56.

$^{19}\text{F}$  NMR ( $\text{CDCl}_3$ , 376 MHz):  $\delta$  -129.69 (m).

IR (thin film,  $\text{CH}_2\text{Cl}_2$ ): 3072, 1761 (C=O), 1368, 1200, 1181, 1109  $\text{cm}^{-1}$ .

HRMS EI (m/z):  $[\text{M}]^+$  calcd for  $\text{C}_8\text{H}_6\text{BrFO}_2$ , 231.9535; found: 231.9540.



**15o: 2-(tert-butyl)phenyl acetate**

Colorless oil.

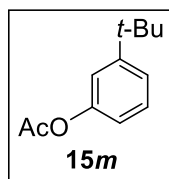
$R_f = 0.59$  in 80% hexanes/20% EtOAc.

$^1\text{H}$  NMR ( $\text{CDCl}_3$ , 400 MHz):  $\delta$  7.41 (d,  $J = 7.8$  Hz, 1H), 7.25-7.15 (multiple peaks, 2H), 7.01 (d,  $J = 7.1$  Hz, 1H), 2.34 (s, 3H), 1.37 (s, 9H).

$^{13}\text{C}\{^1\text{H}\}$  NMR ( $\text{CDCl}_3$ , 175 MHz):  $\delta$  169.71, 149.19, 141.04, 127.31, 126.97, 125.86, 124.11, 34.54, 30.29, 21.78.

IR (thin film,  $\text{CH}_2\text{Cl}_2$ ): 2959, 1764 (C=O), 1485, 1443, 1368, 1209, 1184, 1087  $\text{cm}^{-1}$ .

HRMS EI (m/z):  $[\text{M}]^+$  calcd for  $\text{C}_{12}\text{H}_{16}\text{O}_2$ , 192.1152; found: 192.1152.



**15m: 3-(tert-butyl)phenyl acetate**

White solid.

$\text{Mp} = 38-40$  °C.

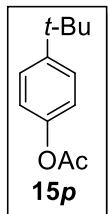
$R_f = 0.59$  in 80% hexanes/20% EtOAc.

$^1\text{H}$  NMR ( $\text{CDCl}_3$ , 700 MHz):  $\delta$  7.31-7.29 (m, 1H), 7.26-7.24 (m, 1H), 7.07-7.06 (m, 1H), 6.91-6.89 (m, 1H), 2.29 (s, 3H), 1.31 (s, 9H).

$^{13}\text{C}\{^1\text{H}\}$  NMR ( $\text{CDCl}_3$ , 175 MHz):  $\delta$  169.77, 153.19, 150.67, 129.01, 123.00, 118.71, 118.67, 34.91, 31.37, 21.34.

IR (thin film,  $\text{CH}_2\text{Cl}_2$ ): 2958, 1758 (C=O), 1584, 1372, 1204, 1187  $\text{cm}^{-1}$ .

HRMS ESI (m/z):  $[\text{M}+\text{H}]^+$  calcd for  $\text{C}_{12}\text{H}_{17}\text{O}_2$ , 193.1223; found: 193.1222.



**15p: 4-(*tert*-butyl)phenyl acetate**

Colorless oil.

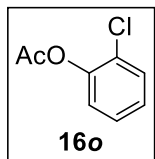
$R_f = 0.59$  in 80% hexanes/20% EtOAc.

$^1\text{H NMR}$  ( $\text{CDCl}_3$ , 700 MHz):  $\delta$  7.38 (d,  $J = 8.5$ , 2H), 7.01 (d,  $J = 8.5$  Hz, 2H), 2.29 (s, 3H), 1.31 (s, 9H).

$^{13}\text{C}\{^1\text{H}\}$  NMR ( $\text{CDCl}_3$ , 175 MHz):  $\delta$  169.88, 148.75, 148.43, 126.47, 120.98, 34.61, 31.55, 21.32.

IR (thin film,  $\text{CH}_2\text{Cl}_2$ ): 2963, 1761 (C=O), 1509, 1366, 1196  $\text{cm}^{-1}$ .

HRMS ESI (m/z):  $[\text{M}+\text{H}]^+$  calcd for  $\text{C}_{12}\text{H}_{17}\text{O}_2$ , 193.1223; found: 193.1221.



**16o: 2-chlorophenyl acetate**

Pale yellow oil.

$R_f = 0.51$  in 80% hexanes/20% EtOAc.

$^1\text{H NMR}$  ( $\text{CDCl}_3$ , 700 MHz):  $\delta$  7.44 (d,  $J = 8.0$  Hz, 1H), 7.26 (t,  $J = 8.0$  Hz, 1H), 7.17 (t,  $J = 8.0$  Hz, 1H), 7.13 (d,  $J = 8.0$  Hz, 1H), 2.34 (s, 3H).

$^{13}\text{C}\{^1\text{H}\}$  NMR ( $\text{CDCl}_3$ , 175 MHz):  $\delta$  168.51, 147.06, 130.32, 127.81, 127.10, 126.92, 123.77, 20.62.

IR (thin film,  $\text{CH}_2\text{Cl}_2$ ): 3071, 1772 (C=O), 1475, 1367, 1183  $\text{cm}^{-1}$ .

HRMS EI (m/z):  $[\text{M}]^+$  calcd for  $\text{C}_8\text{H}_7\text{ClO}_2$ , 170.0134; found: 170.0135.

## 4.7 REFERENCES

- (1) Adapted with permission from Cook, A. K.; Emmert, M. H.; Sanford, M. S. *Org. Lett.* **2013**, *15*, 5428. © American Chemical Society.
- (2) (a) Dick, A. R.; Sanford, M. S. *Tetrahedron* **2006**, *62*, 2439. (b) Jazzar, R.; Hitce, J.; Renaudat, A.; Sofack-Kreutzer, J.; Baudoin, O. *Chem. Eur. J.* **2010**, *16*, 2654. (c) Stokes, B. J.; Driver, T. G. *Eur. J. Org. Chem.* **2011**, 4071. (d) Newhouse, T.; Baran, P. S. *Angew. Chem. Int. Ed.* **2011**, *50*, 3362. (e) Chen, D. Y.-K.; Yoon, S. W. *Chem. Eur. J.* **2012**, *18*, 9452. (f) Yamaguchi, J.; Yamaguchi, A. D.; Itami, K. *Angew. Chem. Int. Ed.* **2012**, *51*, 8960. (g) Wencel-Delord, J.; Glorius, F. *Nature Chem.* **2013**, *5*, 369.
- (3) Neufeldt, S. R.; Sanford, M. S. *Acc. Chem. Res.* **2012**, *45*, 936.
- (4) (a) Lyons, T. W.; Sanford, M. S. *Chem. Rev.* **2010**, *110*, 1147. (b) Muñoz, K. *Angew. Chem. Int. Ed.* **2009**, *48*, 9412.
- (5) Alonso, D. A.; Najera, C.; Pastor, I. M.; Yus, M. *Chem. Eur. J.* **2010**, *16*, 5274.
- (6) (a) Yoneyama, T.; Crabtree, R. H. J. *Mol. Catal. A: Chem.* **1996**, *108*, 35. (b) Ebersson, L.; Jönsson, L. *Liebigs Ann. Chem.* **1977**, 233. (c) Ebersson, L.; Jönsson, L. *J. Chem. Soc., Chem. Commun.* **1974**, 885. (d) Ebersson, L.; Jönsson, L. *Acta Chem. Scand.* **1976**, *30b*, 361. (e) Ebersson, L.; Jönsson, L.

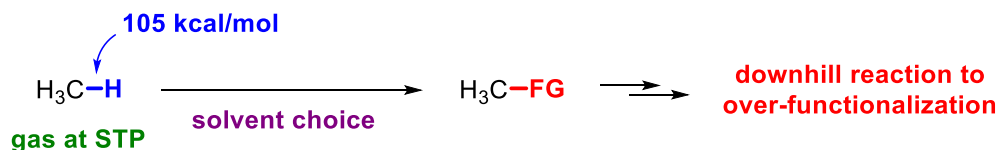
- 
- Acta Chem. Scand.* **1974**, *28*, 771. (f) Ebersson, L.; Gomez-Gonzales, L. *J. Chem. Soc., Chem. Commun.* **1971**, 263. (g) Henry, P. M. *J. Org. Chem.* **1971**, *36*, 1886.
- (7) (a) Gary, J. B.; Cook, A. K.; Sanford, M. S. *ACS Catal.* **2013**, *3*, 700. (b) Emmert, M. H.; Cook, A. K.; Xie, Y. J.; Sanford, M. S. *Angew. Chem. Int. Ed.* **2011**, *50*, 9409.
- (8) For similar effects of pyridine in oxidative C–H olefination, see: Kubota, A.; Emmert, M. H.; Sanford, M. S. *Org. Lett.* **2012**, *14*, 1760.
- (9) For the use of substituted pyridine-ligands in the *meta*-selective C–H olefination of electron deficient arenes, see: (a) Zhang, Y.-H.; Shi, B.-F.; Yu, J.-Q. *J. Am. Chem. Soc.* **2009**, *131*, 5072. (b) Zhang, S.; Shi, L.; Ding, Y. *J. Am. Chem. Soc.* **2011**, *133*, 20218.
- (10) For a recent example of Pd-catalyzed C–H amination where selectivity is dictated by substrate sterics, see: Shrestha, R.; Mukherjee, P.; Tan, Y.; Litman, Z. C.; Hartwig, J. F. *J. Am. Chem. Soc.* **2013**, *135*, 8480.
- (11) For a review on sterically controlled selectivity in C–H borylation reactions, see: Mkhaliid, I. A. I.; Barnard, J. H.; Marder, T. B.; Murphy, J. M.; Hartwig, J. F. *Chem. Rev.* **2010**, *110*, 890.
- (12) For preliminary studies of the influence of MesI(OAc)<sub>2</sub> [versus PhI(OAc)<sub>2</sub>] on the site selectivity of C–H acetoxylation with the Pd(OAc)<sub>2</sub>/pyridine catalyst system, see ref. 7b.
- (13) Emmert, M. H.; Gary, J. B.; Villalobos, J. M.; Sanford, M. S. *Angew. Chem. Int. Ed.* **2010**, *49*, 5884.
- (14) Lee, C. K.; Yu, J. S.; Lee, H.-J. *J. Heterocycl. Chem.* **2002**, *39*, 1207.
- (15) Duthaler, R. O. *Helv. Chim. Acta* **1983**, *66*, 2543.
- (16) Kita, Y.; Tohma, H.; Hatanaka, K.; Takada, T.; Fujita, S.; Mitoh, S.; Sakurai, H.; Oka, S. *J. Am. Chem. Soc.* **1994**, *116*, 3684.
- (17) Das, R.; Chakraborty, D. *Synthesis* **2011**, 1621.
- (18) Nolan, K. A.; Doncaster, J. R.; Dunstan, M. S.; Scott, K. A.; Frenkel, A. D.; Siegel, D.; Ross, D.; Barnes, J.; Levy, C.; Leys, D.; Whitehead, R. C.; Stratford, I. J.; Bryce, R. A. *J. Med. Chem.* **2009**, *52*, 7142.
- (19) Barbero, M.; Cadmuro, S.; Dughera, S.; Venturello, P. *Synthesis* **2008**, 3625.
- (20) Chakraborti, A. K.; Chankeshwara, S. V. *J. Org. Chem.* **2009**, *74*, 1367.
- (21) Paraskar, A. S.; Sudalai, A. *Tetrahedron* **2006**, *62*, 4907.
- (22) Kadam, S. T.; Kim, S. S.; *Synthesis* **2008**, 267.
- (23) Thalji, R. K.; Ellman, J. A.; Bergman, R. G. *J. Am. Chem. Soc.* **2004**, *126*, 7192.

# CHAPTER 5. THE DEVELOPMENT OF CATALYTIC METHANE C–H BORYLATION AND A COMPARISON OF RH AND IR CATALYSTS\*

## 5.1 INTRODUCTION

The increasing quantities of light alkanes that are being harnessed through fracking has spurred renewed interest in the development of methods for their functionalization. In particular, methane, the primary component in natural gas, is abundant and inexpensive; as such, the potential to increase its value through functionalization is high.<sup>1</sup> Despite the urgency, there are a limited number of means to functionalize methane.<sup>2</sup> The dearth of methane functionalization methods are due to four factors (see Figure 5.1): i) as a gas, methane is difficult to handle; ii) the bond dissociation energy (BDE) is the highest of simple alkanes at 105 kcal/mol;<sup>3</sup> iii) the initial functionalization product is usually metastable and can easily be further functionalized;<sup>4</sup> and iv) the choice of reaction medium (solvent) is limited, as typical solvents have C–H bonds that can compete with methane.

**Figure 5.1.** Challenges associated with methane C–H functionalization

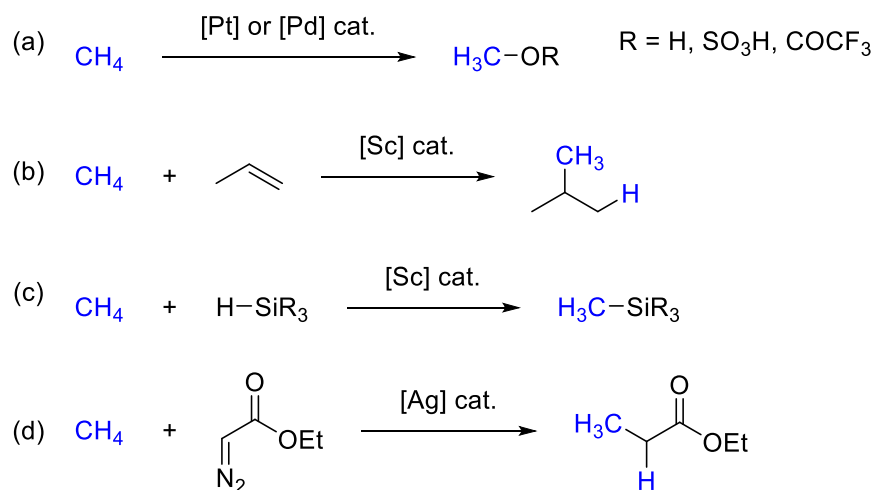


Industrially, methane is primarily used to make syngas.<sup>2a</sup> In the literature, there are few examples of methane functionalization using homogeneous catalysts (Scheme 5.1),<sup>2c</sup> with methane oxidation to methanol derivatives being the dominant reaction (Scheme

\* Work in this chapter was collaborative with Sydonie D. Schimler. Her contribution to this work is the rate data of MeBpin and CyBpin, as well as repeating the screening of reaction conditions to evaluate reproducibility.

5.1a). While there are a number of catalysts and conditions used, they all require aqueous/highly acidic solvents and/or expensive oxidants or have low turnover numbers of the catalyst, which are typically Pd and Pt.<sup>2d</sup> Additional methane functionalization reactions reported by Tilley and coworkers are the hydromethylation of alkenes<sup>5</sup> (Scheme 5.1b) and silylation<sup>6</sup> (Scheme 5.1c) using a scandocene catalyst. However, these methods require long reaction times and proceed with low turnover numbers (typically <10). Finally, Perez and coworkers have recently developed a protocol for carbenoid insertion into the C–H bonds of methane using a silver catalyst (Scheme 5.1d).<sup>7</sup> This reaction uses supercritical CO<sub>2</sub> as the solvent, avoiding the problem of competitive C–H functionalization of the solvent. Despite that advancement, the use of the carbenoid precursor, ethyl diazoacetate, is undesirable as it is unstable and shock sensitive.

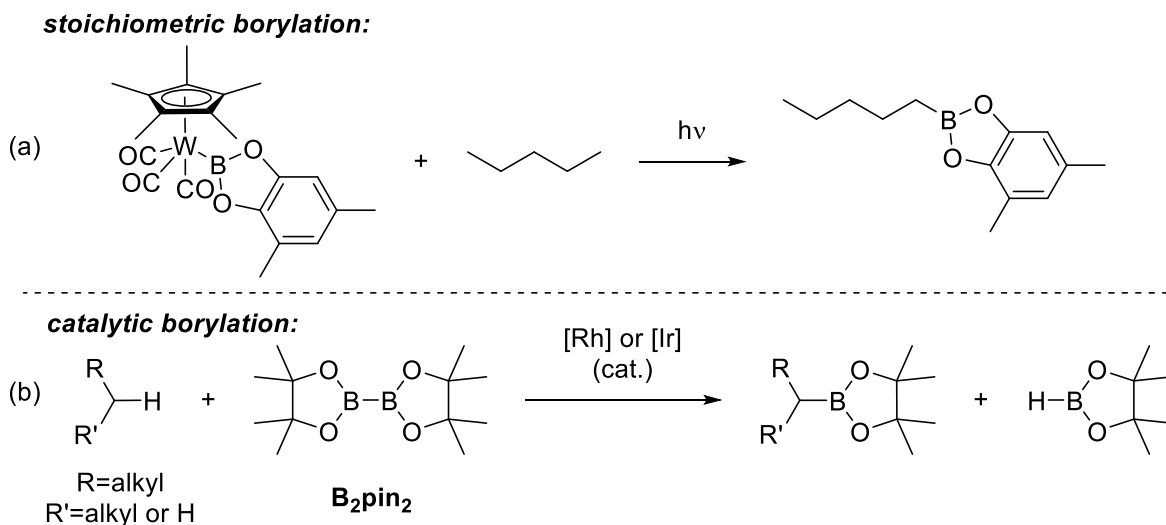
**Scheme 5.1.** Methods of methane functionalization known in the literature



There are additional examples of stoichiometric functionalization of methane in the literature.<sup>8</sup> [Cp\*Ir]<sup>9</sup> and [Cp\*Rh]<sup>10</sup> complexes have been known to activate a variety of C–H bonds via oxidative addition (see Chapter 1), but functionalization of the formed alkylmetal species is rare. One case in which C–H bonds of alkanes are readily functionalized is borylation using diboron reagents (Scheme 5.2).<sup>11</sup> Alkane borylation was first reported as a stoichiometric reaction in which a [W]–B(OR)<sub>2</sub> fragment selectively reacts with the primary position of alkanes such as pentane and ethylcyclohexane to form alkyl-B(OR)<sub>2</sub> (Scheme 5.2a).<sup>12</sup> A catalytic protocol was later developed using Cp\*Rh(η<sup>4</sup>-C<sub>6</sub>Me<sub>6</sub>) (Cp\* = pentamethylcyclopentadienyl) as the catalyst and bis(pinacolato)diboron

(B<sub>2</sub>pin<sub>2</sub>) as the limiting reagent (Scheme 5.2b).<sup>13</sup> This reaction is selective for primary C–H bonds and the substrate is commonly used as solvent,<sup>13c</sup> avoiding competitive solvent C–H bond functionalization. In subsequent reports, the Ir catalyst system ( $\eta^6$ -Mes)Ir(Bpin)<sub>3</sub>/Me<sub>4</sub>Phen (Mes = mesitylene; Me<sub>4</sub>Phen = 3,4,7,8-tetramethyl-1,10-phenanthroline) was used for C–H borylation of secondary C–H bonds.<sup>14</sup> This work built upon prior examples of aryl C–H borylation using ( $\eta^6$ -Mes)Ir(Bpin)<sub>3</sub>,<sup>15</sup> [(COD)Ir(OMe)]<sub>2</sub>,<sup>16</sup> and [(COD)IrCl]<sub>2</sub><sup>15a,16,17</sup> in conjunction with nitrogen-<sup>15b,16,17,18</sup> and phosphorous-based<sup>15</sup> ligands. Despite the high selectivity and activity of these catalysts, methane or other light alkanes were not explored as a substrates.

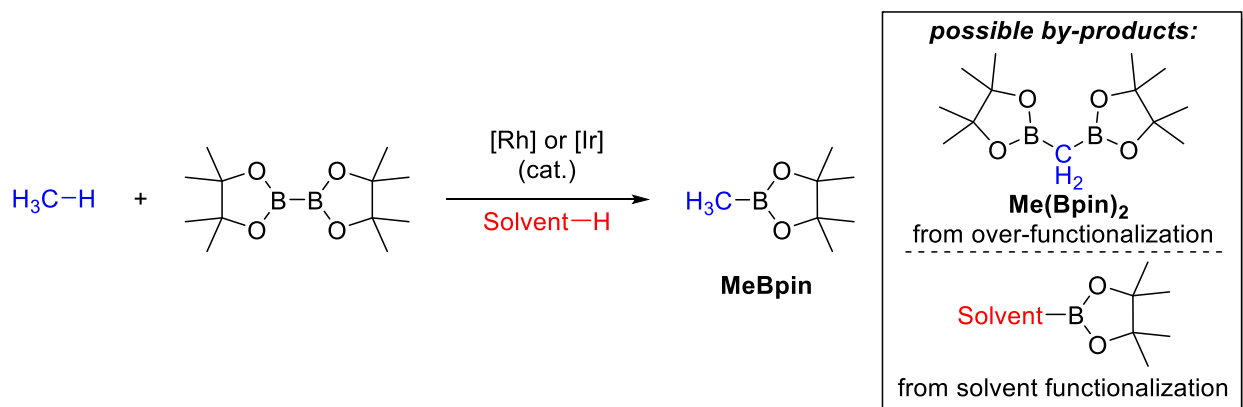
**Scheme 5.2.** (a) Stoichiometric borylation of *n*-pentane using [W]–B(OR)<sub>2</sub> complex. (b) Borylation of 1° or 2° alkanes using a Rh or Ir catalyst and B<sub>2</sub>pin<sub>2</sub>



Based on these precedents, we hypothesized that these catalysts could be used to achieve the C–H borylation of methane (Scheme 5.3). Because of the inherent challenges in methane functionalization, we anticipate the possibility of forming by-products. The first by-product would be from diborylation (represented throughout as Me(Bpin)<sub>2</sub>), in which the product of the first borylation then acts as a substrate. Additionally, if the solvent has C–H bonds, we expect that those C–H bonds can be borylated as well. Discussed below is the development of a catalytic method for the C–H borylation of methane, from initial catalyst evaluation, screening of reaction conditions, a systematic comparison of alkyl C–H bonds, and finally an evaluation of over-functionalization, all the while comparing the best Ir and Rh catalysts.



**Scheme 5.3.** The borylation of methane and potential by-products



## 5.2 RESULTS AND DISCUSSION

Because the  $(\eta^6\text{-Mes})\text{Ir}(\text{Bpin})_3/\text{Me}_4\text{Phen}$  catalyst system showed high activity for both primary and secondary C–H borylation, we began with that catalyst at 3 mol %.<sup>14a</sup> Cyclohexane (CyH) was chosen as the solvent since it is readily available, will solubilize methane, and has been shown to be an effective solvent for the borylation of arenes.<sup>16</sup> The temperature of 150 °C was chosen as the temperature based on prior alkane borylation examples.<sup>13a</sup> Using these conditions, the product of the borylation of methane, MeBpin, was measured by GC-FID in 45% calibrated yield, equaling 15 turnovers (Table 5.1, entry 1). Significant amounts of the expected by-products were observed, diborylated methane ( $\text{Me(Bpin)}_2$ ) and borylated cyclohexane (CyBpin), which are reported as ratios relative to MeBpin formation (two right-most columns of Table 5.1). To identify a more selective catalyst, we next explored other known Ir-catalyst systems. The more-established<sup>16</sup>  $[(\text{COD})\text{Ir}(\text{OMe})_2]$  with  $\text{Me}_4\text{Phen}$  failed to show improvement in yield of MeBpin (entry 2). We next turned to the  $\text{Cp}^*[\text{Ir}]$ -type complexes<sup>19</sup> known to activate methane,<sup>20</sup> but  $[\text{Cp}^*\text{IrCl}_2]_2$  failed, giving only trace product (entry 3). Because of these low yields and/or selectivities, the  $\text{Cp}^*[\text{Rh}]$  system was evaluated. Using the commercially available  $[\text{Cp}^*\text{RhCl}_2]_2$  precatalyst, MeBpin was formed in 51% yield, a slight improvement over the Ir system (entry 4). Encouragingly, the amounts of  $\text{Me(Bpin)}_2$  and CyBpin formed were significantly lower with this Rh catalyst.  $\text{Cp}^*\text{Rh}(\eta^4\text{-C}_6\text{Me}_6)$  is a precatalyst that has shown high activity for the borylation of *n*-octane<sup>13a</sup> and this catalyst, under our conditions,

gave 99% yield of MeBpin (TON = 33; entry 5). Furthermore, it gave high selectivity, with minimal amounts of diborylation and CyBpin formed.

**Table 5.1.** Evaluating Rh and Ir complexes as catalysts for methane borylation

**Rh and Ir complexes evaluated as catalysts:**

(Mes)Ir(Bpin)<sub>3</sub>

[(COD)Ir(OMe)<sub>2</sub>]<sub>2</sub>

[Cp<sup>\*</sup>MCl<sub>2</sub>]<sub>2</sub>  
M = Ir, Rh

Cp<sup>\*</sup>Rh(η<sup>4</sup>-C<sub>6</sub>Me<sub>6</sub>)

**Ligand:**

Me<sub>4</sub>Phen

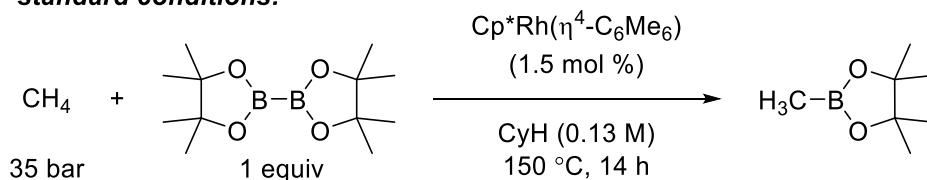
Entry	Catalyst and Ligand	TON for MeBpin	Yield MeBpin <sup>a</sup>	MeBpin: CyBpin	MeBpin: Me(Bpin) <sub>2</sub>
1	(η <sup>6</sup> -Mes)Ir(Bpin) <sub>3</sub> + Me <sub>4</sub> Phen	15	45%	3:1	4:1
2	[(COD)Ir(OMe) <sub>2</sub> ] <sub>2</sub> + Me <sub>4</sub> Phen	2.7	8.3%	9:1	19:1
3	[Cp <sup>*</sup> IrCl <sub>2</sub> ] <sub>2</sub>	<1	<1%	n.a. <sup>b</sup>	n.a.
4	[Cp <sup>*</sup> RhCl <sub>2</sub> ] <sub>2</sub>	17	51%	49:1	16:1
5	Cp <sup>*</sup> Rh(η <sup>4</sup> -C <sub>6</sub> Me <sub>6</sub> )	33	99%	59:1	9:1

<sup>a</sup>Yields are determined by GC-FID using a calibration curve and an internal standard (PhCl or isododecane). <sup>b</sup>n.a.= not applicable; products were formed in yields too low to accurately determine selectivity ratios.

Using Cp<sup>\*</sup>Rh(η<sup>4</sup>-C<sub>6</sub>Me<sub>6</sub>) as the optimal catalyst, a variety of reaction conditions were explored for further optimization (Table 5.2). Because little room for improvement is available under the conditions detailed above (since they resulted in 99% yield), a lower catalyst loading was used to show the dependence of yield on reaction conditions. The standard conditions used for comparison are as follows: Cp<sup>\*</sup>Rh(η<sup>4</sup>-C<sub>6</sub>Me<sub>6</sub>) (1.5 mol %), reaction time of 14 hours, 0.13 M in CyH, 150 °C, and 35 bar CH<sub>4</sub>. The yield resulting from the use of these standard conditions is 74% (entry 1), which equals 49 turnovers. As discussed previously, the yield and TON for 3 mol % catalyst loading is 99% and 33

(entry 2). Therefore, decreasing the catalyst loading decreases the yield, but increases the TON. Further decreasing the catalyst loading to 0.75 mol % showed a similar pattern, with 51% yield and 68 turnovers obtained after 14 h (entry 3). To test whether the catalyst is still active at this time point, the reaction was allowed to progress for 37 h (entry 4) and then for 86 h (entry 5). After 37 h, the yield and TON increased to 69% and 92, respectively; however, after 86 h, only minimal further increases were observed (73% yield and 97 turnovers). Notably, the MeBpin:Me(Bpin)<sub>2</sub> selectivity increased at these low catalyst concentrations.

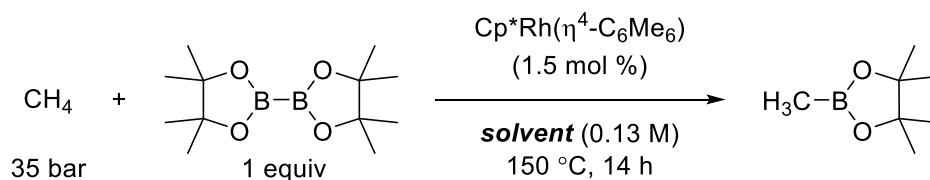
Next, the concentration of the reaction was varied, and increasing the concentration resulted in a decrease in reaction yield, from 74% at 0.13 M (entry 1) to 57% at 0.25 M (entry 6). Lowering the concentration had a minimally positive effect, and the yield increased to 77% at 0.065 M (entry 7). The effect of temperature was evaluated, and it was found that lowering the temperature from 150 °C to 130 °C resulted in a decreased reaction yield to 60% (entry 8), while increasing the temperature to 170 °C led to a slight improvement in the yield, giving 79% (entry 9); however, the MeBpin:Me(Bpin)<sub>2</sub> selectivity decreased to 33:1. The reaction pressure was also varied, and decreasing the pressure from 35 bar to 25 bar had a minimal effect, resulting in 68% yield of MeBpin (entry 10), whereas increasing the pressure to 50 bar led to an increased yield of 84% (entry 11). The selectivities obtained at varied pressures correlate with the amount of methane available: at higher pressures of methane, the selectivity for MeBpin formation versus Me(Bpin)<sub>2</sub> formation is high. Despite this increase in yield at higher pressures, we chose to use 35 bar for practical reasons (one of our reactors is not rated for pressures higher than 55 bar).

**Table 5.2.** Optimization of reaction parameters*standard conditions:*

Entry	Variation from standard conditions	TON for MeBpin	Yield MeBpin <sup>a</sup>	MeBpin: CyBpin	MeBpin: Me(Bpin) <sub>2</sub>
1	none	49	74%	48:1	10:1
2	3 mol % [Rh]	33	99%	59:1	9:1
3	0.75 mol % [Rh]	68	51%	46:1	18:1
4	0.75 mol % [Rh], 37 h	92	69%	41:1	17:1
5	0.75 mol % [Rh], 86 h	97	73%	46:1	14:1
6	0.25 M	38	57%	49:1	6:1
7	0.065 M	51	77%	50:1	8:1
8	130 °C	40	60%	60:1	11:1
9	170 °C	53	79%	33:1	10:1
10	25 bar CH <sub>4</sub>	45	68%	28:1	8:1
11	50 bar CH <sub>4</sub>	56	84%	78:1	16:1

<sup>a</sup>Yields are determined by GC-FID using a calibration curve and an internal standard (PhCl or isododecane).

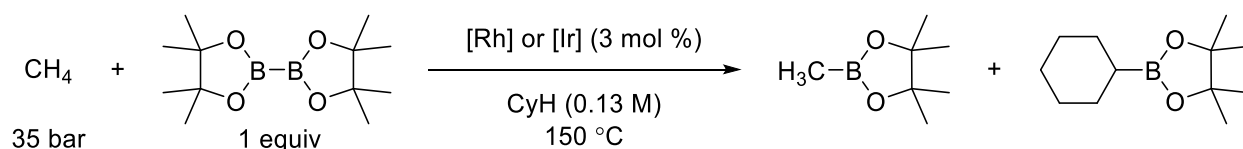
To avoid the functionalization of the solvent cyclohexane, alternative solvents were explored. As seen in Table 5.3, traces of MeBin were detected in reactions conducted in THF, hexafluorobenzene, dichloroethane, and tetrachloroethylene (entries 2-5). Higher yields of 69% and 26% were observed in cyclopentane and perfluorohexane, respectively (entries 6 and 7). These values are still lower than when cyclohexane is used as the solvent and therefore, cyclohexane was used for further studies. Interestingly, the solubility of methane is approximately 2 times higher in perfluorohexane than in cyclohexane (solubility of methane is approximately 30 mM in cyclohexane and 80 mM in perfluoroheptane),<sup>21</sup> suggesting that the yield is not limited by methane solubility.

**Table 5.3.** Testing various solvents for methane borylation

Entry	Solvent	TON for MeBpin	Yield MeBpin <sup>a</sup>	MeBpin:Me(Bpin) <sub>2</sub>
1	Cyclohexane	49	74%	10:1
2	THF	<1	<1	n.a. <sup>b</sup>
3	C <sub>6</sub> F <sub>6</sub>	1	2%	n.a.
4	Dichloroethane	<1	<1	n.a.
5	Tetrachloroethylene	<1	<1	n.a.
6	Cyclopentane	46	69% <sup>c</sup>	10:1
7	Perfluorohexane	17	26%	8:1

<sup>a</sup>Yields are determined by GC-FID using a calibration curve and an internal standard (PhCl or isododecane). <sup>b</sup> n.a.= not applicable; products were formed in yields too low to accurately determine selectivity ratios. <sup>c</sup>8% yield of cyclopentylboronic acid pinacol ester formed (solvent functionalization), as determined by GC-FID using the calibration curve for cyclohexylboronic acid pinacol ester.

Since both active and selective catalysts are required for methane functionalization, we next looked in depth into the selectivity for the optimal Rh and Ir catalysts, Cp\*Rh( $\eta^4$ -C<sub>6</sub>Me<sub>6</sub>) and ( $\eta^6$ -Mes)Ir(Bpin)<sub>3</sub>/Me<sub>4</sub>Phen (Table 5.4). These will henceforth be called [Rh] and [Ir]. First, the selectivity of cyclohexane functionalization versus methane functionalization was examined. We clearly observed a greater selectivity with [Rh] over [Ir]. The selectivity of MeBpin:Me(Bpin)<sub>2</sub> for [Rh] is 59:1 (entry 2), while it is 3:1 for [Ir] upon reaction completion (14 h reaction time, entry 4). Even at early conversions, [Rh] is much more selective for methane over cyclohexane (15:1 for [Ir] and 55:1 for [Rh], entries 3 and 1, respectively).

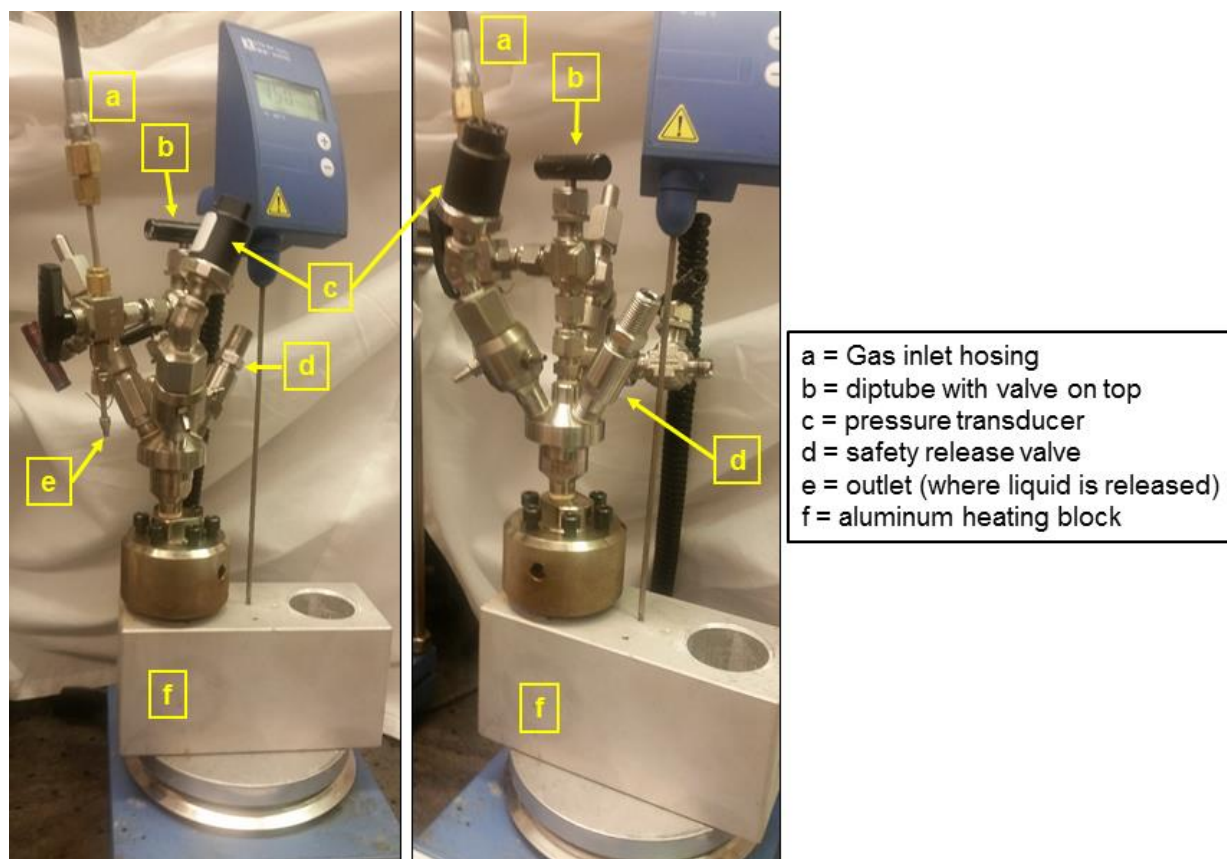
**Table 5.4.** Comparison of Rh and Ir catalysts for CH<sub>4</sub> vs. CyH borylation

Entry	Catalyst	Reaction Time	TON for MeBpin	Yield MeBpin <sup>a</sup>	MeBpin: CyBpin
1	[Rh]	0.5 h	9	27%	55:1
2	[Rh]	14 h	33	99%	59:1
3	[Ir]	2.5 h	8	23%	15:1
4	[Ir]	14 h	15	45%	3:1

<sup>a</sup>Yields are determined by GC-FID using a calibration curve and an internal standard (PhCl or isododecane).

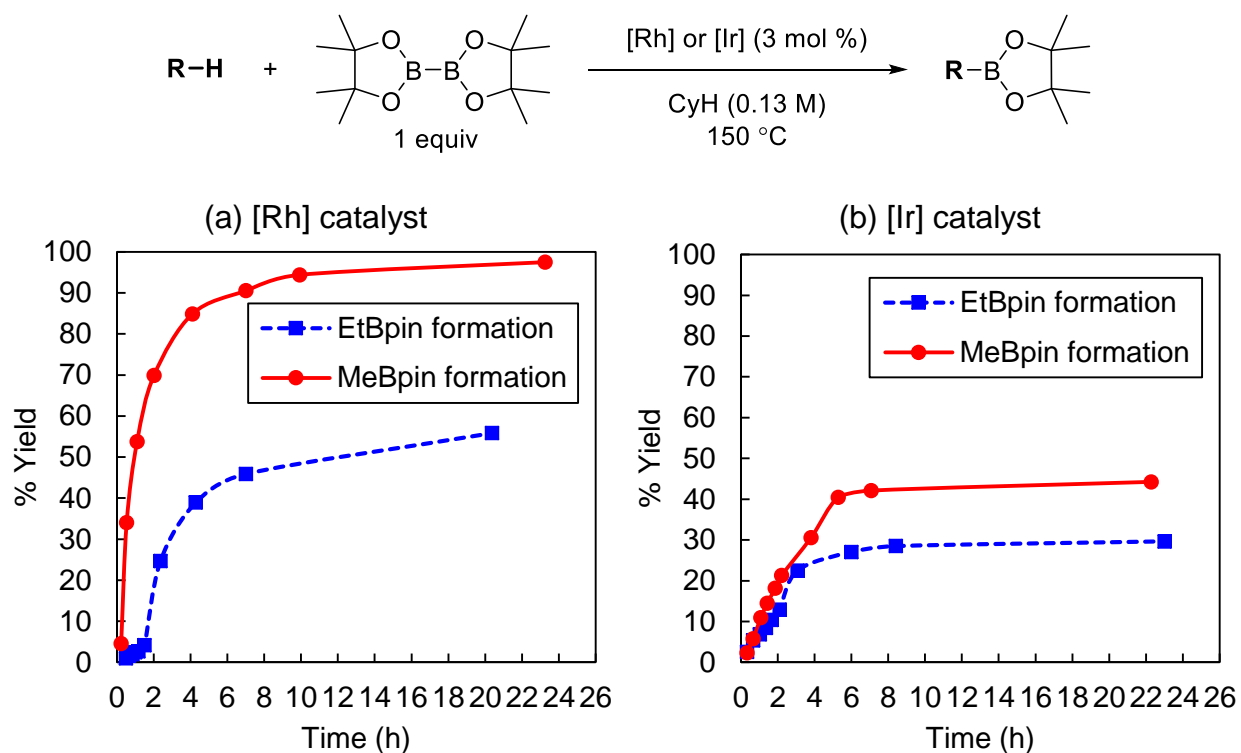
Next, to compare the activity of these catalysts and their affinity for different C–H bonds in detail, we measured the reaction rate for methane, ethane (primary C–H bonds), and cyclohexane (secondary C–H bonds). Since these three substrates represent a spectrum of C–H bonds, the analysis of both catalysts' affinities for each type of C–H bond will result in a more thorough knowledge of their activity. To obtain the rates of reaction for the gaseous substrates (methane and ethane), a modified high pressure reactor was used (Figure 5.2). This reactor has a liquid-sampling diptube (b) that extends to the reaction solution. When opened, the pressure of the headspace drives liquid up through the tube to be sampled via an outlet (e). The reactor is also equipped with a connection to a gas tank (closed during reaction progress) (a), a pressure transducer (c), and a safety release valve (d), and the reactor is heated in an aluminum heating block (f). Aliquots were taken periodically and analyzed by GC-FID to afford the rate data reported with methane and ethane as the substrates. For cyclohexane, rates were measured in 4 mL Schlenk tubes (no positive pressure of gas was added in these experiments) with each time point run as two separate reactions in separate tubes (the reported yields are averages from these two separate reactions).

**Figure 5.2.** Reactor setup for in situ liquid sampling



As can be seen in Figure 5.3a, formation of MeBpin using [Rh] is rapid and immediate. However, an induction period was observed during ethane borylation using [Rh]. The formation of ethylboronic acid pinacol ester (EtBpin), the product of borylation of ethane, is delayed by ~1.5 h, and then formation is rapid. Notably, this effect is not seen using [Ir]. We propose that ethylene, which is a possible contaminant in ethane, can coordinate to Rh of  $\text{Cp}^*\text{Rh}(\eta^4\text{-C}_6\text{Me}_6)$  after or as part of hexamethylbenzene dissociation, forming an ethylene complex.  $\text{Cp}^*\text{Rh}(\eta^2\text{-CH}_2\text{CH}_2)_2$  is a known precatalyst for alkane C–H borylation.<sup>13a</sup> As such, the formation of this species could delay formation of the active borylation catalysts  $(\text{Cp}^*\text{Rh}(\text{H})_2(\text{Bpin})_2)$  and  $\text{Cp}^*\text{Rh}(\text{H})(\text{Bpin})_3$ .<sup>13b,c</sup> Rates of ethane borylation are measured after this induction period. Because the Ir complex added is the tris-boryl complex, there is no prerequisite [M]-boryl complex formation to delay catalysis, as is proposed with [Rh].

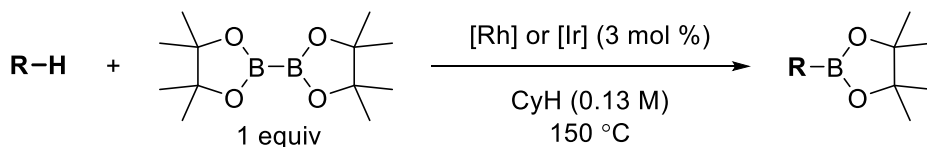
**Figure 5.3.** Time studies for methane and ethane borylation



The rates of reaction for the substrates are seen in Table 5.5. The rate of methane borylation is 84 mM/h using [Rh], which is about 7 times faster than [Ir]. Additionally, [Rh] is especially selective for methane, as seen when comparing the rates for methane (entry 1) and ethane borylation (entry 2), which were measured under otherwise identical conditions (due to the relatively low liquidation pressure of ethane, pressures of 28 bar were used for these rate studies). Indeed, the rate of methane borylation is ~2.5 times faster than that of ethane for [Rh]. Of note, these values are uncorrected for the number of C–H bonds and for their respective solubility (the solubility of ethane (218 mM) is 7 times higher than that of methane (30 mM) in cyclohexane at 1 atm and 25 °C),<sup>21</sup> and if corrected, the relative rate is expected to be significantly higher. [Ir] shows only a slight preference for methane over ethane, with a relative rate of 1.3.



**Table 5.5.** Rates of reaction for methane, ethane, hexane, and cyclohexane using both the Rh and Ir catalysts



Entry	Substrate	Rate with [Rh] (mM/h)	Rate with [Ir] (mM/h)	[Rh]/[Ir] Relative Rate
1	Methane <sup>a</sup>	84	13	6.5
2	Ethane <sup>a</sup>	34	10	1.7
3	Cyclohexane <sup>b</sup>	2.8	0.21	13

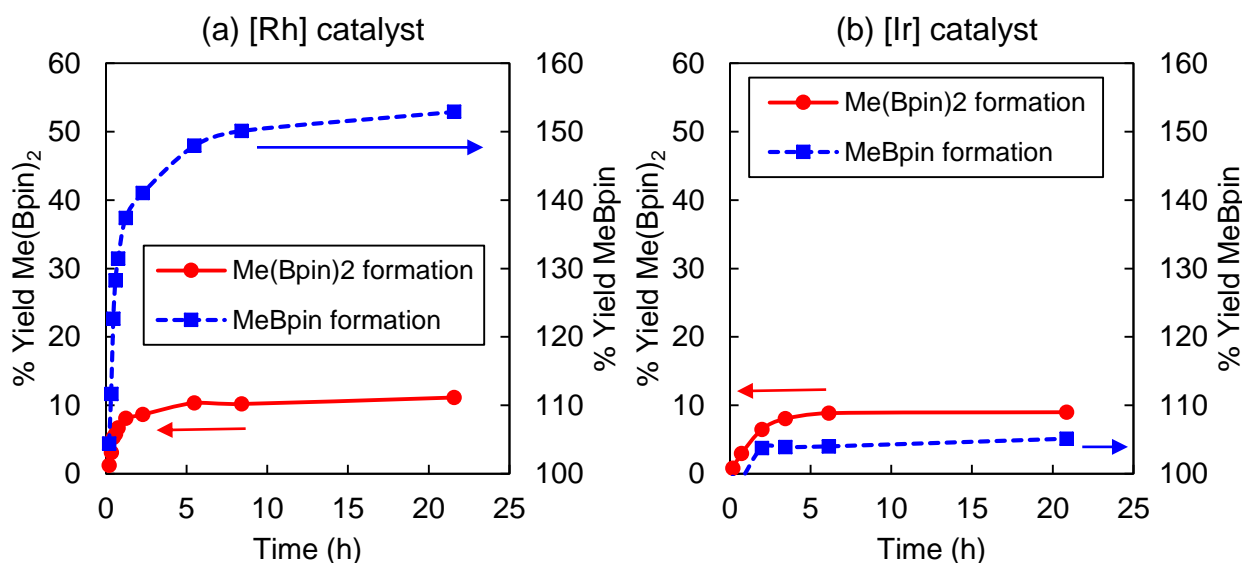
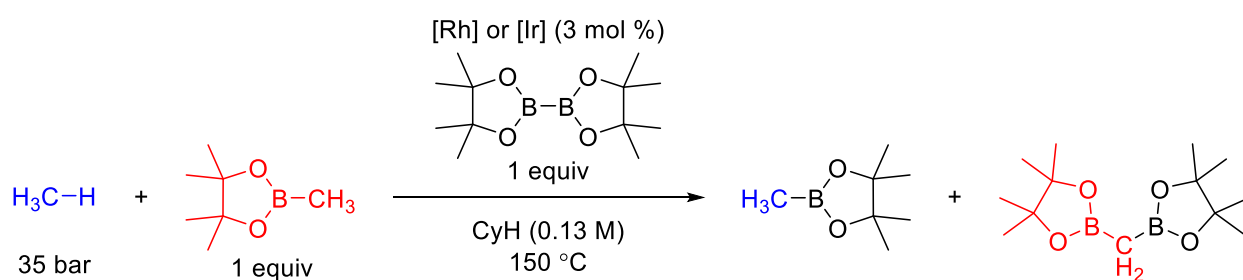
<sup>a</sup>28 bar of the gas was used. <sup>b</sup>Run in neat cyclohexane (72 equiv).

The weakest and most sterically crowded C–H bond tested (and the most statistically abundant) is the cyclohexyl C–H bond (entry 3). Presumably due to the steric environment, it shows the slowest rate in the C–H bond series for both catalysts, with [Rh] being 13 times faster than [Ir]. In general, [Rh] is more active than [Ir]. What is particularly revealing is the preference of [Rh] for methane C–H bonds over the other types of C–H bonds tested. These results show that [Rh] has overcome one of the significant challenges in methane functionalization, which is competitive solvent functionalization.

Another challenge in methane functionalization is over-functionalization. For methane oxidation chemistry, such as conversion to methanol, the products are metastable and are susceptible to further oxidation, to ultimately form CO<sub>2</sub>. This has been circumvented by generating products with electron-deficient groups, such as methyl bisulfate (CH<sub>3</sub>SO<sub>3</sub>H), which are kinetically unreactive towards over functionalization. While this is a successful strategy, it requires acidic solvents.<sup>2c,2d,4,22</sup> Therefore, catalysts that can selectively functionalize methane while avoiding acidic solvents are the optimal choice. Because [Rh] has shown excellent selectivity for methane over other alkyl C–H bonds, we tested its selectivity for methane over MeBpin. As a competition, 1 equiv MeBpin and 35 bar methane were used as reactants in the same reaction vessel. A time course of the reaction is shown in Figure 5.4a. The yield of MeBpin (blue squares, right y-axis) represents the *additional* MeBpin formed from the C–H borylation of methane and the yield of Me(Bpin)<sub>2</sub> (red circles, left axis) represents that formed from the C–H borylation of MeBpin. Because 1 equivalent (100% yield) of MeBpin is present from the

outset, the data starts at 100% yield (right y-axis). As can be seen in Figure 5.4a, the rate of formation of MeBpin is much greater than that of Me(Bpin)<sub>2</sub>, suggesting that there is a preference for methane over MeBpin as substrate. The same competition was performed using [Ir], and it was found that the amount of diborylated product exceeded the amount of newly formed MeBpin. Because one molecule of MeBpin must be formed from methane for every molecule of Me(Bpin)<sub>2</sub> formed to see a change in the % yield of MeBpin, [Ir] shows minimal preference for either substrate, in marked contrast to [Rh].

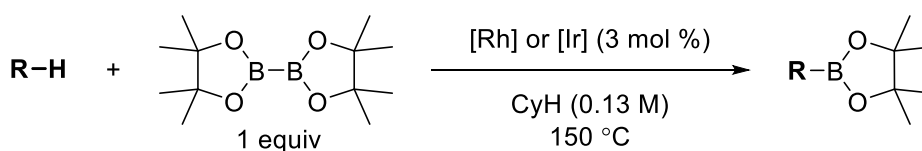
**Figure 5.4.** CH<sub>4</sub> and MeBpin competition for the (a) Rh and (b) Ir catalysts



Next, we measured the rate of each reaction independently. The rates of reaction for methane as the substrate used 35 bar of methane and the rates for MeBpin borylation used 1 equivalent of MeBpin (Table 5.6). Comparing the rates of methane and MeBpin C–H borylation, [Rh] has a clear preference for methane over MeBpin, with a relative rate of 2.4. Interestingly, [Ir] shows a slower relative rate ( $k_{rel}$  is 1.9) for methane borylation

than for MeBpin borylation when the rates are measured separately. The comparison of the relative rates of [Rh] and [Ir] for methane over MeBpin qualitatively reflect that [Rh] is a more selective catalyst than [Ir]. Because the exact concentration of methane under the reaction conditions is unknown, it is difficult to quantify selectivity at this stage. However, the relative rates of the catalysts for methane and MeBpin can be qualitatively compared, and it is clear that [Rh] greatly outperforms [Ir] for both substrates. The Rh/Ir relative rate for methane at 35 bar is 9.2 (entry 1) and for MeBpin is 6.5 (entry 2).

**Table 5.6.** Independent rates for methane and MeBpin



Entry	Substrate	Rate with [Rh] (mM/h)	Rate with [Ir] (mM/h)	[Rh]/[Ir] Relative Rate
1	Methane <sup>a</sup>	101	11	9.2
2	MeBpin <sup>b</sup>	42	6.5	6.5

<sup>a</sup>35 bar of the gas was used. <sup>b</sup>1 equivalent of MeBpin used in 0.13 M cyclohexane.

### 5.3 CONCLUSION

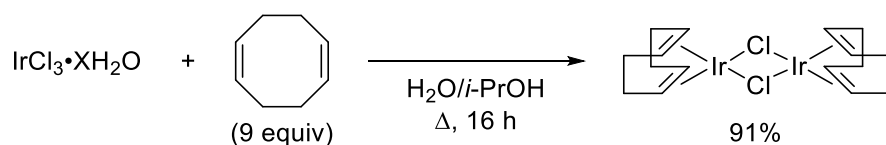
By studying the C–H borylation of methane, two gaps in the literature have been filled. The first is a method to functionalize methane selectively, avoiding solvent functionalization and over-functionalization, which were two major challenges associated with literature methods. The second is a thorough comparison of the activity of the best C–H borylation catalysts known in the literature. We compared the Rh and Ir catalyst systems for their selectivity toward different C–H bonds, information that was lacking in the literature despite much work on these catalysts over the past 15 years. It has become clear through these studies that the Rh catalyst shows excellent activity for the C–H borylation of methane and displays little competitive over-functionalization and functionalization of the solvent.

## 5.4 PERSPECTIVE AND OUTLOOK

Moving forward on the borylation of methane and other light alkanes, the development of new catalysts is of paramount importance. With the improvement of selectivity for methane versus solvent functionalization, the next key step will be improvement of the selectivity for methane versus MeBpin functionalization. Improving this facet of selectivity will entail the development of new catalysts, mechanistic studies, and using diverse boron (diboron and borane) reagents.

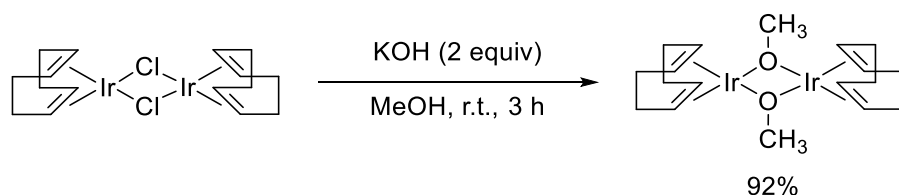
## 5.5 EXPERIMENTAL

### [(COD)IrCl]<sub>2</sub>



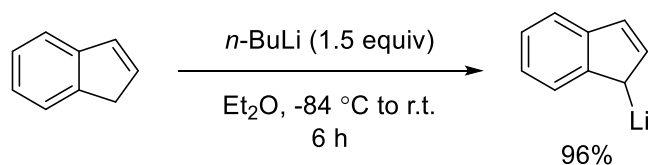
[(COD)IrCl]<sub>2</sub> was synthesized according to a literature procedure:<sup>23</sup> a 500 mL round-bottom flask was charged with IrCl<sub>3</sub>•XH<sub>2</sub>O (4.0 g, approx. 10 mmol, 1 equiv) and a stirbar and the headspace was flushed with nitrogen. Deionized water (65 mL) and *i*-PrOH (120 mL) were sparged with nitrogen and added to the flask. COD (12 mL, 94 mmol, 9.0 equiv) was then added via syringe. The flask was then fitted with a reflux condenser under nitrogen and heated to reflux in an oil bath. After heating for ca. 1 hour, the reaction became homogeneous and orange. After refluxing for a total of 16 h, the reaction was cooled to room temperature and orange crystals formed. Half of the reaction solvent was removed by rotary evaporation and the orange solid was collected by filtration, washing with deionized water. 3.2 g (91% yield) of an orange solid was obtained. <sup>1</sup>H NMR matches that reported in the literature.<sup>24</sup>

## [(COD)Ir(OMe)]<sub>2</sub>



[(COD)Ir(OMe)]<sub>2</sub> was synthesized according to a literature procedure:<sup>25</sup> [(COD)IrCl]<sub>2</sub> (200 mg, 0.30 mmol, 1.0 equiv) was weighed into a Schlenk flask, which was then charged with a stirbar and placed under a nitrogen atmosphere. MeOH (20 mL) was sparged with nitrogen and added to the flask, followed by KOH (34 mg, 0.60 mmol, 2.0 equiv). This mixture was stirred for 3 hours, during which a yellow precipitate formed. This mixture was poured into deionized water (40 mL) which had been sparged with nitrogen. The resulting yellow solid was collected by filtration. The filtrate was cooled to -5 °C for 3 hours and more yellow precipitate was formed. This solid was collected by filtration and combined with the first crop. The combined yellow solids were dried under vacuum over P<sub>2</sub>O<sub>5</sub>, giving 92% yield (183 mg). <sup>1</sup>H NMR matches that reported in the literature.<sup>25</sup>

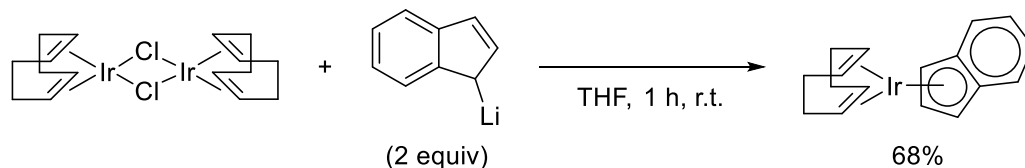
## Indenyl Lithium



Indenyl lithium was prepared by analogy to a literature procedure:<sup>26</sup> under a nitrogen atmosphere, 1*H*-indene (3.3 mL, 29 mmol, 1.0 equiv) was measured into a 500 mL, 3-neck, round bottom flask equipped with a stirbar. Et<sub>2</sub>O (140 mL; from solvent purification system) was added to the flask via cannula. The reaction was cooled to -84 °C in an EtOAc/liquid nitrogen bath and *n*-BuLi (17.1 mL of 2.5 M in hexane solution, 43 mmol, 1.5 equiv) was added dropwise. The reaction was stirred in the bath for 5 min, and then the bath was removed. The reaction was allowed to warm to room temperature and react for 6 hours. The reaction was concentrated to dryness under vacuum. The flask was backfilled with nitrogen and then brought into a nitrogen-filled glovebox. The residue was suspended in pentane (15 mL; purified by solvent purification system) and the solid was

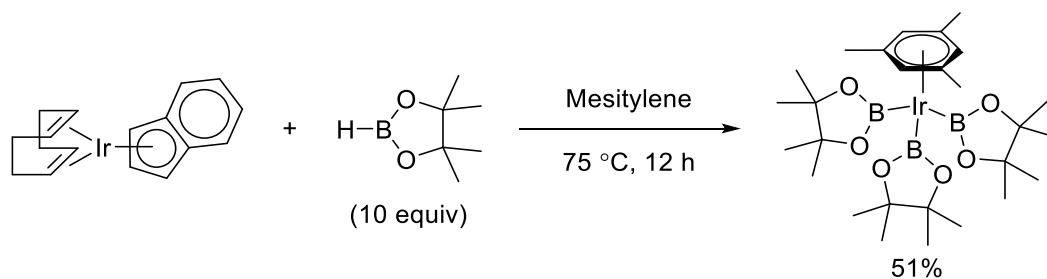
filtered. The solid was washed with pentane (3 x 10 mL), yielding 3.4 g (96%) of a pale yellow solid.  $^1\text{H}$  NMR matches that reported in the literature.<sup>27</sup>

### (COD)Ir(Ind)



(COD)Ir(Ind) was prepared according to a literature procedure:<sup>28</sup> in a nitrogen-filled glovebox, [(COD)IrCl]<sub>2</sub> (1.0 g, 1.5 mmol, 1.0 equiv) was dissolved in THF (20 mL) in a 50 mL round-bottom flask equipped with a stirbar. Indenyl lithium (0.36 g, 3.0 mmol, 2.0 equiv) was then added in one portion to this solution. The reaction was capped and stirred at room temperature in the glovebox for 1 hour, during which the reaction had turned brown. The reaction was concentrated to dryness, giving a brown-red solid. This solid was extracted with pentane (5 x 20 mL). The liquid extractions were combined and concentrated to ca. 20 mL. The resulting dark yellow solid was collected by filtration, giving 0.85 g (COD)Ir(Ind) in 68% yield.  $^1\text{H}$  NMR matches that reported in the literature.<sup>28</sup>

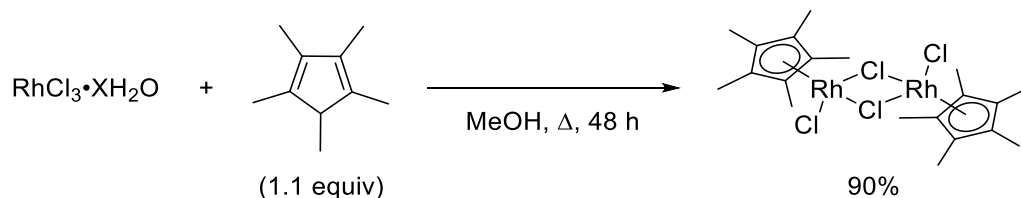
### ( $\eta^6$ -Mes)Ir(Bpin)<sub>3</sub>



( $\eta^6$ -Mes)Ir(Bpin)<sub>3</sub> was prepared according to a literature procedure:<sup>15b</sup> in a nitrogen-filled glovebox, (COD)Ir(Ind) (182 mg, 0.437 mmol, 1.00 equiv), mesitylene (2.0 mL), and HBpin (0.63 mL, 4.37 mmol, 10.0 equiv) were combined in a 20 mL vial equipped with a stirbar. This vial was sealed with a Teflon-lined cap and heated to 75 °C for 12 hours outside the glovebox in a pre-heated aluminum heating block. The reaction was cooled to room temperature and mesitylene was removed under vacuum, resulting in a black sludge. The vial was backfilled with nitrogen and brought into a nitrogen-filled glovebox. Pre-chilled (freezer at -25 °C) (Me<sub>3</sub>Si)<sub>2</sub>O (0.4 mL) was added and the resulting

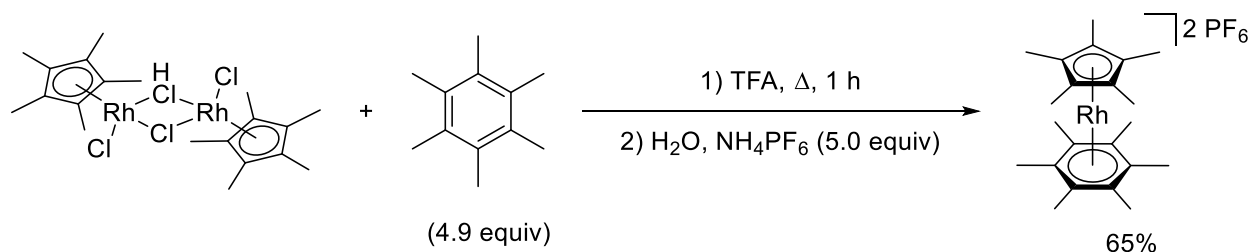
white solid was separated by filtration. The white solid was further dried under vacuum, giving  $(\eta^6\text{-Mes})\text{Ir}(\text{Bpin})_3$  (153 mg, 51% yield).  $^1\text{H}$  NMR matches that reported in the literature.<sup>15b</sup>

### $[\text{Cp}^*\text{RhCl}_2]_2$



$[\text{Cp}^*\text{RhCl}_2]_2$  was prepared according to a literature procedure:<sup>29</sup> a 100 mL round-bottom flask was charged with  $\text{RhCl}_3 \cdot \text{XH}_2\text{O}$  (2.0 g, approx. 8 mmol, 1 equiv) and a stirbar and the headspace was flushed with nitrogen. Methanol (60 mL) was sparged with nitrogen and added to the flask.  $\text{Cp}^*\text{H}$  (1.3 mL, 8.2 mmol, 1.1 equiv) was then added via syringe. The flask was then fitted with a reflux condenser under nitrogen and heated to reflux in an oil bath. After refluxing for a total of 48 h, the reaction was cooled to room temperature. The dark red solid was collected by filtration, washing with a minimal amount of methanol. 2.2 g (90% yield) of  $[\text{Cp}^*\text{RhCl}_2]_2$  was collected as a dark red solid.  $^1\text{H}$  NMR matches the commercial (Alfa Aesar) material.

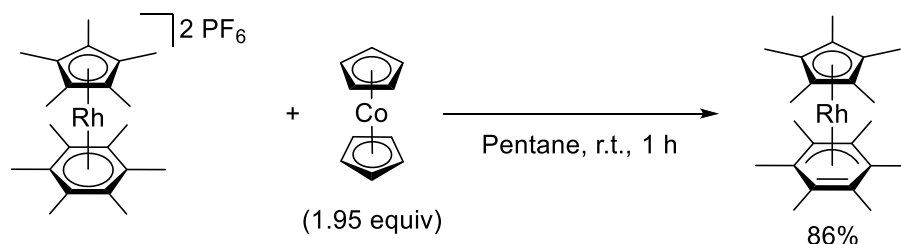
### $[\text{Cp}^*\text{Rh}(\eta^6\text{-C}_6\text{Me}_6)](\text{PF}_6)_2$



$[\text{Cp}^*\text{Rh}(\eta^6\text{-C}_6\text{Me}_6)](\text{PF}_6)_2$  was prepared according to a literature procedure:<sup>30</sup> a 25 mL round bottom flask was charged with  $[\text{Cp}^*\text{RhCl}_2]_2$  (0.90 g, 1.5 mmol, 1.0 equiv), hexamethylbenzene (1.2 g, 7.1 mmol, 4.9 equiv), and a stirbar. The reaction flask was sealed and placed under nitrogen. TFA (17 mL) was then added via syringe and the reaction flask was fitted with a reflux condenser under nitrogen. The reaction was then heated to reflux for 1 hour. After cooling to room temperature, the resulting brown mixture was concentrated to dryness by rotary evaporation. Deionized water (18 mL) was added

and the mixture was filtered. To the filtrate,  $\text{NH}_4\text{PF}_6$  (1.2 g, 7.3 mmol, 5.0 equiv) was added, forming a white precipitate. This mixture was centrifuged (5000 rpm, 20 min) and the liquid was decanted and discarded. The white solid was dried over  $\text{P}_2\text{O}_5$  under vacuum for ca. 3 hours and then recrystallized with acetone and  $\text{Et}_2\text{O}$ . The solid was filtered and rinsed with  $\text{Et}_2\text{O}$ , giving  $[\text{Cp}^*\text{Rh}(\eta^6\text{-C}_6\text{Me}_6)](\text{PF}_6)_2$  as a white solid (1.4 g, 65% yield).  $^1\text{H}$  NMR matches that reported in the literature.<sup>30</sup>

### $\text{Cp}^*\text{Rh}(\eta^4\text{-C}_6\text{Me}_6)$



$[\text{Cp}^*\text{Rh}(\eta^4\text{-C}_6\text{Me}_6)]$  was prepared according to a literature procedure:<sup>31</sup> in a nitrogen-filled glovebox,  $[\text{Cp}^*\text{Rh}(\eta^6\text{-C}_6\text{Me}_6)](\text{PF}_6)_2$  (450 mg, 0.652 mmol, 1.00 equiv) was weighed into a 25 mL round-bottom flask equipped with a stirbar. Pentane (18 mL; from solvent purification system) was added, followed by  $\text{Cp}_2\text{Co}$  (240 mg, 1.27 mmol, 1.95 equiv). This mixture was stirred for 1 hour at room temperature. A green solid was then filtered off and discarded, giving a red filtrate, which was concentrated to dryness under vacuum. The resulting red solid was collected (224 mg, 86% yield).  $^1\text{H}$  NMR matches that reported in the literature.<sup>32</sup>

### General procedure for screening reaction conditions

In a  $\text{N}_2$ -filled glovebox,  $\text{B}_2\text{pin}_2$  (226 mg, 0.890 mmol, 1.00 equiv) and any other solids were weighed into the well of the reactor also containing a magnetic stirbar. Cyclohexane (AcroSeal™) was measured by graduated cylinder and then added to the well of the reactor. The well was then taken outside of the glovebox, and the head assembled. The headspace of the reactor was then flushed 3 times with the gas of use (methane, nitrogen, etc.), and then the reactor was pressurized to the desired pressure. The reactor was then heated to the desired temperature in either a pre-heated oil bath or in a pre-heated aluminum heating block with stirring. To get reliable results, one reactor was setup at a time. After heating for the desired reaction time, the reactors were flash-



cooled in a liquid nitrogen bath (the level of the liquid nitrogen did not surpass the reactor well height) for 5 minutes, which solidified any gases and liquids in the reactor. The reactions were then thawed to room temperature over approximately 1 hour. The internal standard (either PhCl or isododecane) was added via a Hamilton gas-tight microliter syringe, diluted with 5 mL cyclohexane (ACS grade), and an aliquot was taken from this mixture and analyzed by GC-FID. Yields are reported as averages of at least 2 independent reactions.

### **General procedure for time studies and rate data using gaseous substrates**

In a N<sub>2</sub>-filled glovebox, B<sub>2</sub>pin<sub>2</sub> (678 mg, 2.67 mmol, 1.00 equiv) and any other solids were weighed into the well of the reactor also containing a magnetic stirbar. Isododecane was used as the internal standard and it was weighed into a vial and then this was transferred to the reaction well using the reaction solvent, cyclohexane as the transfer medium. Remaining cyclohexane (21 mL total, AcroSeal™) was then added to the well of the reactor. The well was then taken outside of the glovebox, and the head of the reactor was assembled. The headspace of the reactor was then flushed 3 times with the gas of use (methane or ethane), and then the reactor was pressurized to the desired pressure. The reactor was then heated to 150 °C in a pre-heated aluminum heating block with stirring. 0.5 mL aliquots were taken via the liquid sampling fitting, diluted to 1.5 mL with cyclohexane (ACS grade), and analyzed by GC-FID. It was found that the pressure dropped by ~3 bar every time an aliquot was taken; to counteract this, the reactor was immediately re-pressurized to the pressure it reaches at 150 °C after each aliquot was taken. This re-pressurization gave more reliable data.

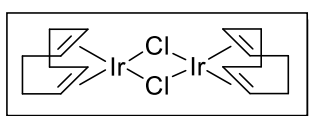
### **General procedure for time studies and rate data using liquid substrates**

*Procedure for the Rh catalyst:* In a N<sub>2</sub>-filled glovebox, stock solution was made by weighing out B<sub>2</sub>pin<sub>2</sub> (650 mg, 2.6 mmol, 1.0 equiv), the liquid substrate (2.6 mmol, 1 equiv), and Cp\*Rh(η<sup>4</sup>-C<sub>6</sub>Me<sub>6</sub>) (31 mg, 0.078 mmol, 0.030 equiv) into a volumetric flask. This was then diluted to 20 mL with cyclohexane (AcroSeal™) and shaken until homogeneous. 1.3 mL aliquots (B<sub>2</sub>pin<sub>2</sub> = 42 mg, 0.17 mmol, 1.0 equiv; [Rh] = 2.0 mg, 0.0051 mmol, 0.030 equiv) were then dispensed into oven-dried 4 mL Schlenk tubes with stirbars. The tubes were sealed with Teflon taps, brought outside the glovebox, and submerged in a pre-

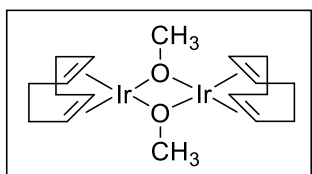
heated oil bath at 150 °C for the given reaction time below. The tubes were flash-frozen in a liquid N<sub>2</sub> bath until solid, and then allowed to thaw to room temperature. PhCl was added as an internal standard, diluting with 2 mL cyclohexane. An aliquot of this mixture was taken for GC-FID analysis. Each data point is the average of 2 simultaneous and independent reactions.

*Procedure for the Ir catalyst:* A stock solution of Me<sub>4</sub>Phen (60 mg, 0.24 mmol) in DCM (5.0 mL) was made and 100 μL aliquots (1.2 mg, 0.0050 mmol, 0.030 equiv) were dispensed into 4 mL Schlenk tubes with stirbars. These were stirred openly to air for 2 hours to allow the DCM to evaporate. These tubes were then brought into a N<sub>2</sub>-filed glovebox. Also in the glovebox, a stock solution was made by weighing out B<sub>2</sub>pin<sub>2</sub> (650 mg, 2.6 mmol, 1.0 equiv), the liquid substrate (2.6 mmol, 1 equiv), and (η<sup>6</sup>-Mes)Ir(Bpin)<sub>3</sub> (54 mg, 0.078 mmol, 0.030 equiv) into a volumetric flask. This was then diluted to 20 mL with cyclohexane (AcroSeal™) and shaken until homogeneous. 1.3 mL aliquots (B<sub>2</sub>pin<sub>2</sub> = 42 mg, 0.17 mmol, 1.0 equiv; [Ir] = 3.5 mg, 0.0050 mmol, 0.030 equiv) were then dispensed into the Schlenk tubes containing Me<sub>4</sub>Phen and a stirbar. The tubes were sealed with Teflon taps, brought outside the glovebox, and submerged in a pre-heated oil bath at 150 C for the given reaction time below. The tubes were flash-frozen in a liquid N<sub>2</sub> bath until solid, and then allowed to thaw to room temperature. PhCl was added as an internal standard, diluting with 2 mL cyclohexane. An aliquot of this mixture was taken for GC-FID analysis. Each data point is the average of 2 simultaneous and independent reactions.

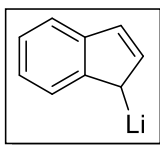
## 5.6 CHARACTERIZATION



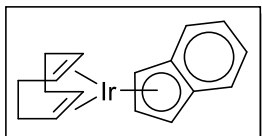
<sup>1</sup>H NMR (DMSO-D<sub>6</sub>, 700 MHz): δ 4.19 (s, 8 H), 2.25 (m, 8 H), 1.80 (m, 8 H).



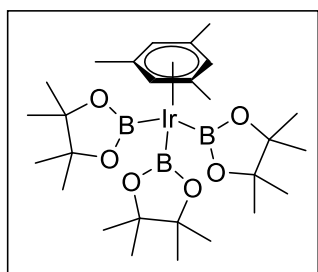
<sup>1</sup>H NMR (CDCl<sub>3</sub>, 700 MHz): δ 3.54 (s, 8 H), 3.24 (s, 6 H), 2.23 (s, 8H), 1.37 (m, 6 H).



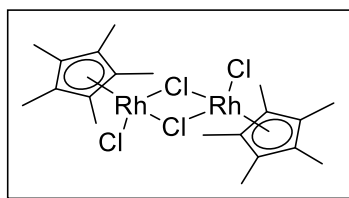
$^1\text{H NMR}$  ( $\text{DMSO-}D_6$ , 400 MHz):  $\delta$  7.08 (dd,  $J = 3.1, 5.9$  Hz, 2 H), 6.35 (t,  $J = 3.3$  Hz, 1 H), 6.20 (dd,  $J = 3.1, 5.9$  Hz, 2 H), 5.71 (d,  $J = 3.3$  Hz, 2 H).



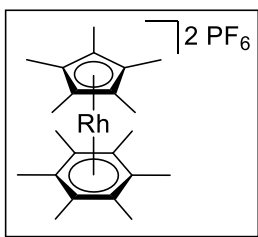
$^1\text{H NMR}$  ( $\text{CDCl}_3$ , 400 MHz):  $\delta$  7.25 (m, 2 H), 7.08 (m, 2 H), 5.96 (m, 1 H), 5.30 (d,  $J = 2.4$  Hz, 2 H), 3.85 (d,  $J = 2.7$  Hz, 4 H), 1.70 (m, 4 H), 1.55 (m, 4 H).



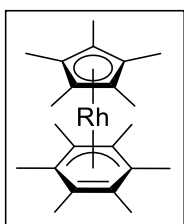
$^1\text{H NMR}$  ( $\text{C}_6\text{D}_6$ , 400 MHz):  $\delta$  5.64 (s, 3 H), 2.25 (s, 9 H), 1.34 (s, 36 H).



$^1\text{H NMR}$  ( $\text{DMSO-}D_6$ , 500 MHz):  $\delta$  1.63 (s, 30 H).



$^1\text{H NMR}$  ( $\text{Aceone-}D_6$ , 400 MHz):  $\delta$  2.58 (s, 18 H), 2.12 (s, 15 H).



$^1\text{H NMR}$  ( $\text{C}_6\text{D}_6$ , 400 MHz):  $\delta$  2.06 (s, 6 H), 1.65 (s, 15 H), 1.42 (s, 6 H), 1.28 (s, 6 H).

## 5.7 REFERENCES

- (1) Hammer, G.; Lübcke, T.; Kettner, R.; Pillarella, M. R.; Recknagel, H.; Commichau, A.; Neumann, H.-J.; Paczynska-Lahme, B. In *Ullmann's Encyclopedia of Industrial Chemistry*, Wiley-VCH Verlag GmbH & Co. KGaA: 2006.
- (2) (a) Crabtree, R. H. *Chem. Rev.* **1995**, *95*, 987. (b) Cavaliere, V. N.; Wicker, B. F.; Mindiola, D. J. In *Adv. Organomet. Chem.*; Anthony, F. H., Mark, J. F., Eds.; Academic Press: **2012**; vol. 60, p 1. (c) Caballero, A.; Perez, P. J. *Chem. Soc. Rev.* **2013**, *42*, 8809. (d) Gunsalus, N. J.; Konnick, M. M.; Hashiguchi, B. G.; Periana, R. A. *Isr. J. Chem.* **2014**, *54*, 1467.
- (3) Anslyn, E. V.; Dougherty, D. A. *Modern Physical Organic Chemistry*, © **2006**, University Science Books.
- (4) Stahl, S. S.; Labinger, J. A.; Bercaw, J. E. *Angew. Chem., Int. Ed.* **1998**, *37*, 2180.
- (5) Sadow, A. D.; Tilley, T. D. *J. Am. Chem. Soc.* **2003**, *125*, 7971.
- (6) Sadow, A. D.; Tilley, T. D. *Angew. Chem., Int. Ed.* **2003**, *42*, 803.
- (7) Caballero, A.; Despagnet-Ayoub, E.; Mar Díaz-Requejo, M.; Díaz-Rodríguez, A.; González-Núñez, M. E.; Mello, R.; Muñoz, B. K.; Ojo, W.-S.; Asensio, G.; Etienne, M.; Pérez, P. J. *Science* **2011**, *332*, 835.
- (8) (a) Crabtree, R. H. *Chem. Rev.* **1985**, *85*, 245. (b) Arndtsen, B. A.; Bergman, R. G.; Mobley, T. A.; Peterson, T. H. *Acc. Chem. Res.* **1995**, *28*, 154. (c) Shilov, A. E.; Shul'pin, G. B. *Chem. Rev.* **1997**, *97*, 2879. (d) Crabtree, R. H. *J. Chem. Soc., Dalton Trans.* **2001**, 2437.
- (9) (a) Janowicz, A. H.; Bergman, R. G. *J. Am. Chem. Soc.* **1982**, *104*, 352. (b) Janowicz, A. H.; Bergman, R. G. *J. Am. Chem. Soc.* **1983**, *105*, 3929. (c) Hoyano, J. K.; McMaster, A. D.; Graham, W. A. G. *J. Am. Chem. Soc.* **1983**, *105*, 7190.
- (10) (a) Jones, W. D.; Feher, F. J. *J. Am. Chem. Soc.* **1984**, *106*, 1650. (b) Periana, R. A.; Bergman, R. G. *Organometallics* **1984**, *3*, 508.
- (11) (a) Ishiyama, T.; Miyaura, N. *J. Organomet. Chem.* **2003**, *680*, 3. (b) Hartwig, J. F. *Chem. Soc. Rev.* **2011**, *40*, 1992. (c) Hartwig, J. F. *Acc. Chem. Res.* **2012**, *45*, 864.
- (12) (a) Waltz, K. M.; Hartwig, J. F. *Science* **1997**, *277*, 211. (b) Waltz, K. M.; Muhoro, C. N.; Hartwig, J. F. *Organometallics* **1999**, *18*, 3383.
- (13) (a) Chen, H.; Schlecht, S.; Semple, T. C.; Hartwig, J. F. *Science* **2000**, *287*, 1995. (b) Hartwig, J. F.; Cook, K. S.; Hapke, M.; Incarvito, C. D.; Fan, Y.; Webster, C. E.; Hall, M. B. *J. Am. Chem. Soc.* **2005**, *127*, 2538. (c) Wei, C. S.; Jiménez-Hoyos, C. A.; Videa, M. F.; Hartwig, J. F.; Hall, M. B. *J. Am. Chem. Soc.* **2010**, *132*, 3078.
- (14) (a) Liskey, C. W.; Hartwig, J. F. *J. Am. Chem. Soc.* **2012**, *134*, 12422. (b) Liskey, C. W.; Hartwig, J. F. *J. Am. Chem. Soc.* **2013**, *135*, 3375.
- (15) (a) Cho, J.-Y.; Tse, M. K.; Holmes, D.; Maleczka, R. E.; Smith, M. R. *Science* **2002**, *295*, 305. (b) Chotana, G. A.; Vanchura, I. I. B. A.; Tse, M. K.; Staples, R. J.; Maleczka, J. R. E.; Smith, M. R. *Chem. Commun.* **2009**, 5731.
- (16) Boller, T. M.; Murphy, J. M.; Hapke, M.; Ishiyama, T.; Miyaura, N.; Hartwig, J. F. *J. Am. Chem. Soc.* **2005**, *127*, 14263.
- (17) Ishiyama, T.; Takagi, J.; Hartwig, J. F.; Miyaura, N. *Angew. Chem., Int. Ed.* **2002**, *41*, 3056.
- (18) Tamura, H.; Yamazaki, H.; Sato, H.; Sakaki, S. *J. Am. Chem. Soc.* **2003**, *125*, 16114.
- (19) Cho, J.-Y.; Iverson, C. N.; Smith, M. R. *J. Am. Chem. Soc.* **2000**, *122*, 12868.
- (20) Hoyano, J. K.; McMaster, A. D.; Graham, W. A. G. *J. Am. Chem. Soc.* **1983**, *105*, 7190.
- (21) Wilhelm, E.; Battino, R. *Chem. Rev.* **1973**, *73*, 1.
- (22) Sen, A. *Acc. Chem. Res.* **1998**, *31*, 550.
- (23) Choudhury, J.; Podder, S.; Roy, S. *J. Am. Chem. Soc.* **2005**, *127*, 6162.
- (24) Grobelaar, E.; Purcell, W.; Basson, S. S. *Inorg. Chim. Acta* **2006**, *359*, 3800.
- (25) Hurst, T. E.; Macklin, T. K.; Becker, M.; Hartmann, E.; Kügel, W.; Parisienne-La Salle, J.-C.; Batsanov, A. S.; Marder, T. B.; Snieckus, V. *Chem. Eur. J.* **2010**, *16*, 8155.
- (26) Wang, H.; Wang, H.; Li, H.-W.; Xie, Z. *Organometallics* **2004**, *23*, 875.
- (27) Tay, B.-Y.; Wang, C.; Stubbs, L. P.; Jacob, C.; van Meurs, M. *J. Organomet. Chem.* **2011**, *696*, 3431.
- (28) Merola, J. S.; Kacmarcik, R. T. *Organometallics* **1989**, *8*, 778.
- (29) White, C.; Yates, A.; Maitlis, P. M.; Heinekey, D. M. *Inorg. Synth.* **1992**, *29*, 228
- (30) Rybinskaya, M. I.; Kudinov, A. R.; Kaganovich, V. S. *J. Organomet. Chem.* **1983**, *246*, 279.

- 
- (31) Bowyer, W. J.; Merkert, J. W.; Geiger, W. E.; Rheingold, A. L. *Organometallics* **1989**, *8*, 191.  
(32) Bowyer, W. J.; Geiger, W. E. *J. Am. Chem. Soc.* **1985**, *107*, 5657.